THE MECHANOBIOLOGY OF NOTCH1 DEFICIENCY IN CALCIFIC AORTIC VALVE DISEASE

By

Joseph Chen

Dissertation

Submitted to the Faculty of the

Graduate School of Vanderbilt University

in partial fulfillment of the requirements

for the degree of

DOCTOR OF PHILOSOPHY

in

Biomedical Engineering

May, 2015

Nashville, Tennessee

Approved:

W. David Merryman, Ph.D.

H. Scott Baldwin, M.D.

Chris B. Brown, Ph.D.

Michael I. Miga, Ph.D.

Hak-Joon Sung, Ph.D.

ACKNOWLEDGMENTS

I would like to thank the Department of Biomedical Engineering at Vanderbilt University for providing me the opportunity to pursue this doctoral degree. The excellent leadership provided by Dr. Todd Giorgio truly has made this experience an enjoyable one. I would like to thank my advisor, Dr. W. David Merryman, for his persistent enthusiasm and support that has allowed me to challenge myself and learn how to succeed in the academic research environment. I would like to acknowledge Drs. H. Scott Baldwin and Chris B. Brown for their significant contributions to my work, and I want to also acknowledge Drs. Michael I. Miga and Hak-Joon Sung for their insight and guidance during these last four and a half years.

I also want to recognize my lab mates for their friendship and support throughout these years. The friendships gained during this time are unique and are filled with experiences that few can fully understand. Many thanks to Josh Hutcheson; MK Sewell-Loftin; Steve Boronyak; Alison Schroer; Meghan Bowler; Nathan Bloodworth; and the three new additions: Cami Johnson, Mark Vander Roest, and Cyndi Hill. I am truly blessed to have these genuinely wonderful people in my life. I wish each of you the best in your future endeavors and look forward to your continued friendship in the coming years. Additionally, I would like to thank Larisa Ryzhova for being the “lab mom” and taking such good care of me both in my scientific endeavors and in my pursuit of delicious baked goods. I also want to thank Charles Fisher for his excellent guidance and support in my

early years as a PhD student. I would like to acknowledge many members of the Baldwin lab: Paige DeBenedittis, Dan DeLaughter, Cristina Harmelink, and LeShana Saint-Jean. Each of you has had a tremendous impact on me in my time here, and I am grateful for you all.

Lastly, I would like to dedicate this dissertation to my family. To my parents, Samuel and Maomi Chen, thank you for your sacrifices and determination to make it in this foreign country, for providing a strong foundation for my brothers and I to attain success, for instilling in us the value of hard work but also giving us the flexibility and support to pursue the things that truly interested us. I thank you for providing me the framework to find God for it is because of His grace that I am who I am today. To my brothers, Tim and Michael, thank you for your presence in my life. The memories I have with you both bring immense joy into my heart and remind me of the blessed life we had in Mississippi. Also, I want to thank Jenn, Caleb, and Levi for adding to my store of happy memories. I am forever indebted to each one of my family members and know quite certainly that without you, I would not have been able to make it through this PhD. So it is with deep gratitude and sincerity that I say that I love you all and am thankful to God for you.

TABLE OF CONTENTS

LIST OF FIGURES

ACRONYMS

αSMA	smooth muscle α-actin
Akt	protein kinase b
AFM	atomic force microscopy
AV	aortic valve
AVEC	aortic valve endothelial cell
AVIC	aortic valve interstitial cell
BMP	bone morphogenic protein
CAVD	calcific aortic valve disease
CN	calcific nodule
DMEM	Dulbecco's modified eagle medium
ECM	extracellular matrix
EDS	energy-dispersive spectroscopy
ELISA	enzyme-linked immunosorbent assay
Erk	extracellular-signal regulated kinase
FBS	fetal bovine serum
GSK-3β	glycogen synthase kinase 3β
MAPK	mitogen-activated protein kinase
mTORC-2	mammalian target of rapamycin complex 2
NICD	Notch intracellular domain
PDK-1	phosphoinositide-depedent kinase 1
PI	propidium iodide
PI3K	phosphoinositide 3-kinase

Runx2	runt related transcription factor 2
SEM	scanning electron microscopy
TEM	transmission electron microscopy
TGF-β	transforming growth factor β

Chapter I

Introduction and Motivation

Calcific aortic valve disease (CAVD) is the predominant valvular disease in the developed world, affecting over five million individuals in the United States alone [1, 2]. CAVD is present within 25% of the population over 65 years of age and is expected to have a significant disease burden in the coming years as the life expectancy of the population increases [2-5]. Presently, treatment for CAVD is limited to surgical aortic valve replacement, a high risk procedure especially for the population affected, and although significant advances have been made to reduce the associated risk with this procedure, a non-surgical treatment option is preferred [6]. Unfortunately, current efforts to develop pharmacological treatments have been largely unsuccessful at preventing or slowing down the progression of CAVD; this lack of efficacy can be attributed to the incomplete understanding of the etiology of CAVD [7, 8]. Thus, focused attention must be placed on elucidating the underlying mechanisms of CAVD initiation and evolution in order to develop novel and effective pharmacological drugs.

CAVD manifests itself as a progressive disease resulting in the obstruction of left ventricular outflow, decreased cardiac output, and eventual heart failure [9]. At the tissue level, normal supple leaflets are transformed into thickened, stiff,

and calcified leaflets, which have dramatically altered biomechanical properties lending to the loss of normal function. These striking changes are attributed to the aberrant behavior of the resident cell population within the valve leaflets, the aortic valve interstitial cells (AVICs), which are believed to play significant roles in leaflet thickening and calcification [10-12]. Under normal conditions, AVICs serve to maintain tissue homeostasis and remodel the leaflets by synthesizing ECM proteins, matrix-degrading enzymes and their inhibitors [13]. However, under pathologic conditions, AVICs become activated and differentiate into two main phenotypes, myofibroblastic and osteoblastic AVICs, which directly contribute to the generation of valvular calcification [14]. Myofibroblastic AVICs are characterized by enhanced smooth muscle α-actin (αSMA) and cadherin-11 and develop cell-death mediated dystrophic calcification, the predominant type of calcification found in 83% of diseased valve explants [15, 16]. Alternatively, osteoblastic AVICs display osteogenic properties as evidenced by Runx2 expression and undergo ossification, which is the active process of bone formation and is present in 13% of calcified valves [15]. Investigating what factors contribute to AVIC differentiation into these pathological phenotypes and further how they generate valvular calcification is essential to the understanding of CAVD etiology.

The development of *in vitro* systems evaluating AVIC mediated calcification has been a vital tool in the study of valvular calcification [12, 17-22]. The seminal paper by Mohler et al. demonstrated that activated AVICs generated hydroxyapatite rich nodular structures *in vitro* called calcific nodules (CNs) [19].

Since this report, significant strides have been taken regarding the understanding of key processes involved in the transformation of AVICs to CNs. It was once thought that CNs exhibited both dystrophic and osteogenic properties and were regulated by myofibroblastic and osteogenic AVICs simultaneously; however, recent studies revealed that dystrophic CNs and osteogenic CNs represent two distinct types of nodules that are generated by unique processes regulated by myofibroblastic and osteogenic AVICs, respectively [17, 23]. The discovery of unique nodule types is novel; however, more studies are needed to fully characterize their similarities and differences. Nonetheless, these findings suggest that development of valvular calcification *in vivo* proceeds primarily through a step-by-step process rather than concurrently. With this in mind, an effort to describe the progression of valvular calcification *in vivo* and further identify which CN pathway is more relevant *in vivo* is paramount in determining how to approach developing pharmacological strategies for CAVD. Optimizing *in vitro* assays to mimic relevant cues that occur *in vivo* may offer new insights towards CN morphogenesis.

It has been demonstrated that CN development is tightly regulated by biomolecular, mechanobiological, and genetic factors [24-30]. Previous studies have focused on describing the effect of biomolecular cues on CN development; however, many mechanobiological and genetic factors that have significant *in vivo* relevance have not been thoroughly assessed. The mechanobiological effect on CAVD is evident in a recent study, which demonstrates that substrate stiffness alone can direct AVIC phenotype and even override the effect of

biomolecuar stimulation [17]. Furthermore, *in vivo*, AVICs reside in an extremely dynamic, unique mechanical environment, which may have significant mechanotransductive impact. Genetic factors, such as Notch1 haploinsufficiency, predispose AVICs for aberrant behavior priming them for valvular disease. Because this genetic mutation represents changes that lead to CAVD *in vivo*, mechanistic studies evaluating signaling alterations are warranted. In an effort to gather insight towards CAVD processes *in vivo*, we believe that investigations into the role of mechanical strain and the effect of Notch1 mutation on AVIC biology and CN formation would provide novel insights towards CAVD etiology that can contribute to the development of effect therapeutics.

The objective of this proposal is to define the roles of mechanical strain and Notch1 haploinsufficiency in the initiation and development of valvular calcification by determining its effect on AVIC phenotype and CN formation. We are intrigued by the physiological and clinical relevance of these inputs and are interested in how these studies can generate new insights in areas that have been largely unexplored. In addition to investigations of AVIC biology and CN formation, characterization studies of CNs will be conducted to more clearly define and differentiate nodule properties. In order to accomplish this objective, we will address the following aims:

1. Clarify the effect of strain on the initiation/progression of CN formation by AVICs in the presence of pro-calcific biomolecules.

2. Describe the biophysical and physiochemical properties of dystrophic and osteogenic models of CN formation.
3. Examine Notch1 deficient signaling and identify its role in modulating AVIC phenotype and CAVD evolution.

To begin, a discussion of heart physiology and pathology will be given with an emphasis on the impact of mechanobiological and genetic factors on valvular disease. Subsequent chapters will address each of the individual specific aims with a focused introduction and description of the methods utilized for each study. Finally, a discussion of the complete dissertation will be provided to highlight the overall impact of the presented work and introduce potential future directions.

.

Chapter II

Background – Aortic Valve Physiology and Pathology

Portions of Chapter II taken from:

> **Simionescu, D.T., Chen, J., Jaeggli, M., Wang B., Liao J., "Form Follows Function: Advances in Trilayered Structure Replication for Aortic Heart Valve Tissue Engineering", *Journal of Health Care Engineering*. 3(2):179-202; 2012.**

2.1 – Heart and Aortic Valve Physiology

2.1.1 Mammalian Heart Physiology

The heart is a vital organ designed to distribute oxygenated blood throughout the vasculature. In an average life span, the heart beats approximately 3 billion times and requires the coordinated action of multiple components [31]. The heart is divided into four chambers: right atrium, right ventricle, left atrium, and left ventricle. Between these chambers, heart valves reside and function to ensure unidirectional blood flow from one chamber to the next (Fig. 2.1). In a normal cardiac cycle, blood is circulated through the four chambers through the coordinated contraction and relaxation of the heart termed systole and diastole, respectively.

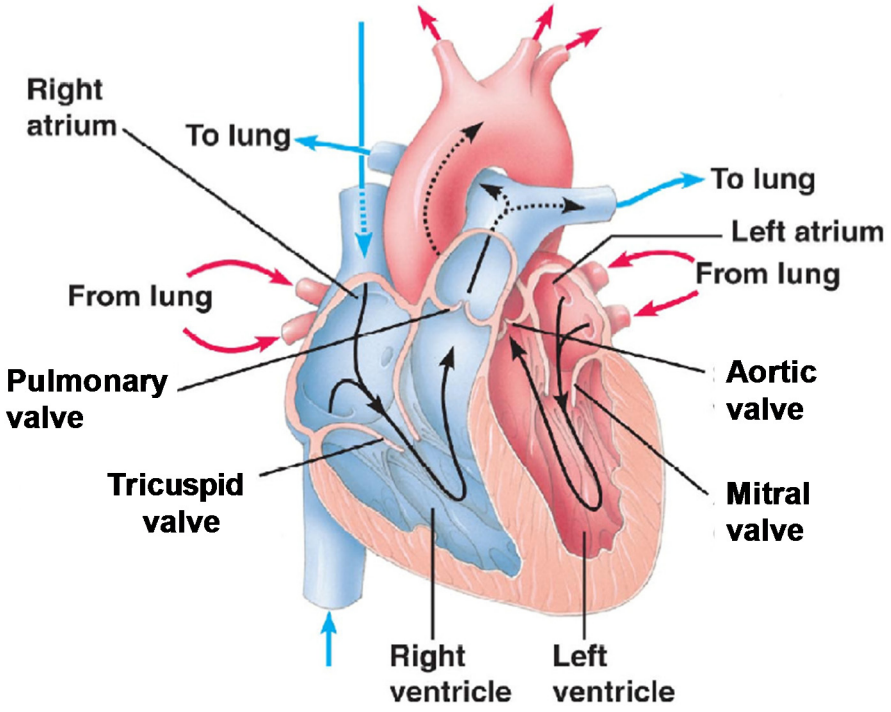

Fig 2.1 – Anatomy of the human heart (www.lamission.edu)

At the beginning of each cardiac cycle, deoxygenated blood enters the right atrium through the vena cava. As the ventricles relax in diastole, the right atrium contracts, pushing deoxygenated blood into the right ventricle through the tricuspid valve. The ventricles begin to contract during systole and pushes blood into the pulmonary system through the pulmonary valves for oxygenation. The now oxygenated blood returns into the heart through the pulmonary veins and fills the left atrium during early diastole. Left atrium contraction then drives the blood through the mitral valve into the left ventricle. Finally, the next ventricular contraction pushes oxygenated blood through the aortic valve from the left ventricle and into the systemic circulation (Fig. 2.2).

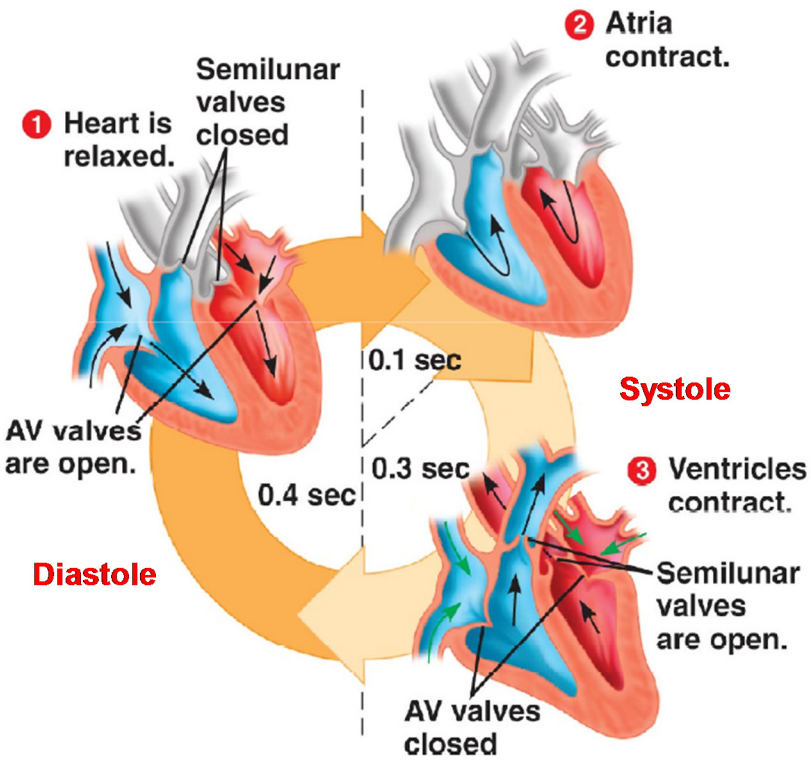

Fig. 2.2 – Two stages of heart function: diastole and systole (www.lamission.edu)

The steady unidirectional circulation of blood through the heart is made possible through the function of the four heart valves: tricuspid, pulmonary, mitral, and aortic. The tricuspid and mitral valves are at the interfaces between the atria and ventricles with the tricuspid controlling blood flow in the right side of the heart and the mitral controlling the left side. These valves are called the atrioventricular valves and represent an intricate apparatus involving chordae tendineae that anchor to the papillary muscles within the ventricle walls (Fig. 2.3).

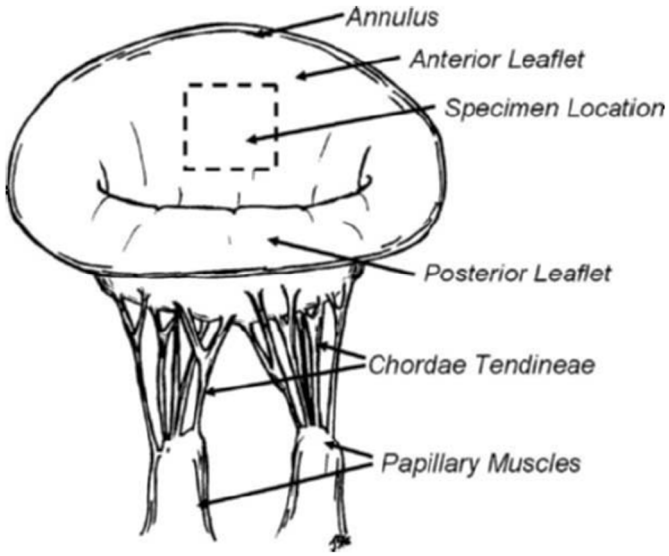

Fig 2.3 – The anatomy of the mitral valve (atrioventricular) (reprinted with permissions from [32]).

The chordae tendineae function to prevent valvular prolapse by providing tension that holds the leaflets in during systole. The structure of the atrioventricular valves is similar with the exception of the number of leaflets within each valve. The mitral valve is often called the bicuspid valve and is comprised of two leaflets, whereas the tricuspid valve contains three. The semilunar valves represent the other type of valve (i.e., the pulmonary and aortic) and are known for their crescent shaped leaflets (Fig 2.4). The pulmonary valve is seated between the right ventricle and the pulmonary system, and the AV is seated between the left ventricle and the aorta, which leads to the circulation to the rest of the body. The heart valves represent remarkable structures that withstand continual cyclical stresses and strains throughout a lifetime. The valvular ultrastructure is designed to operate within this challenging mechanical environment; however, alterations to the applied stress and strain on the heart

valves can lead to the development of valvular disease [33-35]. Moreover, it is no coincidence that the left side of the heart, which experiences the highest stresses and strains, contains the most often diseased valves in the heart.

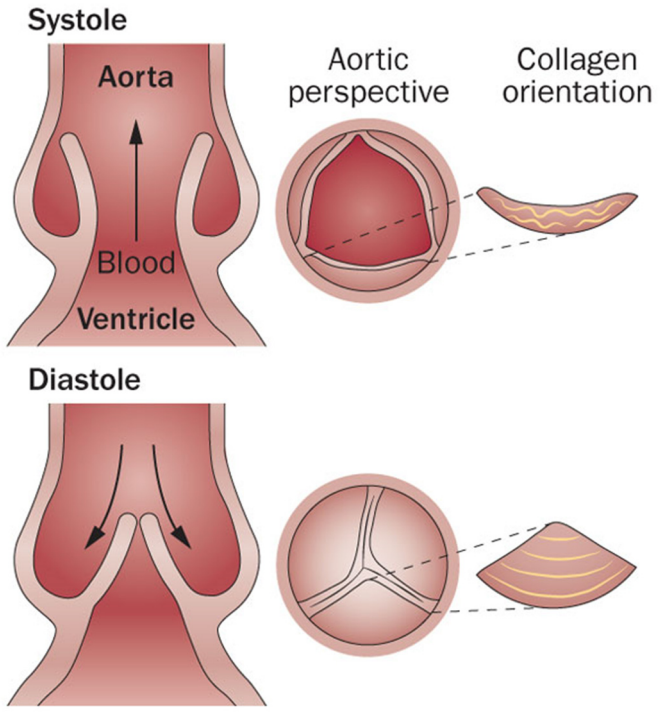

Fig. 2.4 – Structure of aortic valve during systole and diastole (reprinted with permission from [7]).

Diseases of the mitral valves and AVs represent the vast majority of valvular heart diseases [2]. Notably, disorders of the AV comprise over 65% of all valvular heart disease. AV disease was shown to affect ~ 26% of men and women over the age of 65 with increasing prevalence with increasing age [3]. Some form of AV disease was found in 20% of patients aged 65-75 years, 35% in those aged 75-85 years, and 48% in patients older than 85 years [3]. Additionally, it is estimated that the proportion of people over the age of 60 will

increase from 10% to 21% of the total population by 2050 [36]. With the increasing life expectancy of the general population, AV diseases will become a burgeoning global problem [4, 37, 38]. Currently, the only effective treatment is total valve replacement, which is undesirable given the population affected. Estimates of patients requiring valvular replacement is thought to triple in the next 50 years with many affected people in third world countries having no access to this type of treatment [36]. Investigations towards alternative treatments such as pharmacological intervention are needed.

2.1.2 Aortic Valve Physiology

The AV is the most replaced, and researched valve in the heart and undergoes the highest amounts of stress and strain during the cardiac cycle [31, 39]. It consists of three trilayered semilunar cusps attached to the inner wall of the aorta residing within the sinuses of Valsalva [31, 39]. The cusps or leaflets are the main functioning components of the aortic valve and endure the dynamic opening and closing of the valve 40 million times a year and more than 3 billion times during an average lifetime [31]. The highly dynamic environment of the valve illustrates the complex function of the leaflets and pinpoints the importance of processes that are involved in maintaining healthy valve function.

In one cardiac cycle, the AV experiences three modes of biomechanical loading: shear, flexure, and tension [31]. As the valve opens in systole, the leaflets experience shear stress due to the flow of blood on the ventricularis and flexure. As the valve shuts in diastole, the leaflets experience shear stresses on

the fibrosa side, and tensile stresses as the leaflets stretch to coapt. In order for the AV leaflets to fully coapt, the leaflets must undergo significant tensile deformation with circumferential strains ranging from 5-10% and radial strains exceeding 30% [40]. The leaflets are able to withstand the challenging demands based on its structural makeup. The AV leaflet is composed of three layers: fibrosa, spongiosa, and ventricularis (Fig. 2.5A) [41].

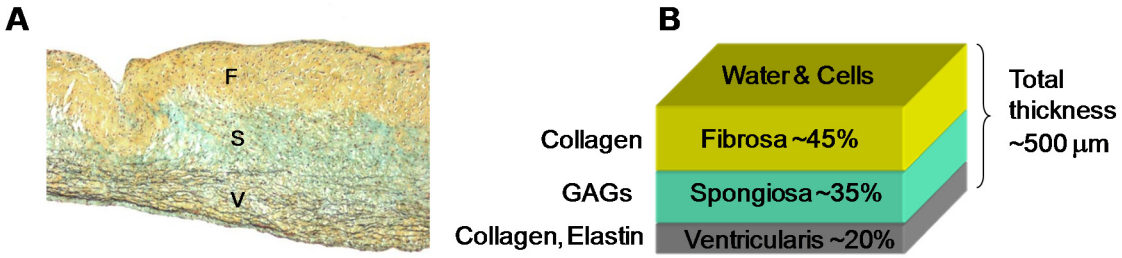

Fig. 2.5 – Aortic valve composition. (A) Movat's Pentachrome staining on an AVL cross section reveals three layers: the fibrosa (F), spongiosa (S), and ventricularis. (B) The fibrosa layer is comprised primarily of collagen, the spongiosa layer is comprised primarily of GAGs, and the ventricularis layer is comprised primarily of elastin and collagen. (Adapted from [42]).

The fibrosa layer is located closest to the aorta and is composed of densely packed circumferentially aligned collagen fibers; this layer is responsible for the mechanical strength and stiffness of the leaflet, which allows it to withstand diastolic forces and prevent leaflet prolapsed into the left ventricle (Fig. 2.5B) [43]. The ventricularis is located closest to the left ventricle and is largely comprised of elastin fibers embedded in a collagenous matrix that play an important role in extending and recoiling during diastole and systole respectively (Fig. 2.5B). Finally, the spongiosa is mainly comprised of proteoglycans and

glycosaminoglycans (GAGs), which acts as a lubricating cushion and bears the applied stresses of valve function (Fig. 2.5B) [44]. The three layers are structurally continuous and work in conjunction with one another to fully satisfy the mechanical demands involved in normal valve function.

Although the structural design of the leaflet makes it mechanically suitable for opening and closing, the structure is still constantly being micro-damaged and therefore subject to repair. The repair mechanisms are carried out by the resident cells of the AV leaflet which include aortic valve endothelial cells (AVECs) and AVICs (Fig. 2.6) [29, 30].

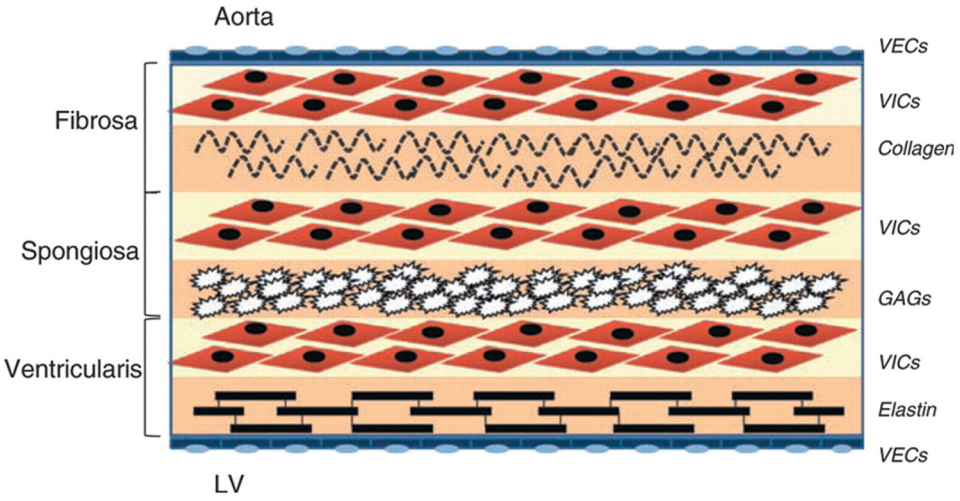

Fig. 2.6 – Cellular makeup of the aortic valve. Valve endothelial cells line the outer surface of the valve, and valve interstitial cells reside in the interstitium of the leaflet, which is comprised of the fibrosa, spongionsa, and ventricularis. (reprinted with permission from [25]).

2.1.3 Aortic Valve Endothelial Cells

Normal vascular endothelial cells possess a crucial job in the maintenance of homeostasis and normal circulatory function. Once thought to only provide a non-thrombogenic surface to the cardiovascular system, it has now been recognized as a highly active cell type with many synthetic and metabolic properties allowing it to regulate homeostasis [45]. Similarly, AVECs form a monolayer on the surface of the AV leaflet and are believed to regulate vascular tone, inflammation, thrombosis, and remodeling [46]. Furthermore, AVECs play roles in the regulation of coagulation and the communication between the underlying cells, AVICs [33, 47]. Regarding the modulation of coagulation, AVECs play primary roles in ensuring that clotting will only occur during injury. This is made possible through a complex procedure involving a plethora of catalysts and antagonists [47, 48]. AVECs also play critical roles in the relaying

of signals to the underlying AVICs. AVECs are known to secrete vasoactive agents such as nitric oxide, prostacyclin, and endothelin to regulate dilation and constriction of the valvular ECM through the control of AVICs [48]. The relationship between AVECs and AVICs has yet to be fully appreciated; however, future studies investigating this intricate interaction may generate insight regarding the initiation of valvular disease [49].

Interestingly, AVECs exhibit characteristics that differ from vascular endothelial cells. For example, Deck et al. reported that AVECs orient themselves circumferentially across leaflets, perpendicular to the direction of blood flow, in contrast to the vascular endothelium, which aligns parallel to blood flow [50]. Notably, AVECs reside in shear conditions that are significantly harsher than vascular endothelial cells suggesting that AVECs may be conditioned to endure higher levels of shear stress by resisting the secretion of coagulation factors. Moreover, AVECs arise from different sources than other types of endothelial cells suggesting that AVECs may represent a phenotypically unique endothelial cell [49]. It is evident that the regulatory role of AVECs makes them an intriguing area of study as AVEC dysfunction always leads to the development of valvular disease.

2.1.4 Aortic Valve Interstitial Cells

AVICs are a heterogeneous cell population residing within the AV leaflet and serve to maintain tissue homeostasis and structural integrity [13, 51, 52]. The interstitial cells are a heterogeneous population comprised primarily of fibroblasts, but also contain smooth muscle cells and myofibroblasts, which are often considered a transient phenotype exhibiting characteristics of smooth muscle cells and fibroblasts [13]. AVICs constantly secrete collagen types I and III, GAGs, matrix metalloproteinases (MMPs) and their inhibitors (TIMPs); also, AVICs secrete matrix degrading enzymes such as GAG-degrading enzymes that mediate remodeling [53-55]. The AVIC population exhibits a dynamic phenotypic spectrum ranging from quiescent fibroblast-like cells (characterized by expression of vimentin, fibroblast surface antigen, low expression of αSMA, and MMP-13), to activated AVICs, assimilated as myofibroblasts (characterized by proliferation, migration, high expression of vimentin, αSMA, and MMP-13) [13, 14, 56-58]. The activated AVICs are considered the pivotal cells that control valve structure and function [14].

Additionally, AVICs exhibit unique properties that differentiate it from other fibroblast cell populations. For example, Schneider et al. observed that normal AVICs secrete proteins and glycosaminoglycans at a dramatically higher rate when compared to other cell types *in vivo* [59]. Further, AVICs display substantial contraction properties that likely play vital roles in the maintenance of AV homeostasis [51, 52]. These results suggest that AVICs resemble a hybrid cell

population with characteristics that sits between fibroblasts and smooth muscle cells.

Interactions between mechanical forces, valvular cells, and the extracellular matrix (ECM) influence remodeling potential and therefore durability of heart valves. It is clear that for proper valve function, there needs to be the maintenance of tissue homeostasis in this challenging mechanical environment. As previously mentioned, the structural design and cellular makeup of the AV leaflet work in conjunction with one another to bear these physiological loads [31, 40, 41, 43]. It is the disruption of these processes that ultimately lead to disease [14].

2.2 Aortic Valve Disease Pathology

CAVD is a progressive degenerative disease that leads to the accumulation of calcifications on the surface of the AV (Fig. 2.7). The disruption of the intricate processes regulating tissue homeostasis is thought to be the initiating factor for valvular disease. Endothelial dysfunction has been highlighted as an important initiator of inflammatory responses that lead to AVIC activation and subsequent valvular disorder [33]. The investigation of both AVECs and AVICs and further in their interactions with one another are critical in elucidation of CAVD etiology; however, this dissertation will focus on the activation of AVICs as they are the main mediators of the morphological tissue level changes that occur as a result of CAVD and therefore hold the highest therapeutic value.

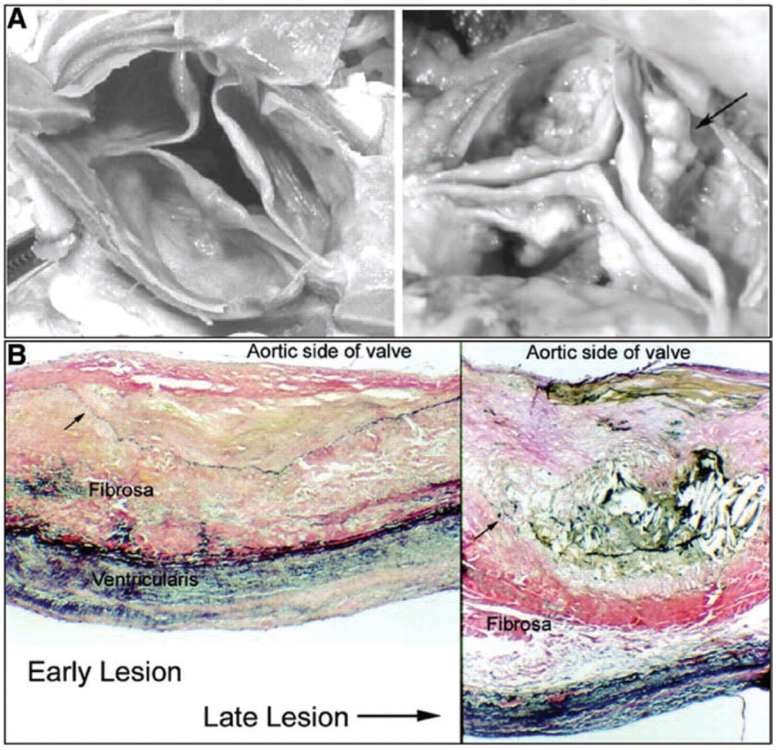

Fig. 2.7 – Gross anatomic specimen of minimally diseased (L) and calcified aortic valve leaflet (R) (A). Histological sections progression of breakdown of ECM with lipid accumulation (B). Verhoff-van Gieson stain 100X (reprinted with permission from [25])

AVIC activation has recently become a heavily studied area of research and involves the differentiation of quiescent AVICs into two main phenotypes: osteogenic and myofibroblastic AVICs [14, 23]. Both phenotypes exhibit unique characteristics that contribute to the development of mutually exclusive forms of valvular calcification. There has been much progress in our understanding of the factors that regulate the activation of each phenotype; however, further studies are necessary to help identify pharmacological targets for therapeutic action.

2.2.1 Osteogenic Aortic Valve Interstitial Cells

Osteogenic AVICs are interstitial cells that undergo osteoblastic differentiation and promote active osteogenesis characteristic of bone formation [14]. Evidence of osteogenic calcification has been confirmed through the use of histomicroscopy and immunomicroscopy and is estimated to be present in 13% of calcified leaflets [15, 60]. Quiescent AVICs undergo osteogenic differentiation through the incubation of calcifying media, which includes organic phosphates and dexamethasone; treatment with bone morphogenetic protein 2 and 4 (BMP 2 and 4) have also been shown to induce osteogenesis but in a less dramatic fashion [61]. Associated markers of osteogenesis include: Runx2, alkaline phosphatase, bone sialoprotein, osteopontin, and osteocalcin. Osteogenic differentiation is highly dependent on the osteoblast specific transcription factor Runx2 [62]. Runx2 expression in fact precedes osteoblast differentiation and is considered an early marker of osteogenesis. Once the cell is committed to the osteoblast phenotype, it undergoes a maturation process to become an active mineralizing cell. The intermediate osteoblast is defined by markers such as alkaline phosphatase and bone sialoprotein, and mature osteoblasts are indicated by the secretion of osteopontin and osteocalcin [14, 63]. Interestingly, Monzack et al. demonstrated that osteogenic AVICs exhibited characteristics that resembled intermediate osteoblast that never progressed toward an advanced stage of mineralization [64]. Further, they hypothesized that the osteogenic AVIC does not possess the same potential as other osteoblasts to undergo robust osteogenesis. These findings suggest that the limited osteogenic calcification

(13%) observed in tissue explants may be a result of the inability of osteogenic AVICs to fully recapitulate the behavior of mature osteoblasts. Further studies are necessary to delve deeper into the mechanistic regulation of AVIC activation towards an osteogenic phenotype.

2.2.2 Myofibroblastic Aortic Valve Interstitial Cells

The myofibroblast has been of interest since it was first discovered in the early 1970s because of its critical role in many patho-physiological processes that include tissue repair and remodeling [65]. Known for their contractile properties, myofibroblasts are important mediators of dermal wound closure and for restoring mechanical stability to tissues and organs that have been injured [66, 67]. However, the persistence and deregulation of this phenotype often leads to tissue deformation through contracture and can disrupt normal organ function. Myofibroblasts are also fundamental in the development of organ fibrosis and has been implicated in a variety of fibrotic diseases affecting the liver, heart, kidney, and lung [68]. Myofibroblasts also contribute to atheromatous plaque formation in the vasculature and has recently been shown to play a significant role in valvular calcification [21].

Myofibroblast activation is a common phenomenon observed in large variety of cell types. Local fibroblastic cells from many organ systems can be recruited during injury and transform into myofibroblasts that rapidly repair and remodel the injured site. Activated myofibroblasts acquire unique characteristics that enable them to facilitate tissue remodeling, which include increased levels of

ECM and cytokine secretion, increased contractility, and enhanced intercellular connections. Initiators of myofibroblast activation include inflammatory cytokines such as TGF-β1 as well as mechanical factors such as substrate stiffness. Myofibroblast differentiation occurs through two stages. Quiescent fibroblasts first differentiate into protomyofibroblasts, which exhibit changes in stress fibers, focal adhesions, and fibronectin secretion [67]. Then, protomyofibroblasts can differentiate into myofibroblasts, which display more complex, mature focal adhesions, increased secretion of ECM proteins, upregulated expression of αSMA, and enhanced cadherin-11 expression [16, 69, 70].

In CAVD, the presence of myofibroblastic AVICs are found in immunohistological sections of diseased valves [71]. In normal healthy valves, the AVIC population expresses little if any αSMA; however, in diseased valves, increased amounts of αSMA are observed throughout the tissue [71]. The localization of myofibroblasts is interestingly in regions corresponding to ECM disruption, degenerative lesions, and fibrosis [21]. Furthermore, myofibroblasts have been implicated in the actual calcification of the valve through cell-death-mediated dystrophic calcification [21, 22].

Activation of quiescent AVICs into osteogenic and myofibroblastic AVICs represent two pathological phenotypes that are shown to be involved in the development of two types of valvular calcification [23]. The study of AVIC activation is immensely complicated; however, much progress has been made to determine how AVICs are directed towards each phenotype. Once osteogenic and myofibroblastic differentiation has occurred, the AVICs proceed to pathways

that lead to the formation and evolution of valvular calcification. *In vitro* assays to study valvular calcification have been developed will be discussed in the following section.

2.2.3 Aortic Valve Calcification

The discovery was AV calcification was first noted by French physician Lazare Riviere in 1663 [72]. He observed large caruncle-like structures that were situated in the aorta obstructing left ventricular outflow to the aorta. Since then, many researchers have hypothesized about the origin of these nodular structures, and it was believed to be a senile, degenerative process that occurred as the valve leaflets became aged and injured [9, 25]. However, in the past 20 years, research investigating the mechanisms of valvular calcification has noted that AV calcification is actually an active process mediated by many cellular and molecular mechanisms. The emerging idea that these active processes can be modulated via pharmacological intervention has peaked interest into this phenomenon and has generated much effort to elucidate AV calcification mechanism.

Mohler et al. observed two major types of calcification in diseased human explants: dystrophic and osteogenic [15]. Dystrophic calcification is more common being found in 83% of diseased explants, and osteogenic calcification was observed in 13% of diseased valves containing calcification [15]. Physiochemical studies have determined that valvular calcification resembles hydroxyapatite, and recent studies have revealed that its biophysical and

structural characteristics may be more complex than previously thought [73]. Descriptive studies evaluating valve calcification have been limited to analyzing end stage valvular calcification because the samples are acquired during valve replacement surgery, which is only conducted when CAVD has become advanced. *In vitro* assays of AV calcification have been developed to investigate the initiation and evolution of valvular calcification and have provided much insight towards the active process of calcification.

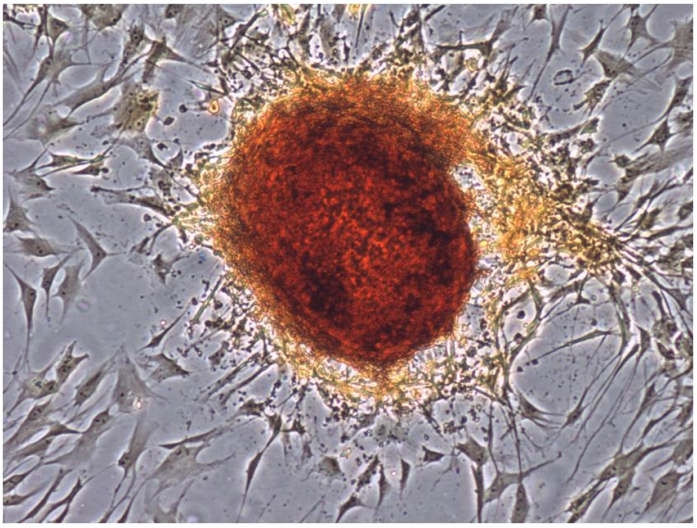

Fig. 2.8 – Calcific nodule stained positively calcification as evidenced by Alizarin red stain.

CAVD is driven by the behavior of the AVICs. Through *in vitro* studies, AVICs have been observed to aggregate and form nodular structures that stain positively for calcification (Fig. 2.8). Although a detailed understanding of the mechanisms involved in CAVD has not yet been established, the general progression of the disease process is well documented. It is clear that CAVD is mediated by the formation of CNs; ambiguity exists in the specific processes

involved in the generation of each nodule [19, 74, 75]. Mohler et al. first described CNs as cellular aggregates that contain an inner ring of apoptotic cells surrounded by an outer ring of living cells [19]. The cells associated with these nodules exhibited osteoblast characteristics and expressed extracellular bone matrix proteins yet exhibited dystrophic characteristics as well. Since this study, the description and characterization of nodules has become an active area of research. Recent studies have helped tease out the complicated processes involved in CN formation. Rodriguez et al. described the core of the nodules as containing different types of mineralization as well as apoptotic cells indicating that there may exist heterogeneity within each nodule [18]. Also, Chen et al. described nodules that did not contain apoptotic cells, noting that different types of nodules may be involved in CAVD [12]. These novel findings began to challenge what a CN was. A survey of the literature reveals that the understanding of CN formation has changed from the idea that CN evolution is a process regulated by both osteogenic and dystrophic simultaneously; it is now recognized as two independent processes generating two distinct CNs.

There are currently two theorized pathways of nodule formation: the dystrophic calcification pathway and the osteogenic calcification pathway [17, 23, 76]. Dystrophic calcification occurs due to the dysregulation of a normal response to injury *in vivo*. Inflammatory cytokines such as transforming growth factor β1 (TGF-β1) induce myofibroblast differentiation of AVICs which is characterized by increased contractility due to αSMA and *de novo* ECM components such as collagen [67, 77]. Failure of the myofibroblasts to apoptose or return to

quiescence leads to the progression of CAVD and dystrophic calcification. The persistence of the myofibroblast leads to contractile events and aggregations that calcify through an apoptosis-mediated process. Specifically, calcification occurs due to a loss of Ca^{2+} and $(PO_4)^{3-}$ homeostasis within the cell leading to the formation of hydroxyapaptite [78]. Conversely, osteogenic calcification does not involve cell death but is an active bone formation process [17]. BMP2 and BMP4 are osteogenic morphogens that are associated with the osteogenic pathway, and it is hypothesized that these biochemicals are secreted by the endothelial cells after injury [79, 80]. In the presence of pro-calcific biochemicals, AVICs differentiate into osteoblast-like cells that have upregulated expression of bone markers and proteins such as runt related transcription factor 2 (Runx2), osteocalcin, and osteonectin [17]. The osteoblastic AVICs undergo active bone formation as evidenced by CN formation *in vitro* and generate morphologically distinct nodules when compared to dystrophic nodules. A gross study of diseased explanted valves revealed evidence of dystrophic calcification in 83% of the valves and osteogenic calcification in 13% corresponding to the two proposed *in vitro* models [15].

The acknowledgement of two distinct pathways has significant implications in our understanding of CAVD development. These findings suggest that valvular calcification proceeds primarily through a step by step process rather than a simultaneous one involving dystrophic and osteogenic pathways at the same time. In order to develop effective therapeutics, consideration of how calcification occurs *in vivo* is essential. Optimizing *in vitro* assays to mimic

relevant cues that occur *in vivo* may offer new insights towards CN morphogenesis.

The examination of the role of biomolecues (TGF-β1 and BMP2,4) in CN morphogenesis has largely been the focus of CN reports in the past; however, mechanical cues and genetic cues, which have been shown to be involved in CAVD, have not yet been thoroughly investigated. Mechanical cues such as mechanical strain are critical regulators of AVIC biology and have been neglected thus far in CN studies. Furthermore, to ascertain the progression and order of *in vivo* calcification, genetic factors that directly contribute valvular calcification *in vivo* may offer clues regarding the roles of both calcification pathways.

2.2.4 The Mechanobiology of Calcific Aortic Valve Disease

Cells are responsible for remodeling their host tissue in response to mechanical forces by regulating their growth, differentiation, protein synthesis, and gene induction [81-83]. Under normal mechanical conditions, the cells are readily taking adaptive measures to maintain tissue homeostasis; however, abnormal mechanical forces can initiate irregular cellular responses that can cause several pathologies [84-87]. A common response to atypical loading conditions is the dysregulation of ECM protein secretion that is responsible for tissue/organ pathologies such as osteoarthritis, tendiopathy, atherosclerosis, and fibrosis in a variety of organ systems [83, 88]. Abnormal mechanical changes have also been linked to the initiation and progression of CAVD.

Robicsek et al. theorized that age-related loss in aortic wall compliance leads to an increase in the mechanical strain imposed on the aortic valve leaflets which ultimately result in aortic valve sclerosis and CAVD [89]. This increased distribution of strain on the leaflets results in elevated strains experienced by the resident AVICs. Goffin et al. showed that αSMA incorporation into stress fibers was directly related to the mechanical tension experienced by fibroblasts [90]. The presumption is that in an environment where there is a higher demand of cell contractility, larger stress fibers are reinforced with αSMA to more efficiently resist the applied load. Furthermore, Wipff et al. showed that lung myofibroblast contraction activates latent TGF-β1 from the ECM revealing a connection between TGF-β1 activation and ECM strain [91]. These changes suggest a potential correlation between strain and dystrophic calcification as Benton et al. demonstrated that increased αSMA expression essential to nodule formation [22]. Additionally, Balachandran et al. demonstrated in an *ex vivo* leaflet tissue study that increased strain in combination with TGF-β1 and osteogenic media resulted in higher amounts of calcification when compared to tissue under physiological strain [92]. However, the role of mechanical strain in CN morphogenesis has yet to be studied.

Recently, AVIC CN formation has been shown to be greatly influenced by mechanical inputs. Yip et al. demonstrated the effect of substrate stiffness on AVIC differentiation and CN formation [17]. On soft substrates, the AVICs differentiated into an osteoblastic phenotype and expressed proteins indicative of bone growth and development. This was further evidenced by the formation of

osteogenic nodules *in vitro.* However, on stiff substrates, the AVICs expressed myofibroblastic markers and developed CNs through the dystrophic pathway. These dramatic changes demonstrate the substantial role of mechanobiologic inputs in AVIC calcification.

Taken together, the impact of mechanical changes in the AV leaflets can lead to significant alterations in AVIC function which have consequences in CN formation. We believe that investigating the strain effects of AVICs in CN morphogenesis, dystrophic and osteogenic, will yield new insight regarding the cellular mechanisms in CAVD.

2.2.5 Genetic Factors and Calcific Aortic Valve Disease

Genetic mutations are responsible for a spectrum of congenital heart defects including cardiomyopathy, tetralogy of Fallot, and valvular malformations [93]. In addition to developmental abnormalities, genetic factors have been shown to contribute directly to cardiovascular disease. Genetic mutations affect the intrinsic behavior and signaling at the cellular level making it an extremely useful model for mechanistic studies of disease. Additionally, the study of the effect of genetic mutations generates insight concerning *in vivo* relevant processes. For valvular disease, Notch1 haploinsufficiency has been implicated in the development of CAVD with 100% penetrance in human patients. Furthermore, Notch1$^{+/-}$ mice revealed a fivefold increase in calcified valve area when compared to wildtype littermates [94]. Although the mechanistic impact of the Notch1 mutation is unclear, it has been observed that this mutation leads to

the upregulation of both canonical TGFβ and BMP signaling, which are both involved in CAVD [95]. Therefore, investigating the Notch1 mutation mechanism will help clarify the roles of TGFβ and BMP signaling in CAVD.

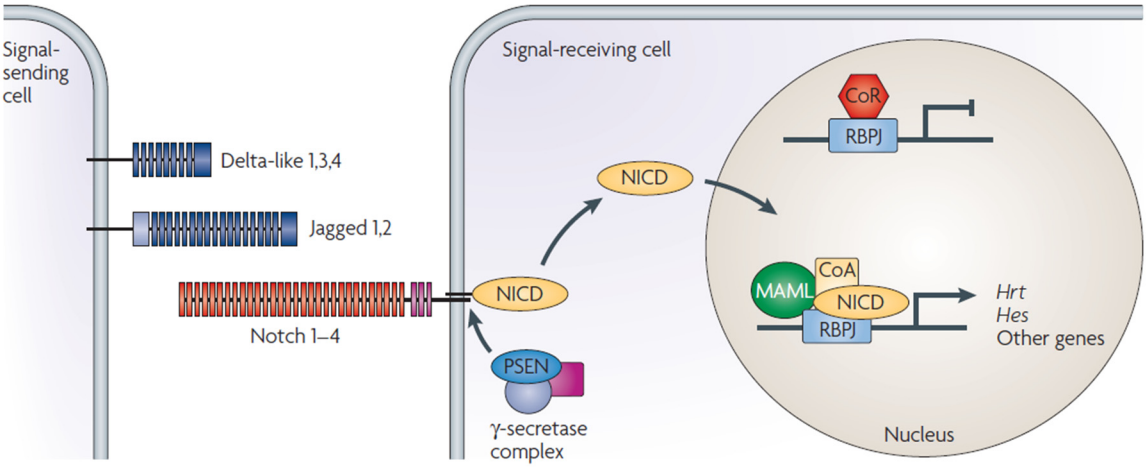

Fig. 2.9 – Canonical Notch signaling. Delta/Jagged ligands from signal-sending cell bind to the Notch receptor and initiates canonical Notch signaling. The NICD is release after γ-secretase cleavage and translocates into the nucleus. In the nucleus, the NICD binds to RBPJ-κ and initiates the transcription of *target genes Hrt and Hes* (reprinted with permission from [93]).

The Notch pathway is conserved pathway that regulates cell fate determination, differentiation, and tissue patterning in a wide range of systems and is an essential signaling mechanism for development as well as tissue maintenance (Fig. 2.9) [93, 96-98]. In the heart, Notch signaling has been shown to be involved in cardiomyocyte differentiation, patterning of various cardiac regions, valve development, ventricular trabeculation, and outflow tract development [97]. The mammalian Notch family includes four receptors (Notch1-4) and five ligands (Jagged1, Jagged2, Delta1, Delta3, and Delta5) [96]. Both Notch receptors and ligands are transmembrane proteins that are composed of

many epidermal growth factor (EGF)-like repeats [97]. Ligand binding from a ligand-presenting cell to a Notch receptor leads to two proteolytic events. The first cleavage event involves the release of the extracellular ligand-bound region of the receptor via ADAM-like metalloproteases, and the second cleavage is mediated by γ-secretase which acts on the transmembrane region and releases the Notch intracellular domain (NICD) [96]. The NICD then translocates into the nucleus and binds to the Recombination signal-binding protein Jκ/CBF1/Su(H)/LAG-1 (RBPJK/CSL) transcription factor and its coactivator Mastermind (Mam) to activate the Notch target genes Hairy/Enhancer of Split (Hes) and Hairy-related transcription factor (Hrt) [93]. Hes and Hrt are transcriptional repressors and have been shown to be enriched in the cardiovascular system during development and remodeling [94, 99].

As previously mentioned, inactivation of Notch signaling has been correlated with CAVD; however, the role of Notch signaling in CAVD is poorly understood. Recently, Nus et al. demonstrated an increase in both canonical TGFβ and BMP signaling with an upregulation of Smad2/3 and Smad1/5/8 in mice with a Notch1 or RBPJκ mutation [95]. Additionally, the Notch1 mutation has been associated with the expression of αSMA and Runx2, hallmarks of the myofibroblast and osteoblast phenotype respectively. Under normal Notch function, Notch target transcription repressors Hrt and Hes physically interact with the αSMA and Runx2 promoters to prevent the expression of those proteins; however, the dysregulation of Notch signaling leads to the removal of Hrt and Hes and subsequent disruption of this regulatory mechanism [95, 99, 100].

These findings demonstrate the relationship between the Notch1 mutation and the dystrophic and osteogenic models of AVIC calcification.

The understanding of CAVD disease mechanism is still unclear because of the ambiguity that exists concerning the roles of TGFβ and BMP signaling and their interactions in CAVD. Notch signaling presents a clinically relevant pathway that reveals increased synthesis and/or signaling of both TGFβ and BMP pathways, which correspond to the proposed models of CAVD. In addition, the Notch1$^{+/-}$ mouse provides an *in vivo* system for the examination of CAVD mechanism. The investigation of the Notch1 mutation will provide a novel system by which the roles of TGFβ and BMP signaling can be clarified and the pertinent mechanisms of CAVD can be elucidated.

Chapter III

Calcific Nodule Morphogenesis Is Strain Dependent

Text for Chapter III taken from:

> **Chen, J.*, Fisher, C.I.*, Merryman, W.D., "Calcific nodule morphogenesis by heart valve interstitial cells is strain-dependent", *Biomechanics and Modeling in Mechanobiology,* 12(1): 5-17; 2012. * = Co-first authorship**

3.1 – Introduction

CAVD is the third leading cause of cardiovascular disease and is now the most common form of acquired valvular disease in industrialized countries [1, 101]. Calcific aortic valves display impaired function through the inability to fully open and close, resulting in abnormal blood flow and increased load imparted to the myocardium [102]. There are no current means of pharmacological intervention for CAVD, and the only effective treatment is surgical replacement [1, 103, 104]. The evolution of CAVD is hypothesized to be initiated by abnormal responses of AVICs, the residential cell type responsible for maintaining valve integrity [105]. For example, AVIC aggregation and formation into CNs have been useful *in vitro* model systems that have revealed various stimuli that cause these pathologic responses [17, 19, 20, 22, 35, 106]. Because AVICs are greatly

influenced by cytokines such as TGF-β1 and mechanical cues such as substrate composition and stiffness, these stimuli have been primarily studied and are thought to contribute to the pathology of CAVD. Specifically, TGF-β1 is a potent inducer of myofibroblast differentiation in AVICs and has been shown to be enriched in sclerotic valves and promotes calcification of *in vitro* cultures [21, 107]. Substrate composition and interaction with AVIC integrins also regulates the likelihood of aggregation and calcification [108-110]. AVIC differentiation can also be regulated mechanically *in vitro*; compliant substrates lead to AVIC differentiation into osteoblast-like cells which actively secrete bone matrix, while stiff substrates lead to myofibroblast differentiation [17]. In diseased explants, contributions from both myofibroblastic and osteogenic processes are present; dystrophic calcification and ossification has been observed in 83% and 13% of explanted diseased valves, respectively [15]. The details concerning how these stimuli work together to activate AVICs and produce the CAVD phenotype, however, remain largely unknown.

While the mechanical cues that AVICs respond to are not limited to substrate composition and stiffness, mechanical strain during the cardiac cycle may also contribute to CAVD. *In vivo*, compliance changes in the aortic wall alter the deformation profile of aortic valve leaflets. Under normal physiological conditions, the perimeter of the aortic valve annulus increases approximately 15% at the beginning of diastole, which allows for maximum radial deformation [102, 111]. However, with age the aorta stiffens [112], causing the annulus to stiffen, minimizing the radial strain. This results in higher loads and deformations

in the circumferential collagen fibers, the principle axis along which AVICs reside, and exposes them to greater mechanical strain. Studies exposing either AVICs or freshly excised, whole valve leaflets to varying levels or regimens of strain have shown responses such as structural changes to withstand this increased loading [34, 42, 113], but the effect of increased strain *in vivo* is unknown. Furthermore, few studies have used mechanical strain to investigate mineralization of AVICs to identify its role in CAVD [35, 42, 114]. Therefore, an investigation that applies strain in combination with other stimuli to impact AVIC calcification will provide new insights into the progression of CAVD.

To assess the extent strain mediates calcification of AVICs, we used an *in vitro* Flexcell system to apply varying levels of equibiaxial strain to AVICs in the presence or absence of TGF-β1. The incubation of TGF-β1 prior to the application of strain accelerated the nodule formation process by increasing monolayer tension that initiated aggregation and nodule maturation. Both TGF-β1 and mechanical strain revealed cell-cell adhesion forces that inhibited motility and promoted aggregates to calcify. Further, we identify a novel property of strain magnification using linear elasticity theory to better approximate the *in vitro* mechanical environment that supports CN growth. The results show that strain is an important contributor to nodule formation and regulates the mechanobiology of AVIC monolayers.

3.2 – Methods and Materials

3.2.1 Cell Isolation and Culture

Porcine aortic valve leaflets were excised from sacrificed animals within 10 minutes of slaughter at a local abattoir. Leaflets were stored in phosphate buffered saline (PBS) at 4° C to ensure survival. Within 3 hours (h) of sacrifice, AVICs were isolated as previously described [115]. Briefly, after the removal of the endothelium, the leaflet was diced and digested in a 1 mg/ml collagenase solution (Worthington Biochemical Corp., Lackwood, NJ) for 1 h at 37° C and 5% CO_2. The collagenase solution with the remaining tissue was passed through a cell strainer to collect a cell solution which was centrifuged at 1500 RPM for 5 min to obtain the cell pellet. The pellet was resuspended in Dulbecco's Modified Eagle Medium supplemented with 10% fetal bovine serum (FBS) (Atlanta Biologicals; Lawrenceville, GA), 1% penicillin/streptomycin antibiotic (Cellgro; Manassas, VA), and 0.2% Amphotericin B (Sigma; St. Louis, MO). The cells were seeded into T-75 tissue culture flasks and incubated at 37° C and 5% CO_2 with media changes every three days. All cells were frozen for storage after the second passage.

3.2.2 Strain and TGF-β1 Treatments

AVICs were trypsinized at ~80% confluence, counted with a hemocytometer, and seeded onto Bioflex Pronectin culture plates (Flexcell International Corporation) at a density of 50,000 cells/cm^2 in 3 ml of media. No cellular aggregates pre-existed during the cell counting or in culture. Cells were given 2

days to reach confluence in growth media and were then treated with 6 combinations of TGF-β1 and strain (Figure 1) over 48 h. Depending on the protocol, cultures were either treated with 1 ng/ml porcine TGF-β1 (R&D Systems; Minneapolis, MN) or kept in growth media. The media was changed daily during experimentation. For cultures undergoing strain, cells were subjected to cyclic equibiaxial strain via the Flexcell-4000 tension system (Flexcell International Corporation) at a frequency of 0.75 Hz, the maximum frequency for generating vacuums that ensure ≥15% strains each cycle. Various strain levels were applied using different diameter loading posts (Flexcell International Corporation). 5% (31 mm posts), 10% (28 mm), 15% (25 mm or 28 mm), and 20% (25 mm) strain were used in these experiments to represent a range that corresponds to both physiological and pathological strain levels. Control groups were incubated on Bioflex Pronectin culture plates in static conditions in the same tissue culture incubator housing the Flexcell system. All experiments were performed using AVICs spanning passages 4-7 with no apparent differences in results across these passages.

3.2.3 Calcific Nodule Quantification

After treatment, AVICs were rinsed twice with PBS and fixed in 3.7% neutral buffered formaldehyde for 15 min. AVICs were rinsed with PBS and, unless immediately stained, stored at 4^{o}C for up to several days. Each 35 mm well was rinsed with deionized water (dH_2O) and stained with 1 ml of 14 mM Alizarin red S (Sigma) (in dH_2O, pH 4.1, where undissolved particulates were removed by brief

centrifugation and then with a 0.45μm filter) for 30 min with agitation to determine calcium deposition. After staining, the cells were washed 4 times with dH_2O to remove excess dye. Positively stained nodules were manually counted under the microscope. Nodules were defined as round, having a minimum 100 μm diameter (twice that of the long axis of individual cells), sufficient staining intensity, containing elongated cells in a radial pattern around the periphery of the nodule, and adjacent to a region devoid of cells.

3.2.4 Enzyme-linked Immunosorbent Assay

After treatment, AVICs from all samples were incubated for 15 min at room temperature and then scraped in lysis buffer (Cell Lytic M (Sigma), 10% protease inhibitor cocktail (Sigma), 1% phosphatase inhibitor cocktail (Sigma)). Lysates were centrifuged at 16,000*g for 20 min and the top 80% volume of supernatant collected and stored at -80^{o}C until use. Lysates from all samples were assayed for total protein content using a Bradford assay and diluted to a final protein concentration of 5 μg/ml in carbonate/bicarbonate buffer (pH 9.6) (Sigma). These antigen solutions were added to 96 well plates and incubated at RT overnight to allow the proteins to adsorb to the plate surface. αSMA was then quantified via ELISA [116]. We confirmed antibody specificity using an αSMA peptide (Abnova; Walnut, CA) using standard Western blot, and our results are within the linear range of detection using this peptide in each ELISA assay performed (results not shown).

3.2.5 Wound Assay

AVICs were seeded onto standard 6 well tissue culture plastic plates or Flexcell Pronectin plates at a seeding density of 60,000 cells/cm^2 and allowed to reach confluence in normal growth media. The cells were treated with either 0, 1, or 5 ng/ml of TGF-β1 for 24 h. After treatment, the media was replaced with normal growth media. To apply the wound, a 200 µl pipette tip (diameter~820 µm) was used to create a cross-shaped incision through the monolayer. The wells were rinsed with fresh media to remove any floating, cellular debris. Images were acquired on a tissue culture microscope immediately after incision. Wound area was quantified in ImageJ. After selecting five approximately equal-spaced locations in the horizontal and vertical directions, separation distances were averaged to represent wound width and height and multiplied together to determine wound area.

3.2.6 Characterization of Apoptosis and Inhibition with ZVAD

AVICs were rinsed with PBS and stained with Annexin V conjugated with Alexa fluor 488 (5% solution in Annexin binding buffer; Invitrogen) for 15 minutes to detect apoptotic cells. Propidium Iodide (PI) (0.4% solution in Annexin binding buffer; Invitrogen) was used as a counter-stain for necrotic cells. Apoptosis and necrosis images were taken after 3, 12, and 24 h of equibiaxial strain using a fluorescence microscope (Nikon TE300 Inverted Tissue Culture Microscope).

Apoptosis inhibition studies were performed using ZVAD-FMK (R&D Systems), a general caspase inhibitor. After TGF-β1 supplemented media was

removed from AVICs, media supplemented with ZVAD in concentrations of 20 or 50 μM was added to each well and incubated for 30 min prior to application of 15% strain.

3.2.7 Statistical Analysis

Results were analyzed as mean ± SE. ANOVA and Holm-Sidek tests were performed as needed. Statistical significance was defined as $p < 0.05$.

3.3 – Results

3.3.1 Calcific Nodule Formation is Dependent on the Order of TGF-β1 and Mechanical Strain Treatment

We previously investigated the effects of TGF-β1 and mechanical strain on valve leaflets to test their role in the differentiation of AVICs into the myofibroblast phenotype [35, 42]. Also, there have been multiple other studies that have examined mechanical strain and TGF-β1 treatment on fibroblasts [66, 67, 90, 117]. The order of addition has been varied in multiple ways: simultaneous TGF-β1 incubation with strain [35, 42], pretreatment with TGF-β1 for several days prior to application of strain [90], and the application of mechanical tension prior to TGF-β1 incubation [66, 117]. Because it is speculated that myofibroblast differentiation precedes CN morphogenesis, we sought to test the order of addition of TGF-β1 and mechanical strain.

We exposed the AVICs to six combinations of TGF-β1 and strain over 48 hours and then stained the wells with alizarin red to detect the presence of CNs.

Static culture, TGF-β1, and strain alone did not generate CNs after 48 h and only an unperturbed cell monolayer was observed (Fig. 3.1A-C). AVICs strained first for 24 h and then treated with TGF-β1 for 24 h generated no CNs with only a monolayer observed (Fig. 3.1D); however, when AVICs were incubated first with TGF-β1 for 24 h and subsequently strained for the next 24 h, a large number of CNs were generated, intensely stained with alizarin red (Fig. 3.1E). Simultaneous treatment of TGF-β1 and strain generated CNs after 48 h; however, these nodules were smaller and faintly stained in comparison to the prior case (Fig. 3.1F). These results suggest that pretreating AVICs with TGF-β1 prior to strain produces the optimal nodule formation after 48 h. To our knowledge, static culture studies in the literature report aggregation and mature nodule formation occur between 3 days [20] and 3 weeks [12] after reaching confluence. Studies that utilize larger concentrations of TGF-β1 (≥ 5 ng/ml) observe nodule formation with shorter culture duration [19-21] while others using lower concentrations of TGF-β1 or other media supplements require longer durations in culture [12, 18, 109] . Also, most studies are unclear about differentiating between initial aggregation events and the extent of calcification needed to define a nodule since this conversion can take over one week [20]. Thus, a sequential treatment of TGF-β1 and strain appears to be most efficient for forming mature calcified nodules.

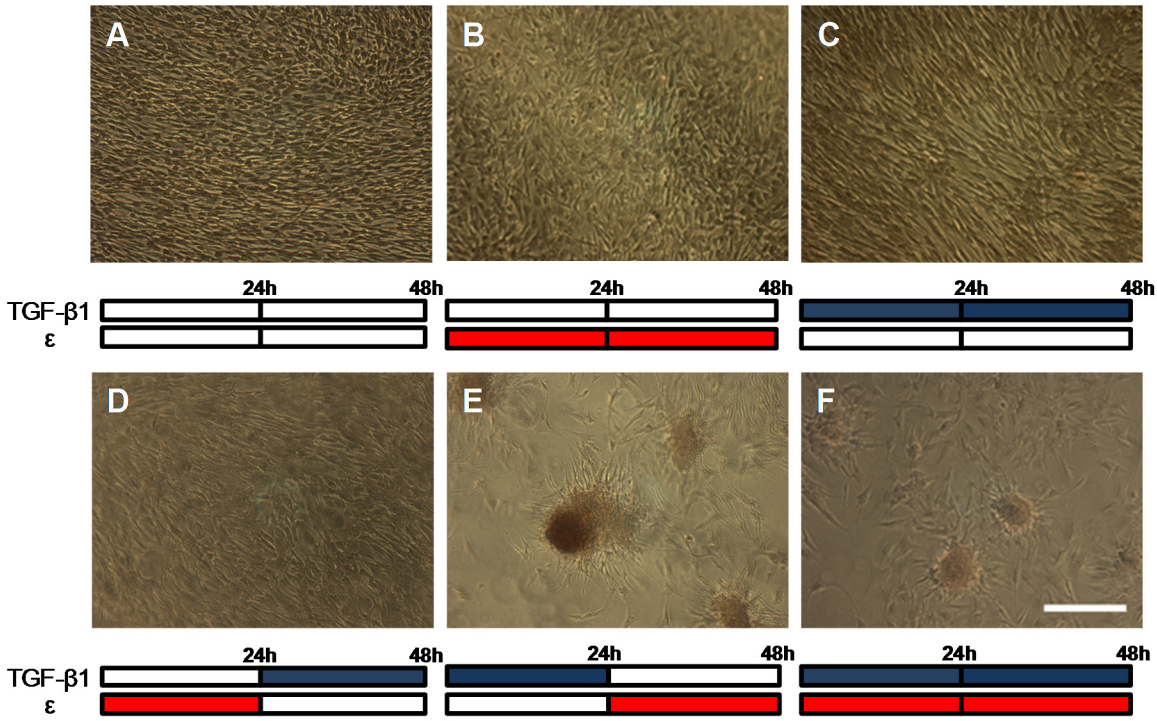

Fig. 3.1 – Calcific nodule formation following combination treatments of 15% equibiaxial strain (red bars) and 1 ng/ml of TGF-β1 (blue bars) over 48 hrs. Control (A), strain only (B), and TGF-β1 only (C) all show unperturbed monolayers, as does strain followed by TGF-β1 (D). TGF-β1 followed by strain reveals large, mature calcific nodules (E), while simultaneous TGF-β1 and strain cause small, less mature nodules (F). All treatments stained with Alizarin red to identify calcification. n >15, scale bar = 250 μm.

3.3.2 Variables Regulating Nodule Formation

To determine how TGF-β1 and mechanical strain influence nodule formation, we individually varied the concentration of TGF-β1 incubation and the extent of strain. First, we incubated AVICs with various TGF-β1 concentrations (0 – 5 ng/ml) and then applied 15% cyclic strain (Fig. 3.2A). We observed greater numbers of CNs with increasing TGF-β1 concentrations, suggesting that the likelihood of nodule formation is actively regulated by changes to the cells induced by TGF-β1. To assess the role of mechanical strain, we pretreated AVICs with 1 ng/ml TGF-β1 for 24 h and then subjected them to different magnitudes of strain (0 – 20%). We observed increasing number of CNs with increasing strain (Fig. 3.2B). We note that at lower levels of TGF-β1 and strain, amorphous cellular aggregates were observed that stained poorly with alizarin red and were not included in the nodule count. These results suggest that threshold levels of both TGF-β1 and strain are needed to produce mature nodules.

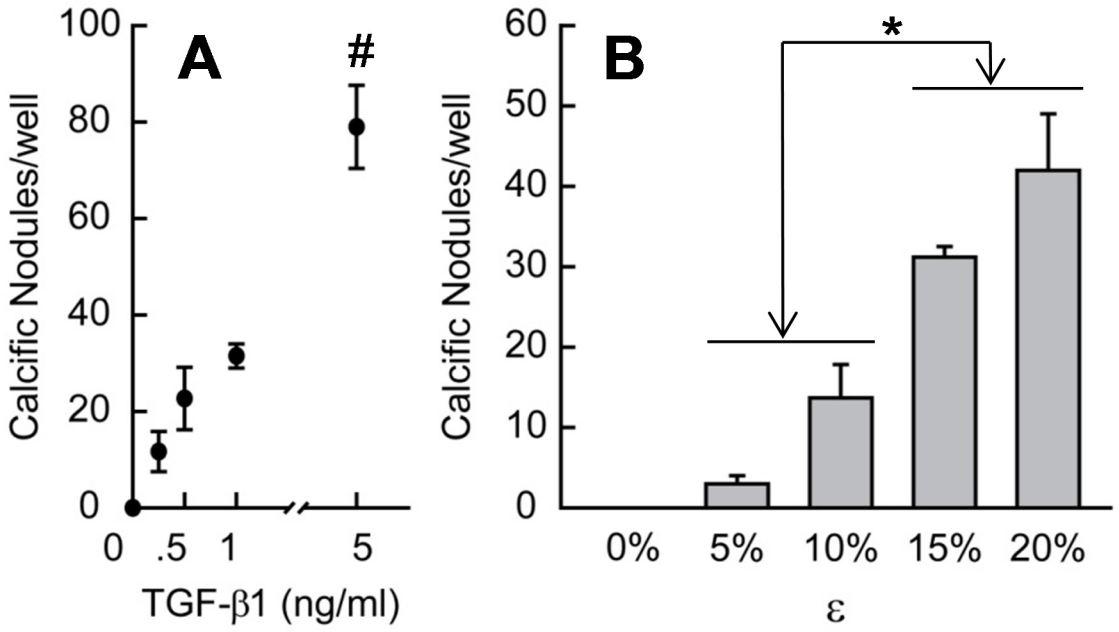

Fig. 3.2 – Nodule formation as a function of TGF-β1 concentration (A) and strain magnitude (B). For A, 24 h of 15% equibiaxial strain was applied after 24 h of each TGF-β1 concentration. For B, all groups were treated with 1 ng/ml TGF-β1 for 24 h prior to each strain being applied for 24 h. All bar graphs and points represent mean $\pm$ SE ($n \geq 3$), * = $p<0.05$, # = $p<0.01$.

3.3.3 Mechanical Damage Reveals TGF-β1 Enhancement of VIC Monolayer Tension

The response of statically cultured AVICs treated with TGF-β1 suggests that the aggregation process occurs via monolayer disruption due to αSMA mediated contractility [22]. Because TGF-β1 incubation is well established at increasing αSMA expression in AVICs [21], we first wanted to assess how the 24 h TGF-β1 incubation affected the AVICs in our system. We used an ELISA assay to measure the expression of αSMA in these monolayers and observed a ~2.2 fold increase after 24 h that was dose-dependent (Fig. 3.3A). These results confirm that TGF-β1 induces the same magnitude effect on the Bioflex Pronectin culture plates as tissue culture plastic [21].

After verifying the effect of TGF-β1 on αSMA expression, we tested how TGF-β1 alters the mechanics of the monolayer by subjecting AVIC cultures to a wound assay. Because greater αSMA expression increases contractility, we speculate that higher αSMA expression will translate to greater tension in the AVIC monolayer. AVICs treated with TGF-β1 opened larger wounds after the incision (Fig. 3.3B). This opening effect is not unique to monolayers cultured on the Flexcell membranes because a similar increase is observed for monolayers cultured on standard tissue culture plastic (Fig. 3.3B). Interestingly, the wounds created in non-TGF-β1 treated wells were approximately the size of the pipette tip on both materials indicating that the tension in these monolayers is negligible and also that the cell-cell associations may be weak relative to cell-substrate interactions. Regardless of substrate, the increase in tension is due to TGF-β1, however, further increases in tension did not appear with larger dose of TGF-β1. This increase in tension could explain observations of monolayer disruption and aggregation, particularly upon application of strain. Strain would then be insufficient to promote aggregates when the monolayer tension is small (Fig. 3.1B). The response of AVICs to TGF-β1 is likely not limited to an increase in monolayer tension in order to fully describe how it promotes nodule formation (Fig. 3.2A).

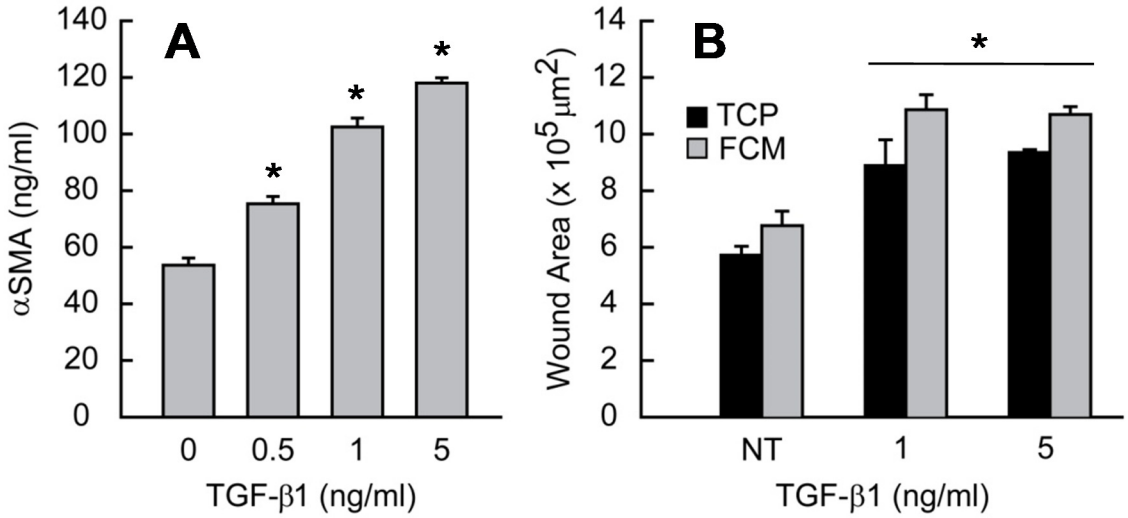

Fig. 3.3 – αSMA expression increases with increasing dose of TGF-β1 (A).Mechanical damage reveals TGF-β1 effects on monolayer integrity. Monolayers were scraped with a 200 μl pipette tip in a cross pattern. Initial wound area increases with TGF-β1 pretreatment on TCP and FCM (B). All bar graphs and points represent mean ± SE (n≥2), *p<0.05.

3.3.4 Time Course of Calcification: Nodule Maturation Spreads From Center Outward, From Early to Late Stage Apoptosis

To investigate how aggregates remodel into CNs, we analyzed images at intermediate time points over the 24 h after initiating the application of strain. Because CNs are associated with apoptotic processes [17, 19, 20, 109, 118], we speculated that apoptosis develops over time. Annexin V was used to stain the membranes of apoptotic cells, and propidum iodide (PI) was used to stain necrotic cells that have lost their cell membrane. Prior to application of strain, the monolayer treated with TGF-β1 sparsely binds either stain indicating cell viability (Fig. 3.4A). At 3 h, aggregates contain faint amounts of both stains, but at 12 h, necrotic cells were prominent towards the center of the aggregate, and many of the cells in the aggregate were apoptotic. After 24 h, the core of the nodule is mostly necrotic and the apoptotic AVICs only appear in an intense ring around

the periphery of the nodule. Viable cells, which contain neither stain, appear to radiate out of the periphery of the nodule. This phenotype appears to dominate at the 24 hour time point and suggests that nodule maturity occurs from the inside and spreads to the edges with the transition from an apoptotic state to a necrotic state.

To determine if apoptosis is required for nodule maturation, we used the general caspase inhibitor ZVAD to inhibit apoptosis. ZVAD has previously been demonstrated to inhibit calcium deposition in nodules [20]. Media supplemented with ZVAD was added just prior to application of 15% cyclic strain. After 24 h, ZVAD treated wells contain significantly fewer mature nodules (Fig. 3.4B). Larger concentrations of ZVAD did not statistically reduce nodules any further (data not shown). These wells also contain many amorphous regions of higher cell density, distinct from the monolayer, that resembled aggregates. These regions stained poorly with annexin and PI, suggesting they were mostly composed of living cells. These regions were adjacent to areas devoid of cells, flatter than mature nodules, and did not appear to have cells migrating out to reestablish the cell monolayer.

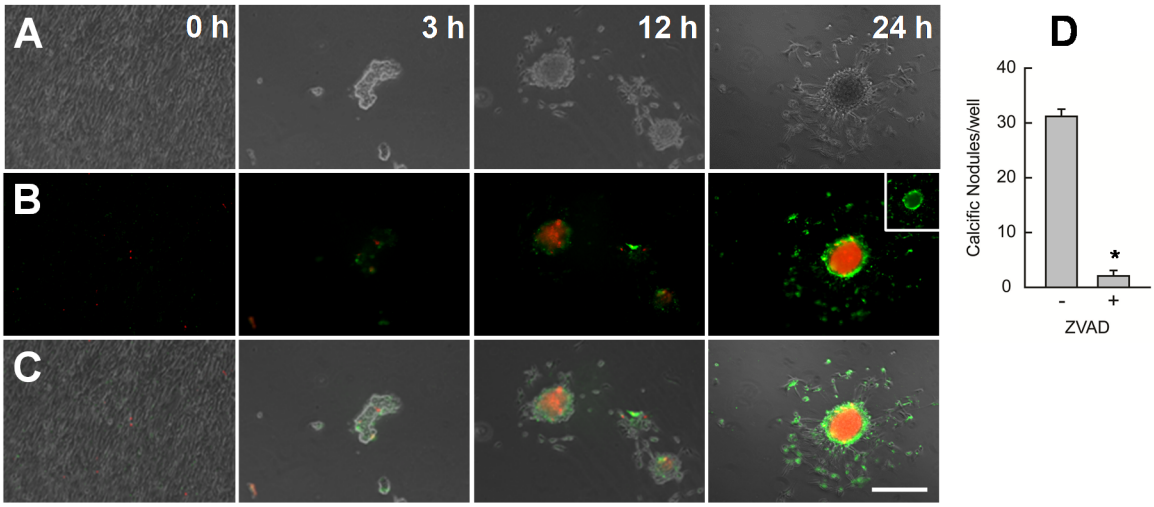

Fig. 3.4 – Nodule maturation spreads from the inside out and is dependent on apoptosis. Cultures were removed from strain at 3, 12, and 24 h and stained with Annexin V (green) and PI (red) to identify apoptosis and necrosis respectively. Phase only (A), fluorescence only (B), phase and fluorescence overlay (C). Lack of stain at 0 h indicates cell viability and monolayer integrity. Stain intensity increases with time as apoptosis is replaced by an intense necrotic core. Inset represents green channel only showing apoptotic ring at the nodule periphery. Inhibition of apoptosis with ZVAD reduces the number of mature nodules per well (D). A minimum of 3 wells were observed at each time point. *$p<0.05$, scalebar = 250 µm.

To verify that nodule maturation correlates with calcification, we stained samples with alizarin red at the same time points above (Fig. 3.5). We have previously observed that fixation with formaldehyde results in non-specific or saturated alizarin red binding; therefore no fixation was used in order to distinguish variations in calcification with time. Alizarin red intensity increases with time in aggregates, which seems to parallel with the PI staining pattern. After 24 h, nodules contain an intense alizarin red staining indicating a high density of solid calcium deposition.

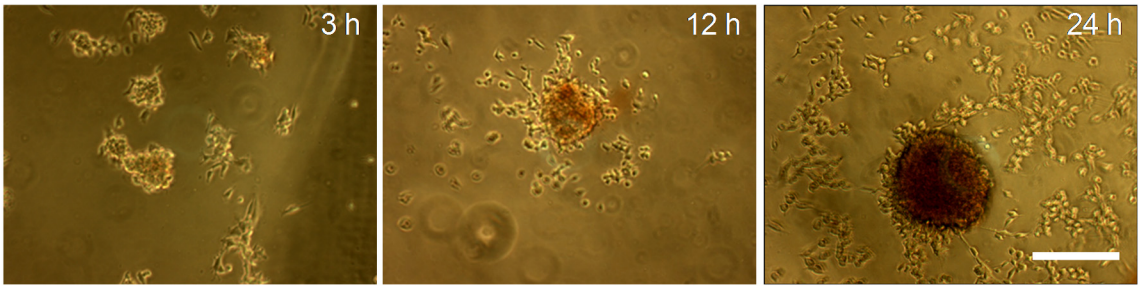

Fig. 3.5 – Nodules calcification occurs concomitantly with maturation. Cultures were removed from strain at 3, 12, and 24 h and stained with Alizarin red S. Stain increases intensity with time. No fixation was used prior to staining causing cells to round up. A minimum of 3 wells were observed for each case. Scalebar = 250 μm.

3.3.5 Nodule Maturation is Dependent on Mechanical Strain

Since the application of strain initiates aggregate formation, we wanted to determine if continuous exposure to strain promotes nodule maturation. After 24 h pretreatment with TGF-β1, AVIC monolayers were equibiaxially strained at 15% for 5 min to initiate aggregation. Strain was removed, and these samples were then left at static conditions for 24 h. At 3 h, aggregates were observed to still be present in the well (Fig. 3.6A). Around the aggregates, cells were

migrating radially outward (Fig. 3.6A; arrows). Interestingly, samples under continuous cyclic strain for the same duration had far fewer migratory cells around the aggregates (Fig. 3.6B; arrow). This suggests that strain inhibits AVIC motility and tends to keep a large portion of the cells in the aggregate.

At 24 h, many AVICs continued to migrate out of the aggregates in the static condition to further distances relative to the center of the aggregate, and the aggregates also appear to have flattened out, blending in with the rest of the monolayer (Fig. 3.6C). In contrast, samples exposed to continuous strain had very limited cell migration from the aggregates resulting in a mature nodule phenotype (Fig. 3.6D). Staining of aggregates that appeared after 5 min of strain revealed a limited presence of necrosis and faint staining for apoptosis (Fig. 3.6E). As before, strain for 24 h led to a prominent apoptotic ring surrounding the necrotic core (Fig. 3.6F). TGF-β1 pretreated static samples not exposed to any strain over 24 h remained as a monolayer (Fig. 3.1C) and did not stain for apoptosis or necrosis (data not shown) having the same appearance as images taken at t=0. These results suggest that continuous cyclic strain regulates more than just causing mechanical damage to a monolayer, but also whether cells can emerge and migrate out of an aggregate. This also indicates that aggregation does not automatically proceed to nodule maturation because the cells do not undergo apoptosis. Furthermore, cyclic strain does seem to promote apoptosis and the likelihood of becoming the mature nodule phenotype indicative of mineralization.

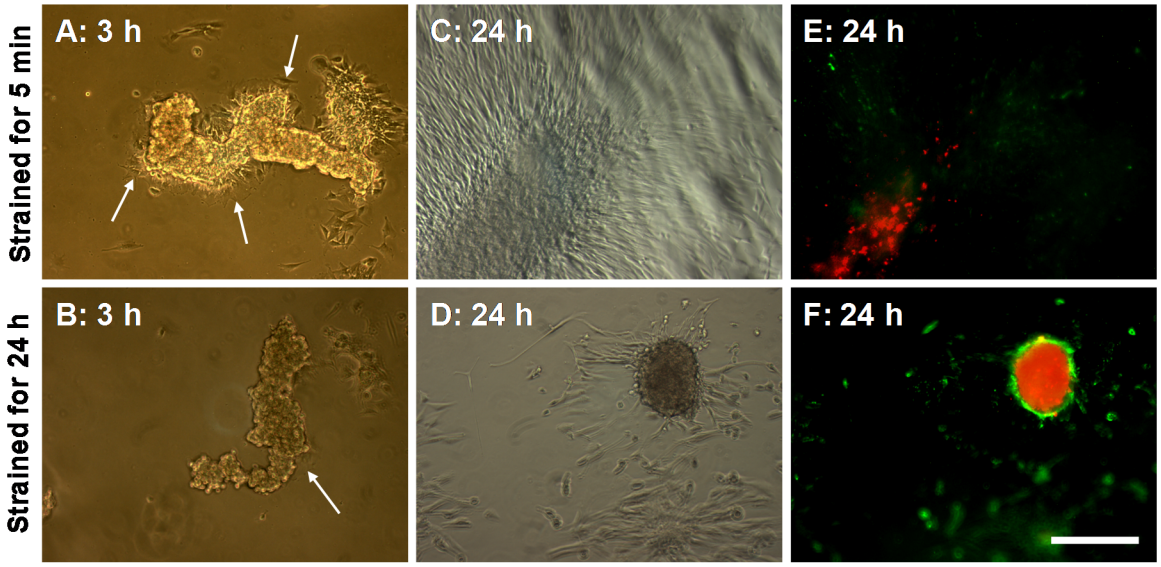

Fig. 3.6 – Nodule maturation is dependent on continued strain. Aggregation was induced with exposure to 5 min of strain. Cultures were either removed from strain (A,C,E) or continued to receive cyclic strain for 24 h (B,D,F). Images were collected at 3 and 24 h and stained with Annexin V (green) and PI (red) to identify apoptosis and necrosis respectively. Arrows point to AVIC migration emerging from the aggregate but seem to be inhibited with strain. Flattened aggregates with minimal apoptotic staining (E) were not observed in cultures under 24 h strain. A minimum of 3 wells were observed for each case. Scalebar = 250 μm.

3.4 – Discussion

3.4.1 Strain Accelerates Calcific Nodule Formation and Mimics Dystrophic Calcification

While the dynamic mechanical environment of AVICs has been shown to influence both function and pathology, it was unclear, prior to the current study, whether mechanical strain contributes to calcification reminiscent of aortic valve disease. Most models of CN formation have not explored the role of mechanical strain in this process. By applying an equibiaxial strain field to confluent AVICs, we have identified that mechanical strain can both initiate and accelerate the aggregation of AVICs to form CNs. We show that TGF-β1 and mechanical strain must be provided in a specific sequence in order to generate CNs. Our results indicate a rapid onset of nodule formation, taking approximately 48 h from the beginning of treatment, for the formation of significant numbers of large, mature nodules (Fig. 3.1E, Fig. 3.4). These results suggest that AVIC differentiation and remodeling are active processes that occur with short exposure to TGF-β1 (24 h) and are revealed by the application of sufficient mechanical strain for an equivalent duration (24 h). This was confirmed using simultaneous exposure to TGF-β1 and strain, a closer mimic to the physiological environment (Fig. 3.1F). In this model, calcification results from cells in the aggregate undergoing apoptosis, consistent with a retrospective study demonstrating that 83% of diseased heart valves in humans are indicative of dystrophic calcification [15].

3.4.2 Strain Reveals TGF-β1 Mediated Remodeling of AVICs and Initiates Aggregation

Our results indicate that strain performs multiple roles in nodule formation. First, strain reveals TGF-β1 mediated remodeling of the cell monolayer. TGF-β1 increased αSMA expression in the monolayer (Fig. 3.3A). Higher αSMA expression in AVICs caused by TGF-β1 treatment has been shown to increase contractility on unconstrained collagen gels [22, 115]. On constrained substrates, we predicted higher contractility should functionally increase tension in the cell monolayer. These TGF-β1 effects were confirmed with a wound assay in which the wound area was larger with addition of TGF-β1, inferring enhanced contractility (Fig. 3.3B), and explaining how mechanical damage to the monolayer via strain initiates the formation of AVIC aggregates (Fig. 3.4A). Increasing contractility and monolayer tension must also be complemented with tight cell-cell associations. Once mechanical damage occurs, aggregates form because the energy from relieving the tension combined with adhesion strength between cells must be greater than adhesion of the cells with the underlying substrate. Evidence of TGF-β1 remodeling adherens junctions that both strengthens these associations and induces mechanical damage under stress [16, 119, 120], may also be important for understanding how αSMA generated tension leads to the aggregation of a sheet of cells.

Common features that generate CNs have been heavily dependent on the experimental context. To study CN formation via TGF-β1 pathway, most of the published studies were performed on tissue culture polystyrene or a minimum of 120 kPa stiffness. TGF-β1 stimulation of AVICs [23] is highly dependent on

substrate stiffness, and the Flexcell silicone membranes (~930 kPa) in our study are a closer approximation to valve tissue stiffness [121]. Further, when studies utilize a minimum of 5 ng/ml TGF-β1 treatment in static culture, nodules are observed within 2-5 days[19, 21]. For lower or no TGF-β1 treatment in static culture, other studies observe fewer nodules within this time period and may require as long as 3 weeks [12, 18]in culture to be characterized. Such aggregation events have been mostly explained in the context of contractility, and multiple studies that inhibit contractility have shown reduced nodule formation [22, 106, 122, 123]. In combination with substrate stiffness and surface coatings that also play important roles, we speculate that the amount of TGF-β1 exposure and time in culture are separate variables that regulate AVICs responses. These variables may determine the generating of an imbalance of tension in the cell monolayer capable of the events needed for aggregation to occur and regulate the migratory capacity that determines whether aggregates dissipate. Our results demonstrate that when strain is applied, lower levels of TGF-β1 and shorter durations are just as sufficient to create the conditions that lead to nodule formation. These results support a paradigm that cell-generated forces and externally applied forces are both needed to reveal properties that better represent physiological conditions.

3.4.3 Strain Promotes Maturation of Calcific Nodule via Apoptosis

Another role of strain is its regulation of nodule maturation. By maintaining cyclical strain for 24 h, CNs were more likely to form from initial aggregates (Fig. 3.4A and Fig. 3.6D,F). Aggregates under strain were more likely to undergo apoptosis and generate large necrotic cores that were consistent with staining for calcification (Fig. 3.5). These results suggest that aggregation does not automatically proceed to mineralization and additional regulatory mechanisms govern this transition. Together, these data suggest that strain regulates AVIC behavior in multiple points of nodule development.

A common feature in nodule formation is the dependence on apoptosis. Studies that inhibit apoptosis reduced nodule formation, but the aggregation process still occurred [20]. Interestingly, inhibition of contractility also reduced apoptosis and nodule formation [108]. The addition of strain in the present study shows that apoptosis occurs as early as 3 h after aggregation and becomes prominent after 12 h (Fig. 3.4A). In static cultures, similar apoptosis staining is observed after 5 – 7 days [17, 20, 109], while two studies showed that strain increases both apoptosis and calcification in valvular tissues [35] and vascular cells [114]. Our results show a dramatic and rapid conversion from apoptosis to necrosis in the central core of a mature nodule when strain is applied over the final 12 h. A very intense ring of apoptosis surrounds the periphery of the nodule, and, to our knowledge, has not been previously reported. We show that this conversion appears to be strain dependent and correlate with reduced cell migration from cells incorporated in the aggregate.

While our data and other current models can produce CNs *in vitro*, it is not clear if these mechanisms can predict nodule formation that arises during CAVD *in vivo*. Tissue level studies of valve leaflets exposed to both TGF-β1 and pathological strain suggest that a homogeneous distribution of cells shift to a heterogeneous distribution of cell aggregates containing apoptotic cells [35], consistent with our model system. Many other groups have also found evidence correlating calcification and apoptosis in AVICs [24, 124]that possibly explain the events occurring in 83% of diseased heart valves[15]. This compendium of evidence supports apoptosis as one mechanism that may contribute to this pathology. Many of the remaining challenges at the cellular level involve identification of the signaling pathways and enzymes that initiate calcification and its location, whether intracellular or extracellular in origin, and temporal changes occurring over decades [125, 126] *in vivo*. Additional investigations are needed probing interactions between AVICs, endothelial cells [127], and other cell types that control these processes at the tissue level. To understand the impact of the mechanical environment on these mechanisms, we first need a better approximation how externally applied forces can change within an AVIC monolayer.

3.4.4 Calcific Nodule Maturation by Strain Magnification: Modified Lamé Solution

The line between physiological and pathological strain levels has been used as an explanation for the impact of high strain on nodule formation. At the tissue level, the line was drawn between 10% and 15% uniaxial strain as

significant differences in calcification were observed [35], and we also observed a significant increase in nodule formation at 15% and 20% strain (Fig. 3.2B). Recognizing that nodule maturation occurs symmetrically from the center outward during exposure to strain (Fig. 3.4, Fig. 3.6) and that calcification must also change material properties, as predicted in multiscale models[126], it is unclear how small differences in strain magnitude generate such large effects. Using principles of linear elasticity, mechanical strain magnitudes can be calculated for the defined geometry of our experimental system to more closely approximate the mechanical environment. We use a modified Lamé solution of a thick-walled cylinder to calculate the strain field at the periphery of the nodule that becomes altered at the junction between two different materials. The model derivation, numerical predictions, and limitations are described in the Appendix. By assuming a circular disc that contains a small rigid core (Fig. 3.7A), the mechanical changes to the applied equibiaxial strain field provides a new hypothesis to examine the process of nodule formation. The strain fields shift from equibiaxial to uniaxial which necessitates that the strains increase in one orientation and decrease or become compressive in the other orientation. For rigid cores, the radial strains can increase up to two-fold and eliminate circumferential strains whereas loss of contact and absence of cells increase circumferential strains at the expense of radial strains (Fig.3.7B,C,D).

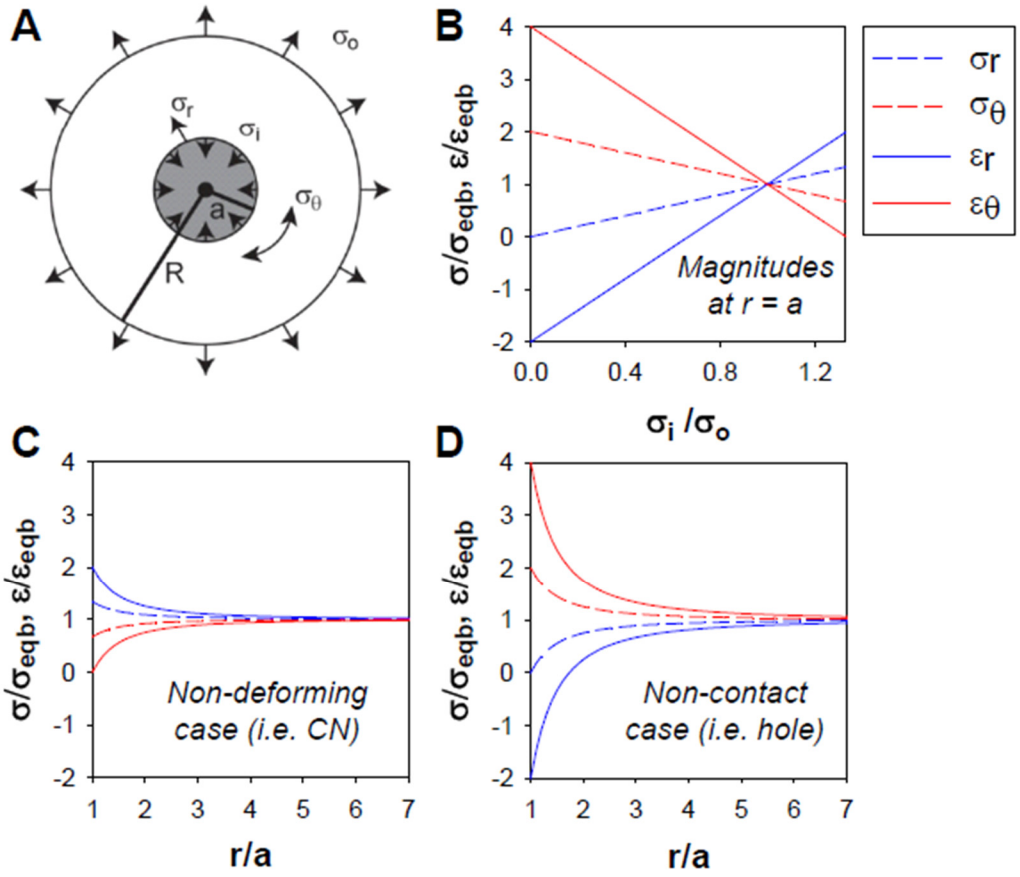

Fig. 3.7 – Strain enhancement model: Modified Lamé solution. External (σ_o) and internal (σ_i) stresses applied to a ring (radius = R) surrounding a circular core (radius = a) (A) used to calculate radial and circumferential stresses and strains at the core periphery (r = a) normalized to the equibiaxial case (B). Normalized gradient of stresses and strains as a function of the core radius were calculated for the non-deforming case ($\sigma_i = 4\sigma_o/3$) (C) and the non-contact case ($\sigma_i = 0$) (D). For all cases, R >> a. Normalized magnitudes indicate the extent of magnification of applied stresses and strains at the periphery of the circular core suggesting how small increases in strain can have significant impact on cells.

With these numerical predictions, we can better account for the changes we observed in the monolayer when applying strain. Assuming a uniform monolayer has homogenous material properties, in contrast, a TGF-β1 treated monolayer should create an imbalance in tension due to local heterogeneity of contractility and remodeling of cell-cell contacts..Weak areas in the monolayer will more likely rip when challenged by externally applied forces, and regions with tighter cell-cell associations will be primed to become the foci where cell sheets would accumulate into aggregates and have sufficient rigidity to promote strain enhancement. As we have shown with TGF-β1 treatment and lower strains approximated to be physiological (Fig. 3.2B), the monolayer seems to withstand these forces or aggregates dissipate resulting in fewer nodules formed (Fig. 3.6). However, we speculate that at pathological strains, the increased magnitude of strain due to the strain enhancement cannot be tolerated, increasing the propensity for creating greater numbers of nodules (Fig. 3.2). Furthermore, strain enhancement may also be responsible for triggering the biological changes necessary for apoptosis and perhaps the conversion to necrosis that can explain how the necrotic core spreads from the center outward. Fully mature nodules may also alter the strain field creating more aggregation events that feed this nodule and cause it to increase in diameter. These events could explain how strain would accelerate nodule maturation and form dense CNs. More broadly, this concept of strain enhancement may also be applicable in other tissues that are exposed to cyclical strain such as myocardium and lung tissues. Scar tissue in these regions may have different material properties from the surrounding

tissue, and this principle could explain pathological responses in terms of greater strains than would normally be expected. Identification of principles that can be tested at the 2D environment act as a first approximation that can be extrapolated to the 3D environment [128].

3.5 – Conclusion

Our results suggest multiple biological checkpoints that regulate nodule formation and can assist in explaining the causes of CAVD. The complex interplay of biological changes induced by TGF-β1 is revealed by mechanical strain (including cell tension, cell contacts, migration, apoptosis, necrosis, and calcification), arguing that multiple active processes must occur to create the final pathological phenotype. Future efforts that can better classify these phenotypes for human patients will provide more specific strategies for pharmacological treatment.

Chapter IV

Cadherin-11 is a Critical Regulator of Calcific Nodule Morphogenesis

Text for Chapter IV taken from:

Chen, J.*, Hutcheson, J.D.*, Sewell-Loftin, M.K., Ryzhova, L.M., Fisher, C.I., Su, Y.R., Merryman, W.D., "Cadherin-11 Regulates Cell-Cell Tension Necessary for Calcific Nodule Formation by Valvular Myofibroblasts." *Arteriosclerosis, Thrombosis, and Vascular Biology*, 33: p 114-120; 2013. * = Co-first authorship

4.1 – Introduction

The differentiation of quiescent fibroblasts to activated myofibroblasts represents a normal physiological response to injury *in vivo*; however, persistence of the myofibroblast population contributes to a spectrum of fibrotic disease [67, 68, 77, 129]. Activated myofibroblasts are characterized by increased contractility due to αSMA, and in normal physiology, these cells remodel the ECM by secreting proteases for matrix breakdown and *de novo* ECM components such as collagen [67, 77]. Failure of the myofibroblasts to apoptose or return to quiescence in pathological cases causes impairment of organ systems due to elevated contractions and accumulation of ECM

components. One disease in which the myofibroblast is thought to play a crucial role is calcific aortic valve disease (CAVD) [1, 9, 19, 24, 103, 130].

Increased αSMA expression in AVICs, the resident fibroblast population in the aortic valve, has been observed in excised fibrotic leaflets [71]. Increased expression of the profibrotic cytokine TGF-β1 has also been observed in these leaflets, and accordingly, TGF-β1 has been shown to lead to myofibroblast activation of AVICs *in vitro* [21, 71, 110]. Additionally, in *ex vivo* models of CAVD, TGF-β1 works synergistically with mechanical strain to lead to collagen accumulation, characteristic of early CAVD, and formation of bone-like CNs, an endpoint of CAVD [42, 92]. Two distinct CN morphologies have been observed: dystrophic calcification driven by myofibroblastic phenotypes [20, 22, 131] and ossification driven by osteogenic phenotypes [12, 17]. In diseased explants, dystrophic calcification and ossification has been observed in 83% and 13% of explanted diseased valves, respectively [15].

In vitro, dystrophic nodule formation involves myofibroblast differentation of AVICs. Upregulation of αSMA during myofibroblast differentiation by TGF-β1 leads to an increase in mechanical tension between AVICs and subsequent aggregation into nodules, which calcify through apoptotic processes [21, 109]. When αSMA expression is suppressed, CNs are unable to develop thereby revealing the essential role of acquired contractility within AVICs in CN formation [22]. Confoundingly, preventing phosphorylation of Erk1/2 with a MEK1/2 inhibitor leads to increased αSMA expression [132] yet prevents CN formation [123],

suggesting the requirement of another essential component of nodule formation that has yet to be revealed.

Along with increased αSMA expression, myofibroblast differentiation has been associated with changes in cadherin expression. Specifically, in lung fibroblasts, TGF-β1 induced myofibroblast differentiation leads to an increase of cadherin-11 (aka OB-cadherin) and a decrease of N-cadherin [16]. Increased cadherin-11 expression has been implicated in various pathologies including pulmonary fibrosis and arthritis [133, 134]. Functionally, the transition to cadherin-11 yields stronger intercellular connections that improve force development in myofibroblast populations. Recent works have shown that elevated intercellular tension along with increased contractility drive CN formation of AVICs *in vitro* [22, 131]. Therefore, we hypothesize that TGF-β1 induced cadherin-11 expression through an Erk1/2 dependent pathway is essential for robust cell-cell connections necessary for generating intercellular tension required for CN formation.

To test this hypothesis, we quantified the expression and contributions of cadherin-11 in CN formation of AVICs. Here, we show that TGF-β1 induced myofibroblast differentiation of AVICs leads to upregulation of αSMA and cadherin-11 expression in an Erk1/2 dependent fashion, corresponding to increased functional contractility and cell-cell connection strength, respectively. Subsequent knockdown of cadherin-11 inhibits the ability of AVICs to generate CNs similar to knockdown of αSMA [22], demonstrating that both proteins are necessary for dystrophic CN morphogenesis.

4.2 – Methods

4.2.1 AVIC isolation and culture

Porcine aortic valve leaflets were excised from sacrificed animals within 10 minutes of slaughter at a local abattoir. Leaflets were stored in PBS at 4°C to ensure survival. Within 3 h of sacrifice, AVICs were isolated as previously described [115]. Briefly, after the removal of the endothelium, the leaflet was minced into 1 mm^2 pieces and digested in a 1 mg/ml collagenase solution (Worthington Biochemical Corp., Lakewood, NJ) for 1 h at 37° C and 5% CO_2. The collagenase solution with the remaining tissue was passed through a cell strainer to collect a cell solution which was centrifuged at 1500 RPM for 5 min to obtain the cell pellet. The pellet was resuspended in Dulbecco's Modified Eagle Medium (DMEM) supplemented with 10% FBS (Atlanta Biological; Lawrenceville, GA), and 1% Antibiotic-Antimycotic (Gibco; Grand Island, NY). The cells were seeded on tissue culture dishes and incubated at 37° C and 5% CO_2 with media changes every three days. AVICs were cyropreserved after the second passage and all experiments in this study were performed using AVICs between passages 3-6.

4.2.2 Calcific Nodule Treatments and Analyses

AVICs were seeded onto BioFlex Pronectin culture plates (Flexcell International Corporation) at a density of 60,000 cells/cm^2 in 3 ml of media. After reaching confluence (~48 h), AVICs were treated with 1 ng/mL TGF-β1, 10 μM U0126, a MEK1/2 inhibitor that prevents Erk1/2 phosphorylation, or U0126 +

TGF-β1 for 24 h, after which they were subjected to 15% cyclic equibiaxial strain via the Flexcell-4000 tension system (Flexcell International Corporation) at a frequency of 0.75 Hz for 24 h. The specific sequence of TGF-β1 for 24 h followed by 15% cyclic strain results in the formation of dystrophic CNs [131].

To quantify nodule counts following treatments, AVICs were rinsed twice with PBS and fixed in 3.7% neutral buffered formaldehyde for 15 min. AVICs were rinsed with PBS and, unless immediately stained, stored at 4^{o}C for up to several days. Each 35 mm well was rinsed with deionized water (dH_2O) and stained with 1 ml of 14 mM Alizarin red S (Sigma) (in dH_2O, pH 4.1, where undissolved particulates were removed with a 0.45μm filter) for 30 min with agitation to determine calcium deposition. After staining, the cells were washed 4 times with dH_2O to remove excess dye. Positively stained nodules were manually counted under the microscope.

To examine the morphology of the nodules formed following treatments, wells were rinsed with PBS and stained with Annexin V conjugated with Alexa fluor 488 (5% solution in Annexin binding buffer; Invitrogen) for 15 minutes to detect apoptotic cells. PI (0.4% solution in Annexin binding buffer; Invitrogen) was used as a counter-stain for necrotic cells. Images were taken with a Nikon TE300 inverted tissue culture fluorescence microscope.

4.2.3 Wound Assay

A wound assay to quantify the level of intercellular tension was performed as described previously [131]. Briefly, AVICs were seeded on tissue culture polystyrene 6-well plates at 60,000 cells/cm^2 and allowed to adhere overnight. AVICs were treated with either 1 ng/ml TGF-β1, 10 μM U0126, or a combination of these treatments for 24 h. Prior to the introduction of a wound to the monolayer with a pipet tip, the extracellular growth media was washed away and replaced with DMEM media containing 1.8 mM Ca^{2+} or DMEM diluted with Ca^{2+} free PBS to give a final concentration of 0.45 mM Ca^{2+} 5 min prior to wounding in order to select for function of different cadherins. All cadherins require extracellular Ca^{2+} for function; however, cadherin-11 functions at lower Ca^{2+} concentrations than normal cadherins such as N-cadherin. Previous studies have identified 0.3 – 0.8 mM as a threshold concentration range in which cadherin-11 is functional but N-cadherins display reduced functionality in this range [135]. Immediately after wounding, each well was imaged, and wound areas were calculated using ImageJ analysis software.

4.2.4 Protein and mRNA Assays

AVIC activation was quantified by assaying for αSMA protein expression using an indirect ELISA as described previously [131, 136]. AVIC mRNA was isolated per manufacturer protocol using RNeasy isolation kit (Qiagen). A cDNA library using forward (CAAGTTAGTGTACAGTATCCTGG) and reverse

(GTCTTTAGCCTTCACTCT TCC) primers was then created with Oligo d(T) and RNAse inhibitor (Applied Biosystems) using M-MLV reverse transcriptase enzyme (Promega). Finally, qPCR was performed on a HT7900 sequence detection system (Applied Biosystems, VUMC DNA Resource Core).

4.2.5 Immunofluorescence

AVICs were plated on fibronectin functionalized coverslips and treated with 1 ng/mL TGF-β1, 10 μM U0126, or U0126 + TGF-β1 for 24 h. The cells were then fixed in 3.7% formaldehyde, permeabilized with 0.1% Triton X-100, and blocked with 1% bovine serum albumin for 1 h at room temperature. A primary antibody to cadherin-11 (2 μg/ml, Santa Cruz) was added to the coverslips for 3 h at room temperature. After thorough washing in PBS, a fluorescently labeled secondary antibody (Alexa Fluor 488, Invitrogen) was added to the coverslip for 1 h. The coverslips were then washed and sealed with ProLong Gold antifade reagent (Invitrogen) overnight prior to imaging with a Nikon Eclipse E800 equipped with a Spot RT3 camera.

4.2.6 siRNA Knockdown

The necessity of cadherin-11 expression in CN morphogenesis was assessed using siRNA knockdown. Cadherin-11 specific siRNA was designed using specialized algorithms, and 40 pM each of three different siRNA plasmids (CCAAGTTAGTGTACAGTAT, GGGATGGATTGTTGAA, CCTTATGACTCCATC

CAAA, Sigma) were pooled and transfected into AVICs using Lipofectamine 2000 (Invitrogen) for 6 h. AVICs were allowed to recover overnight prior to the addition of TGF-β1 and strain as described above. Live/Dead stain was conducted to assess cell viability (Supplemental Data); Western blotting was used to confirm knockdown efficiency.

4.2.7 Immunohistochemistry and von Kossa staining

Fresh frozen 5-7 μm sections in OCT were obtained from the Vanderbilt Heart and Vascular Institute Main Heart Registry and stored at -20^{o}C until use. For immunofluorescence, sections were warmed at room temperature prior to removal of OCT with PBS. Tissue sections were stained for 4h at room temperature using a rabbit primary antibody to cadherin-11 at a 1:25 dilution (Cell Signaling, Danvers, MA), rinsed 3X in PBS with 0.01% Triton-X 100, incubated with an Alexa-Fluor 647-conjugated goat-anti-rabbit secondary antibody at a 1:300 dilution (Invitrogen, Grand Island, NY, USA) and a primary antibody to αSMA directly conjugated with Cy3 at a dilution of 1:300 (Sigma-Aldrich, St. Louis, MO), and finally washed 3X in PBS with 0.1% Triton-X 100. Excess moisture was carefully wicked away before samples were mounted in ProLong Gold AntiFade with DAPI (Invitrogen) and allowed to dry overnight at room temperature. All sections were imaged using the Nikon Eclipse TE-2000 microscope. Adjacent valve sections were analyzed using a von Kossa calcium staining kit (PolySciences Inc., Warrington, PA).

4.2.8 Statistical analyses

The data are reported as the mean of all replicates, and error is given as standard error of the mean ($n \geq 3$). Statistical significance between treatments was determined by one-way ANOVA, and pairwise differences were identified using post-hoc Holm-Sidak testing.

4.3 – Results

4.3.1 αSMA Expression is Not Sufficient for Calcific Nodule Formation in Strain Environment

Consistent with previous results [132], treating AVICs with either 1 ng/ml TGF-β1 or 10 μM U0126 leads to a significant increase in αSMA mRNA and protein expression (Fig. 4.1A). A combination of these treatments also significantly increases αSMA expression compared to non-treated controls. As shown previously [131], AVICs treated with TGF-β1 prior to the addition of strain form significantly more CNs compared to non-treated, strained control AVICs (Fig. 4.1B), and CNs were determined to be dystrophic with an apoptotic ring surrounding a necrotic core (Fig. 4.1C). The addition of U0126 to the TGF-β1 treatment prevents this increase in CN formation.

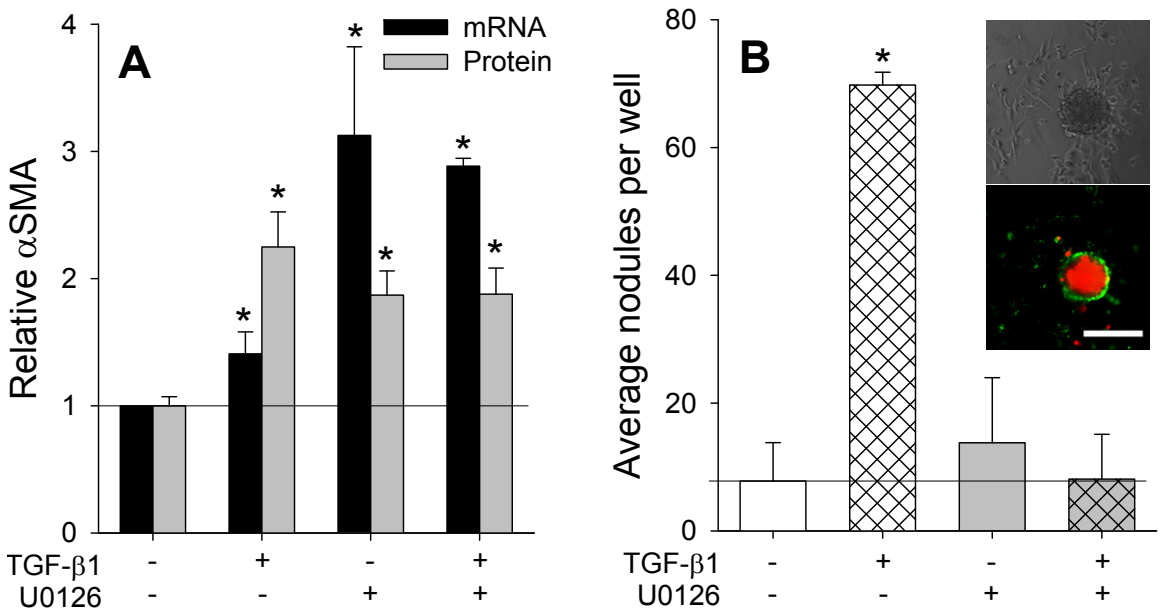

Fig. 4.1 – The effect of MEK1/2 inhibition on hallmarks of dystrophic calcification. AVICs were treated TGF-β1, U0126, U0126 + TGF-β1 and assayed for αSMA and calcific nodule formation. MEK1/2 inhibition causes αSMA expression (A) but suppresses dystrophic calcific formation (B) in AVICs, both in the presence and absence of TGF-β1. Scalebar = 250 μm. All error bars indicate standard error of the mean. * indicates significant difference ($p < 0.005$) versus control.

4.3.2 Erk1/2 Inhibition Does Not Affect Canonical TGF-β1 Signaling

U0126 is designed to be a specific inhibitor to MEK1/2, the kinase directly upstream of the MAPK Erk1/2. Therefore, we assessed the effect of TGF-β1 and U0126 treatments on Erk1/2 phosphorylation in AVICs. Treating AVICs with TGF-β1 for 1 h significantly increased Erk1/2 phosphorylation (Fig. 4.2A), and this phosphorylation is completely inhibited by the U0126 treatment. We were next determined potential off target effects of U0126 treatment at other common TGF-β1 signaling proteins. TGF-β1 treatment for 1 h induces significant phosphorylation of its canonical transcription factor Smad3 (pSmad3) in a manner that is not inhibited by U0126 treatment (Fig. 4.2A). In addition to Smad3, we have previously shown that 1 h of TGF-β1 treatment leads to

phosphorylation of the MAPK p38 that is necessary for TGF-β1-induced αSMA expression in AVICs [136]. Treating AVICs with U0126 does not inhibit TGF-β1 p38 phosphorylation (Fig. 4.2A). Consistent with the pSmad3 results, treating AVICs with TGF-β1 for 24 h leads to a significant increase in PAI-1 promoter luciferase activity that is not inhibited by U0126 treatment (Fig. 4.2B).

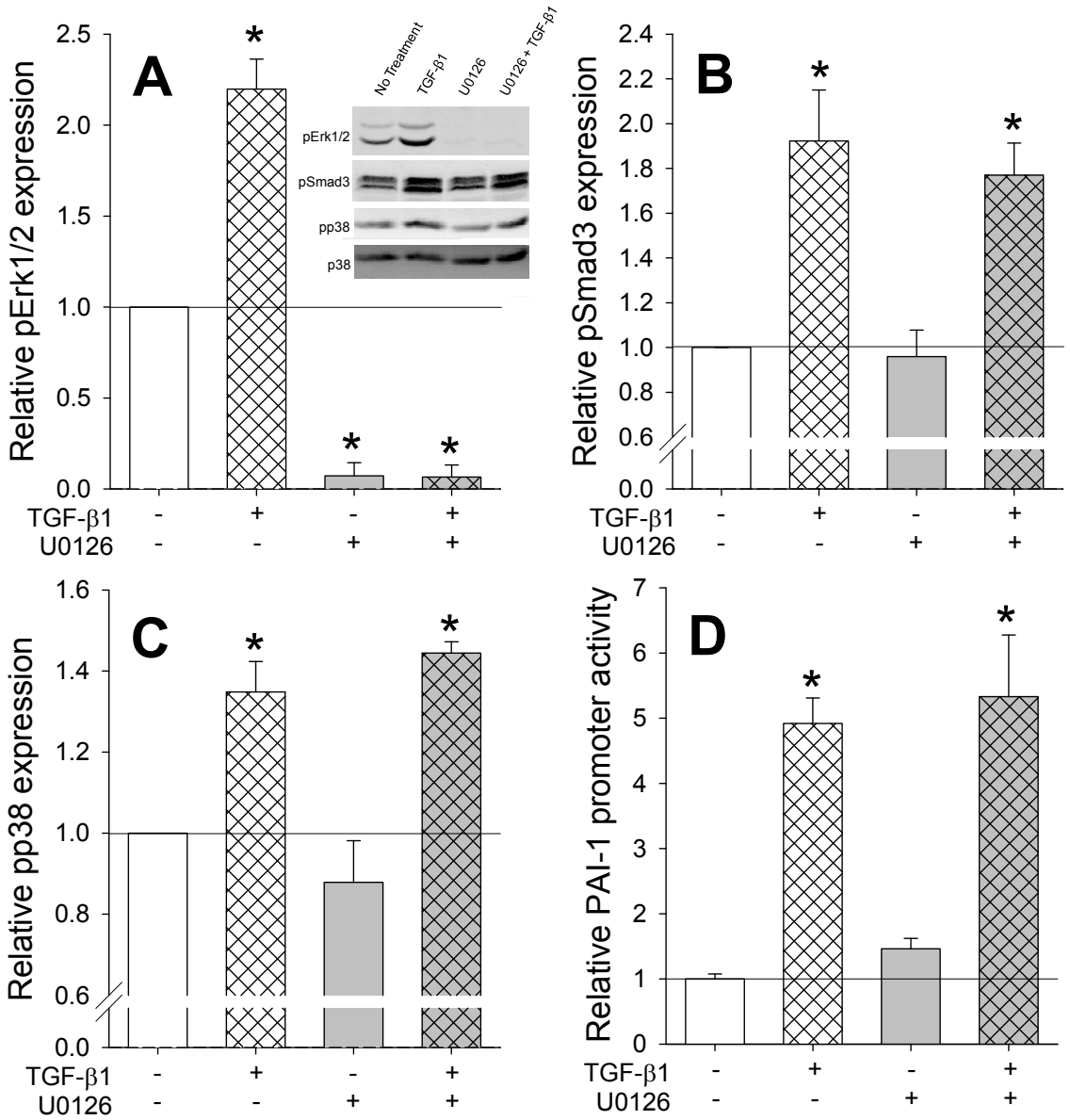

Fig. 4.2 – U0126 does not interfere with canonical TGF-β1 signaling. U0126 is a specific MEK1/2 inhibitor as indicated by the complete inhibition of pErk1/2 (A) but no change in pSmad3 (B) or pp38 (C). Inset in A shows representative blots and A-C are average densitometry from three independent experiments. Similar to the pSmad3 results, U0126 does not inhibit PAI-1 promoter activity following TGF-β1 treatment (D). All error bars indicate standard error of the mean. * indicates significant difference ($p < 0.005$) versus control.

4.3.3 Erk1/2 Inhibition Suppresses TGF-β1 Induced Expression of Cadherin-11

AVICs treated with TGF-β1 for 24 h exhibit a significant increase in cadherin-11 mRNA that is inhibited by treating AVICs with U0126 (Fig. 4.3A). Immunofluorescence images also indicate changes in cadherin-11 expression and cellular localization following the TGF-β1 and U0126 treatments (Fig. 4.3B). TGF-β1 treated AVICs exhibit cadherin-11 expression as indicated by FITC fluorescence between adjacent cells (with nuclei indicated by DAPI staining). Expression of cadherin-11 was not observed in AVICs treated with U0126 or in non-treated controls.

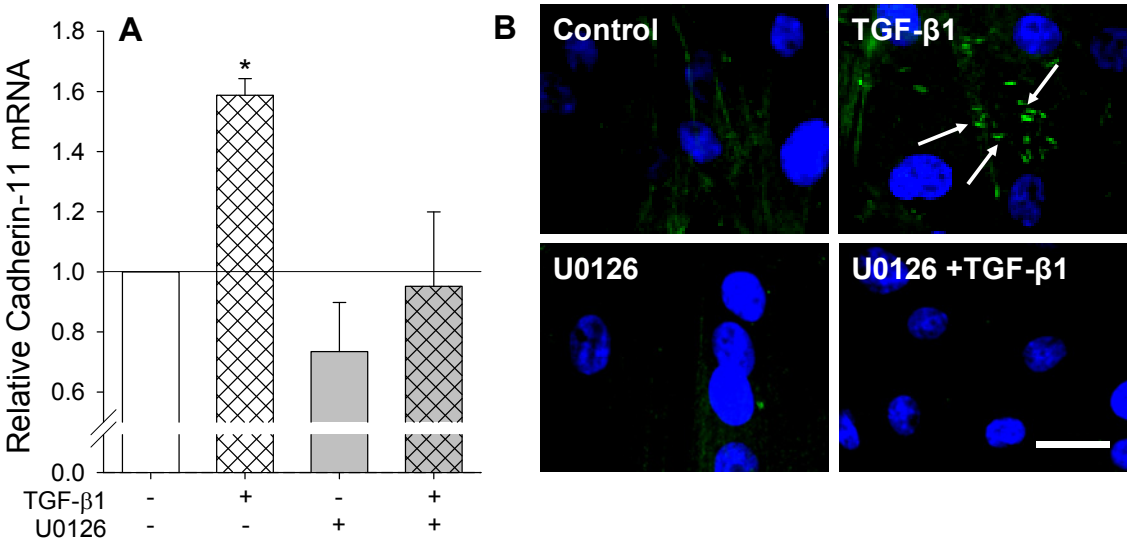

Fig. 4.3 – TGF-β1 incubation for 24 h increases cadherin-11 expression in AVICs. (A) qPCR reveal a 1.58 fold increase in cadherin-11 mRNA in samples treated with TGF-β1 and a decrease in cadherin-11 mRNA with inhibition of MEK1/2. (B) Immunostaining shows cadherin-11 in TGF-β1 groups with minimal to no stain in other treatment groups. Scalebar = 10 μm. All error bars indicate standard error of the mean. * indicates significant difference ($p < 0.005$) versus control.

4.3.4 Cadherin-11 is Required for Elevated Intercellular Tension and Calcific Nodules

Given that TGF-β1 induces expression of cadherin-11 in a manner that is inhibited by U0126, we next determined if upregulation of this protein plays a role in increased intercellular tension that is believed to lead to the formation of dystrophic CNs *in vitro*. When a wound is introduced to statically cultured AVICs in 1.8 mM Ca^{2+}, a concentration that allows all cadherins to function, all treatment groups display increased intercellular tension as shown by larger wound areas compared to non-treated controls (Fig. 4.4A). However, when a wound is applied to AVICs in 0.45 mM Ca^{2+} media, a concentration that permits functionality of cadherin-11 but below the functional concentration for typical cadherins, only TGF-β1 treated AVICs exhibit a significantly increased wound area, and this area is even greater than AVICs treated with TGF-β1 and wounded in high Ca^{2+} media.

To determine if cadherin-11 expression is necessary for CN formation, we used siRNA to knockdown cadherin-11 in AVICs. AVICs treated with lipofectamine transfection reagent alone or in combination with a non-specific scramble siRNA construct generated robust CNs following TGF-β1 treatment for 24 h and mechanical strain for an additional 24 h; however, AVICs transfected with siRNA specific to cadherin-11 exhibit dramatically reduced CN morphogenesis (Fig. 4.4B). No significant differences were observed for cell morphology and growth.

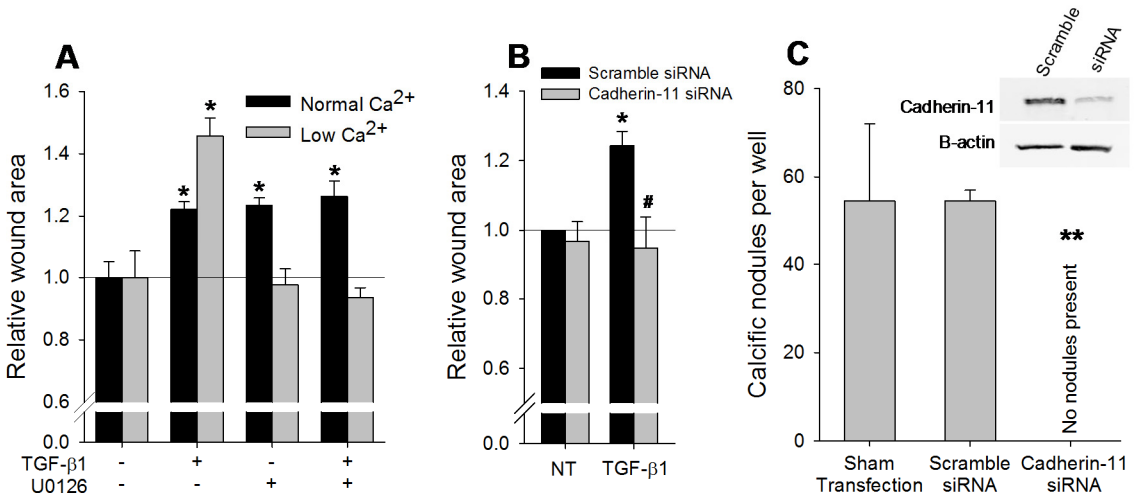

Fig. 4.4 – Cadherin-11 generates intercellular tension through αSMA that enables calcific nodule morphogenesis. (A) Wound assay reveals strength of intercellular connection which correlates to wound area. At normal Ca^{2+} levels, with all cadherins functional, TGF-β1, U0126, and U0126 + TGF-β1 treatments all increased wound area size due to increased αSMA expression. However, at low Ca^{2+} levels, where cadherin-11 is still functional and others are not, TGF- β1 treated cells created a large wound. (B) siRNA knockdown of cadherin-11 decreases TGF-β1 initiated wound area to control levels. (C) siRNA knockdown of cadherin-11 prevents calcific nodules. All error bars indicate standard error of the mean. * indicates significant difference ($p < 0.005$) versus control. # indicates significant difference ($p < 0.05$) versus Scramble. ** indicates significant difference ($p < 0.005$) versus Sham and Scramble.

4.3.5 Expression of Cadherin-11 is Elevated in Calcified Human Aortic Valves

We evaluated non-calcified and calcified aortic valves from human explants with Von Kossa staining for calcification and immunohistochemistry for cadherin-11 and αSMA expression. Von Kossa staining revealed dramatic differences in the diseased valve with a significant accumulation of stain throughout the whole tissue (Fig. 4.5A,B). Immunostaining of the valves revealed the presence of cadherin-11 in non-calcified valves but very little αSMA expression. Cadherin-11 was mostly present near the periphery of the tissue confirming previous findings of its presence in the endothelium[79] (Fig. 4.5A). However, in the calcified valve, an intense stain was observed for both cadherin-

11 and αSMA (Fig. 4.5B). Furthermore, in contrast to the peripheral staining observed in the healthy leaflet, cadherin-11 was detected throughout the interstitium in the diseased leaflet.

Analysis of the mRNA from the tissue samples revealed a 50 fold increase of cadherin-11 mRNA in calcified samples when compared to non-calcified samples (Fig. 4.5C). Also, a close to 10 fold increase over non-calcified specimen was observed for αSMA mRNA levels in calcified samples.

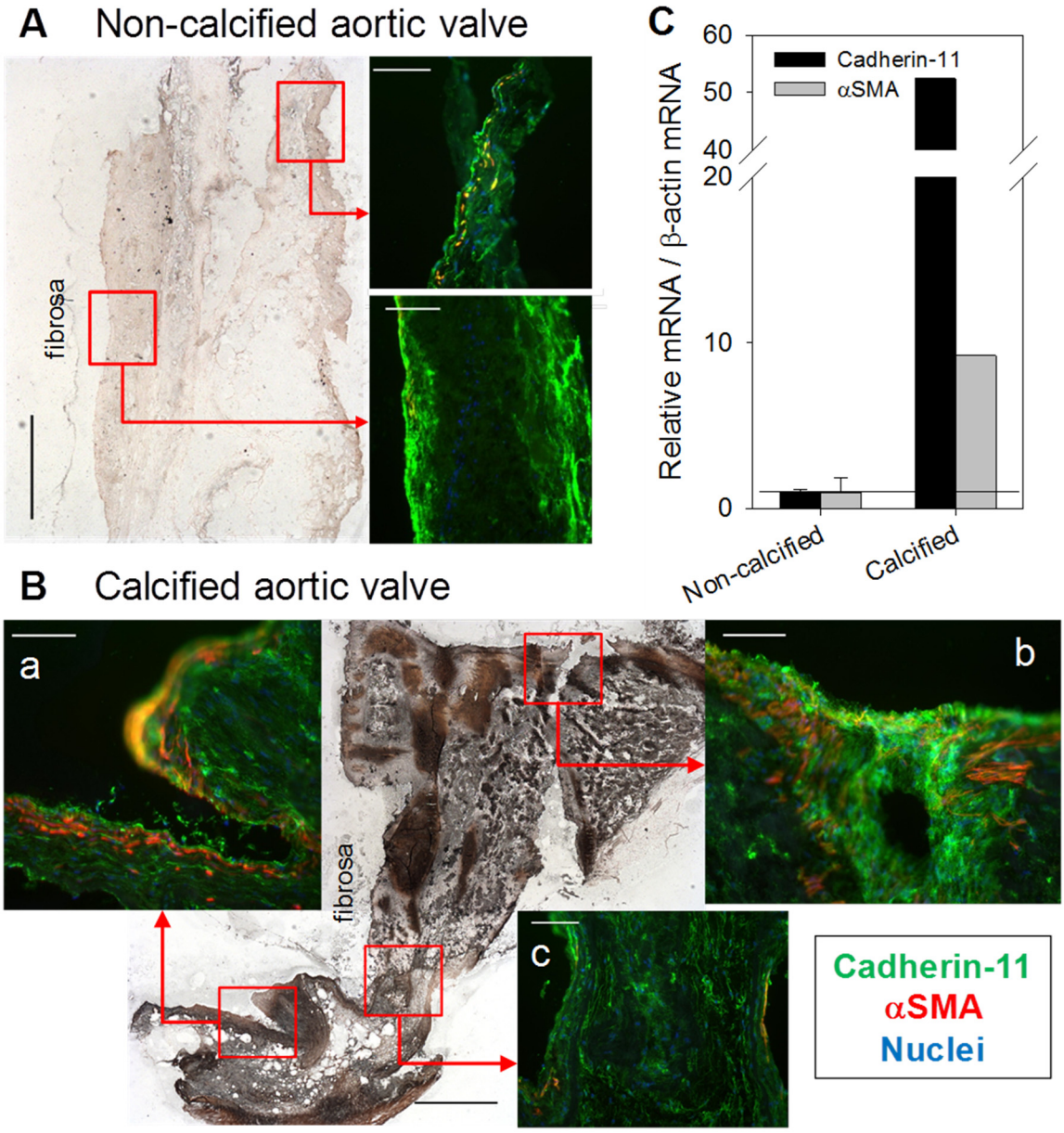

Fig. 4.5 – Cadherin-11 and αSMA expression are increased in calcified human aortic valve leaflets. (A) Immunostaining of a non-calcified leaflet reveals cadherin-11 expression along the periphery of the leaflet, sparse αSMA staining, and very little calcification indicated by the von Kossa stain. (B) Calcified leaflet shows enriched cadherin-11 and αSMA co-localization in areas of significant calcification (panels a and b), as seen in the von Kossa stain, but not in areas where calcification is less intense (panel c). (C) mRNA for cadherin-11 and αSMA are increased in the calcified leaflet (n=1) compared to the non-calcified leaflets (n=2). Scalebar = 500 μm for von Kossa, = 100 μm for immunofluorescence.

4.4 – Discussion

Dystrophic calcification in CAVD has been associated with the pathological differentiation of AVICs to myofibroblasts, which is characterized by increased αSMA expression. Treating AVICs with U0126, however, indicates that the presence of αSMA is not sufficient to drive dystrophic calcification, leading to the hypothesis that there exist other relevant mechanisms that have not been elucidated. Here, we present evidence that TGF-β1 treatment of AVICs leads to expression of the atypical cadherin, cadherin-11, and expression of this intercellular adhesion protein is necessary for the development of dystrophic CNs *in vitro*.

Previous *in vitro* studies on dystrophic CN formation revealed the importance of αSMA as a mediator of the process. TGF-β1 treatment of AVICs led to increased expression of αSMA, which reinforces stress fibers and produces a more contractile cell. Benton et al. showed this increased contractility leads to contraction events that result in cell aggregates that develop into CNs through an apoptosis driven pathway [22]. Recently, we found that mechanical strain exacerbated the formation of these aggregates by introducing a force imbalance on the monolayer whereby increased intercellular tension is overcome by the addition of externally applied strain [131]. This led us to theorize that TGF-β1 induced myofibroblast populations possessed higher intercellular tension than quiescent fibroblasts, thus making them more sensitive to mechanical strain and subsequent nodule formation.

Interestingly, distinct differences in cadherin expression have been observed in fibroblast and myofibroblastic populations with fibroblasts expressing N-cadherin and myofibroblasts expressing cadherin-11 [16]. Cadherin-11 junctions withstand two-fold higher forces when compared to connections formed with N-cadherin [120]. Furthermore, upon application of forces, cadherin-11 expressing cells will continue to hold on and eventually rip at the plasma membrane while N-cadherin expressing cells release from each other [16]. These stronger intercellular contacts are organized by and work synergistically with increased αSMA expression leading to the accumulation of tension within myofibroblast populations. To test the effect of cadherin-11 on elevated intercellular tension, we utilized a wound assay as described previously [131]; however, in this study we varied the concentration of extracellular Ca^{2+} to select for function of different cadherins. All cadherins require the presence of extracellular Ca^{2+} in order to function, but atypical cadherins such as cadherin-11 have a higher Ca^{2+} affinity (K_D ~ 0.2 mM) than normal cadherins [135]. Therefore, cadherin-11 functions at lower Ca^{2+} concentrations than normal cadherins such as N-cadherin (K_D = 0.7mM). This difference in cadherin Ca^{2+} affinity is reflected in the wound assay results. At the higher Ca^{2+} concentration, all cadherins are functional. TGF-β1 and U0126 treatments both lead to an increase in αSMA, thus an increase in AVIC contractility; therefore, these two treatment groups cause significant tension as the AVICs pull on each other in the monolayer, ultimately leading to large increases in wound area. When the extracellular Ca^{2+} is lowered such that only cadherin-11 is functional, intercellular tension does not build in the

U0126 treated AVICs, and the wound area for this treatment group is not significantly different than non-treated controls. However, for TGF-β1 treated AVICs in the low Ca^{2+} case, the presence of cadherin-11 in AVICs treated with TGF-β1 alone allows intercellular tension to build in the monolayer, leading to a significant increase in wound area compared to non-treated control samples. Additionally, since typical surface-adhesion cadherins are weaker in the low Ca^{2+} case, the increased force imbalance leads to an even larger wound area for AVICs treated with TGF-β1 compared to the high Ca^{2+} case. Illustrating the importance of increased tension conferred by cadherin-11 expression in nodule formation, when siRNA is used to knockdown the expression of cadherin-11, intercellular tension is reduced and CNs fail to form after TGF-β1 treatment and mechanical strain. This indicates that robust cell-cell connectivity in conjunction with contraction events are both necessary for CN formation.

A proposed function of cadherin-11 in CN morphogenesis is described here. Activated AVICs express two mechanotransductive proteins due to TGF-β1: αSMA and cadherin-11. With the change in protein expression, there is a dramatic change in the physical interactions between the cells in the monolayer. Intercellular tension increases as the cells become tightly connected due to cadherin-11 and as the cells become contractile due to αSMA. Eventually, the increased tension throughout the monolayer generates an imbalance of forces possibly due to cadherin-11 expression differences within individual cells. The application of external forces, such as large tissue deformation during valve closure, increases this tension imbalance leading to apoptosis of the weaker cell

and creating aggregates as the initiating step of CN morphogenesis. CNs mature as cells near the periphery of the aggregate experience strain magnification due to the non-deformity of the nodule, leading to apoptosis and calcification as we proposed recently [131].

Expression of cadherin-11 by TGF-β1 is blocked by pre-treating AVICs with U0126, an inhibitor to MEK1/2. MEK1/2 is a MAPK kinase that when activated leads to phosphorylation of the MAPK Erk1/2. TGF-β1-induced phosphorylation of Erk1/2 has been observed in a wide-variety of cell types and has been shown to be necessary for numerous cellular responses [137-139]. Activation of Erk1/2 has also been shown to suppress αSMA expression in mouse embryonic fibroblasts [140]. Consistently, U0126 treatment leads to a significant increase in αSMA expression in AVICs. Our previous results indicate that TGF-β1-induced expression of αSMA in AVICs requires phosphorylation of a different non-canonical MAPK p38 [136]. Therefore, it seems that these two non-canonical pathways may independently lead to expression of proteins that are characteristic of pathological differentiation of AVICs. In contrast, canonical TGF-β1 signaling leads to increased expression of PAI-1, and we have hypothesized that upregulation of PAI-1 through activation of the canonical Smad2/3 pathway may be involved a negative feedback of TGF-β1 signaling [136]. Therefore, the results of these studies suggest a divergence in TGF-β1 signaling that leads to AVIC myofibroblastic differentiation through activation of non-canonical pathways (p38 and Erk1/2) that each lead to a different cellular outcome that may be very important in CAVD, while canonical Smad pathways may not be directly involved

in pathological signaling for CAVD. Additionally, Erk1/2 phosphorylation has been shown to be required for mechanically-induced calcific mineralization by calcifying vascular cells [114], suggesting that these pathways may be important in a variety of calcification processes. We believe that the results of this study suggest a therapeutic approach for CAVD by targeting either of these non-canonical pathways or direct inhibition of cadherin-11 function.

In order for the current work to realize a larger clinical impact, the *in vitro* mechanisms and AVIC outcomes identified in this study should be examined *in vivo*. We have confirmed the presence of cadherin-11 in human aortic valves and have also observed a dramatic increase in cadherin-11 expression in calcified valves, which supports our *in vitro* findings; however, *in vivo* research into the mechanisms of CAVD is currently limited by the lack of an animal model that accurately recapitulates human pathology. Nonetheless, we believe that identification of cadherin-11 may provide a useful tool for better understanding the pathogenesis of CAVD, and our results may have implications beyond solely elucidating mechanisms of CN formation. AVIC myofibroblast activation is believed to be one the earliest processes in CAVD; however, early valvular changes are difficult to detect in patients. Very few markers of this differentiation are known, and the most commonly used ones such as αSMA do not lend themselves to imaging techniques due to their cytosolic expression. Since cadherin-11 is a transmembrane protein, it allows for targeting via molecular imaging tracers and may provide a molecular fingerprint for the onset of CAVD.

Chapter V

Biophysical Analysis of Dystrophic and Osteogenic Calcific Nodules

Text for Chapter V taken from:

> **Chen, J., Peacock, J.R., Branch, J., Merryman, W.D., "Biophysical Analysis of *in vitro* Models of Valvular Calcification", *Journal of Biomechanical Engineering*, 137(2); 2015.**

5.1 – Introduction

The pathogenesis of CAVD involves the deposition of calcium rich nodules on the fibrosa layer of aortic valve leaflets [9, 141, 142]. The presence of these structures significantly impedes proper opening and closing of the valve leading to left ventricular pressure overloading and eventual heart failure [9, 143]. Two major types of valvular calcification have been observed in diseased excised tissue: dystrophic and osteogenic [23]. Dystrophic calcification is the predominant form of valvular calcification being found in 83% of diseased valves and is described as an amorphous crystalline material [15]. Osteogenic calcification is present in 13% of valves containing dystrophic calcification and is identified by the presence of osteoid matrix reminiscent of active bone formation [15]. At present, there exists only surgical intervention for CAVD, which although

effective, include a 3% mortality rate and is only utilized at the end stage disease [144, 145]. Efforts to describe the mechanisms of valvular calcification may lead to the development of novel pharmacological treatments for CAVD [7, 146, 147].

The etiology of CAVD has been extensively studied through the development of valvular calcification *in vitro* models [17, 19-23, 109, 118, 123, 146, 148-150]. These models describe the formation of CNs via AVICs in unique culture conditions and are thought to mimic the dystrophic and osteogenic calcification found in diseased explanted aortic valve leaflets [15, 23]. The CNs generated from each model appear morphologically similar in that they are cellular aggregates but form via distinct mechanisms and have unique features. Dystrophic nodules form on stiff substrates, are characterized by cell death, and involve the differentiation of quiescent AVICs into activated myofibroblasts via inflammatory cytokines such as TGF-β1 [20, 22, 151, 152]. Conversely, osteogenic nodules form on compliant substrates through the active secretion of bone matrix via osteogenic AVICs [17, 23, 60]. These *in vitro* systems have helped identify many important mediators of dystrophic and osteogenic calcification; however, there exist ambiguity regarding what distinguishes each type of CN [153]. The physiochemical composition and biophysical properties of the two nodule types remain largely undefined and their relationship to *in vivo* valvular calcification is unclear [17]. Clarifying the properties of CNs is necessary to more clearly delineate the two nodule types and provide a correlation between mechanistic changes and biophysical properties.

Few studies have been conducted to describe the physiochemical properties of CNs. Cloyd et al. examined CNs formed using calcifying media supplemented with TGF-β1 with techniques such as scanning electron microscopy (SEM), transmission electron microscopy (TEM), and Raman spectroscopy [153]. Strikingly, these CNs were not mineralized but rather were rich in collagen content indicative of myofibroblast remodeling. This is in contrast to a study demonstrating, via TEM, that CNs formed in calcifying media without TGF-β1 contained a mineralized core [12]. Additionally, a seminal study investigating CN formation using infrared spectroscopy revealed that the CNs formed with TGF-β1 treatment exhibited a spectrum corresponding to the presence of hydroxyapatite in the nodule center [19]. Taken together, these studies suggest that all CNs are not equal and their properties are highly dependent on their culture conditions. Furthermore, these contrasting findings highlight the uncertainty that exists regarding CN properties and necessitate additional studies evaluating the physiochemical and biophysical properties of dystrophic and osteogenic CNs.

In this study, we utilize SEM coupled with X-ray Energy Dispersive Spectrometry (SEM-EDS) and atomic force microscopy (AFM) to define CN characteristics through two published *in vitro* systems of dystrophic and osteogenic calcification [17, 148]. We found that both nodule types contained Ca and P content; however, the regions where calcification forms was dramatically different. Dystrophic nodules had little to no surface calcification, whereas osteogenic nodules had an abundance of calcified spheres on the surface similar

to what has been observed *in vivo* [73]. Also, both nodules had regions that did not contain calcification and exhibited modulus readings similar to that of cells. These data reveal a heterogeneous make up of both nodules that has not been previously described. Furthermore, characteristics specific to dystrophic and osteogenic types were identified. Collectively, these findings ascribe unique characteristics to CN types and provide evidence connecting *in vitro* and *in vivo* valvular calcification.

5.2 – Methods

5.2.1 AVIC Isolation and Culture

Porcine aortic valve leaflets were excised from sacrificed animals within 10 minutes of slaughter at a local abattoir. Leaflets were stored in PBS with 1% penicillin/streptomycin (Cellgro; Manassas, VA) at 4°C to ensure survival. Within 3 hours (h) of sacrifice, AVICs were isolated as previously described [115]. Briefly, after the removal of the endothelium, the leaflet was diced and digested in a 2 mg/ml collagenase solution (Worthington Biochemical Corp., Lackwood, NJ) for 1 h at 37° C and 5% CO_2. The collagenase solution with the tissue was passed through a cell strainer to collect a cell solution which was centrifuged at 1500 RPM for 10 minutes to obtain the cell pellet. The pellet was then resuspended in Dulbecco's Modified Eagle Medium (DMEM) supplemented with 10% FBS (Atlanta Biologicals; Lawrenceville, GA), and 1% penicillin/streptomycin antibiotic. Cells were either cryopreserved at passage 0 to preserve a quiescent

phenotype or seeded on tissue culture dishes and incubated at 37° C and 5% CO_2 with media changes every three days [154].

5.2.2 Calcific Nodule Assays

Dystrophic and osteogenic CNs were generated according to published *in vitro* systems [17, 23, 148, 149]. For dystrophic CN formation, AVICs were cultured on BioFlex Pronectin culture plates (Flexcell International Corporation, Hillsborough, NC) at $6x10^4$ cells/cm^2 in normal growth media and were given a day to reach confluence. After AVIC confluence, normal growth media was removed and replaced with growth media supplemented with 5 ng/ml porcine TGF- β1 (R&D Systems, Minneapolis, MN) for 24 h. The plates were then subject to equibiaxial strain via the Flexcell-4000 Tension System at a strain magnitude of 15% and a frequency of 0.75 Hz for 24 h.

Osteogenic CN were developed on 24 kPa polyacrylamide hydrogels fabricated as previously described [17, 155, 156]. Briefly, amino-silanated coverslips were prepared and utilized as a surface for hydrogel polymerization. 24 kPa hydrogels (10% Acrylamide, 0.225% Bis-acrylamide) were produced via free radical polymerization and functionalization was performed via Sulfo-SANPAH conjugation of 10 μg/ml fibronectin to the polyacrylamide substrate. P0 AVICs were plated onto the hydrogels at a density of $1x10^4$ cells/cm^2 and allowed to attach overnight. Cells were then treated with osteogenic media consisting of DMEM supplemented with 10% FBS, 1% penicillin/streptomycin antibiotic, 10

mM β-glycerophosphate, 10 μg/ml ascorbic acid, and 10 nM dexamethasone for six days.

5.2.3 Calcific Nodule Staining and Analysis

CNs were assayed for calcium deposition using the Alizarin red stain [157]. CNs were rinsed with three times with PBS, fixed with 3.7% neutral buffered formaldehyde for 15 minutes, and rinsed again with PBS. For microscopic analysis, 1 mL of 14 mM Alizarin red solution was added to AVIC cultures for 30 minutes. After staining, the wells were washed with deionized water (dH_2O) to remove excess dye. Positively stained nodules were determined by visible red color.

To confirm cell viability properties in each CN type, Annexin V/PI and Calcein AM/PI stains were utilized. Dystrophic nodules were rinsed with PBS and stained with Annexin V conjugated with Alexa fluor 488 (5% solution in Annexin binding buffer; Invitrogen) for 15 minutes to detect apoptotic cells. PI (0.4% solution in Annexin binding buffer; Invitrogen) was used as a counter-stain for necrotic cells. Osteogenic nodules were rinsed in PBS and stained with fluorescently labeled Calcein AM (0.3% solution in PBS) to detect living cells and PI (0.3% solution in PBS) to detect dead cells. Images were taken with a Nikon TE300 inverted tissue culture fluorescence microscope.

5.2.4 SEM and X-ray Energy Dispersive Spectroscopy

For SEM-EDS analysis, CN samples were fixed in 2.5% gluteraldehyde in 0.1 M sodium cacodylate buffer solution for 1 h at room temperature and 24 h at 4°C. Samples were subsequently washed three times with sodium cacodylate buffer. CNs were then dehydrated by a series of ethanol washes (30%, 50%, 70%, and 95%, ethanol) for 15 minutes each. Dehydration was completed with two 15 minute washes with 100% ethanol. Samples underwent critical point drying and were then placed on carbon tape mounted on aluminum stubs. Silver paint was applied on the carbon tape to reduce charging effects and samples were scanned in environmental SEM (ESEM) mode.

A Phillips/FEI Quanta 650 field emission electron microscope with ESEM capability and equipped with an Oxford Instruments X-Max 50 mm^2 Silicon Drift Detector (SDD) and was used to collect backscattered images and semi-quantitative chemical data of representative nodules and cells from the osteogenic and dystrophic samples. EDS spectra were generated on >3 nodules of each nodule type with >5 scans per nodule. The SEM was operated in ESEM mode at 130 Pa to avoid carbon coating and to reduce sample charging. A spot size of 3.5, a working distance of 10 mm, and a voltage of 10 keV were used to collect all backscattered electron SEM images and EDS data. A voltage of 10 keV was chosen because it has sufficient energy to exceed the critical excitation energy of the Ca K shell (3.6905 keV). A beam measurement of 200,000 counts was performed on a titanium standard prior to collecting EDS data. Point spectra were collected for 60 seconds which corresponded to $\geq$ 80,000 area counts. All

EDS data was populated in the Oxford Aztec software and the Aztec default standards were applied during the post-processing quantitative analysis.

5.2.5 Atomic Force Microscopy

AFM data and corresponding bright-field images were captured with a Catalyst Bioscope AFM (Bruker AXS, Madison WI, USA) and a non-conductive silicon nitride cantilever with a blunted pyramidal tip (f_0 = 15 kHz, k = 0.03 N/m) suitable for biological samples was used for all measurements. The AFM was calibrated each day in fluid using a relative calibration method as previously described [158]. Briefly, the AFM was operated in Peak Force Quantitative Nanomechanical Mapping Mode, and deflection sensitivity was measured on a glass slide. The cantilever spring constant was calculated using the thermal tune method built in to the AFM software. Three to six 15 x 15 μm area scans were taken on a Bruker-provided poly(dimethyl siloxane) calibration standard (E = 2.5 MPa) in order to adjust peak force set-point and amplitude, as well as tip radius. These parameters were kept constant after calibration. Scans of samples ranged from 5 x 5 μm to 30 x 30 μm in area.

For all experiments, live non-fixed samples were scanned to prevent potential artifacts due to fixation. Three cells or nodules were scanned with three different regions scanned for each. Median modulus values for each region were determined from the modulus distribution and a single median modulus value was calculated for each cell or nodule by averaging the three regional median

modulus values. Median stiffness values for the AVICs (n=3) and CNs (n=3) were then calculated as the mean ± SEM

5.2.6 Statistical Analyses

The data are reported as the mean of all replicates, and error is given as standard error of the mean. Statistical significance between treatments was determined by one-way ANOVA and Holm-Sidek tests.

5.3 – Results

5.3.1 Dystrophic and Osteogenic Calcific Nodules Exhibit Differences in Morphology and Cell Viability

CN formation via dystrophic and osteogenic culture systems generated distinct CNs consistent with previous findings [17, 148]. Bright field images reveal morphological differences with dystrophic nodules exhibiting aggregates with elongated cells in a radial pattern along the periphery of the nodule (Fig. 5.1A,B) and osteogenic nodules having flattened cells lining regions of the aggregate (Fig. 5.1D,E). Additionally, dystrophic nodules were generally larger than osteogenic CNs. Using the calcium stain Alizarin red, both dystrophic and osteogenic CNs stained positively in the nodule center (Fig. 1 A,D). Stains for cell viability were conducted on both nodule types to confirm the cell death mediated and active bone forming calcification of dystrophic and osteogenic systems respectively. Annexin V/PI stain on dystrophic nodules revealed an intensely stained necrotic core with Annexin V positive apoptotic cells lining the periphery

of the CN (Fig. 5.1C). Conversely, Calcein AM/PI staining of osteogenic nodules showed no uptake of PI stain but an incorporation of Calcein AM stain confirming the presence of living cells within the nodule (Fig. 5.1F).

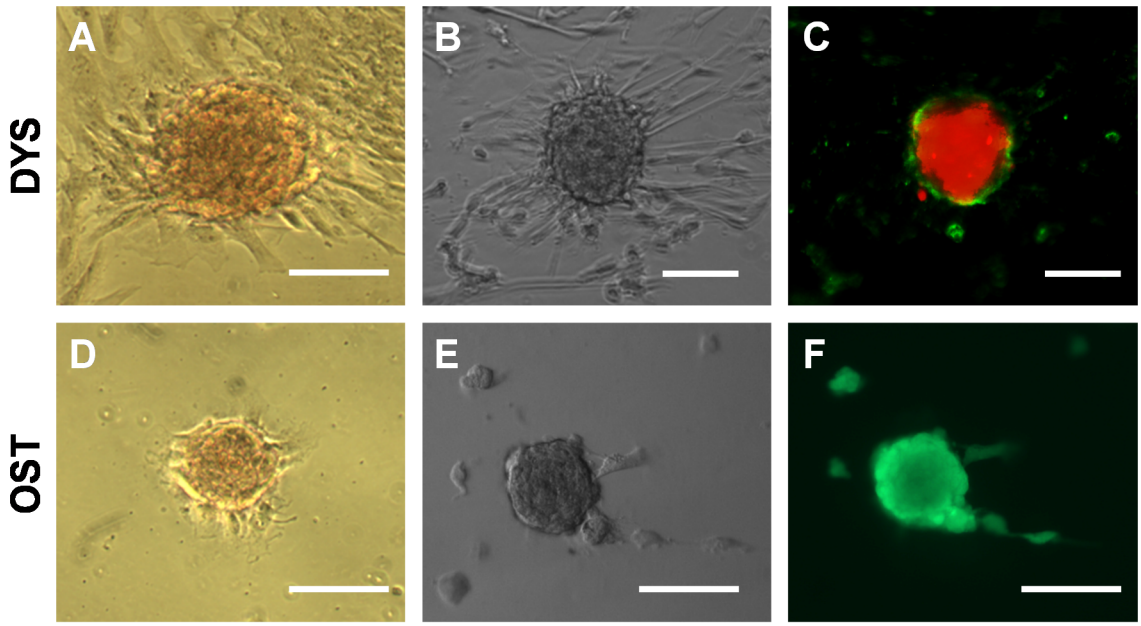

Fig. 5.1 – *Dystrophic and osteogenic calcific nodules exhibit differences in morphology and cell viability*. (A,D) Dystrophic CNs and Osteogenic CNs stain positive for Alizarin Red. (B,E) Brightfield images reveal morphological differences between dystrophic and osteogenic nodules. (C) Annexin/PI stain show strong uptake of PI stain in the nodule center with an Annexin V positive ring around dystrophic nodules while Calcein AM/PI stain show living cells within the osteogenic nodules and no uptake of PI stain. Scalebar = 100 µm

5.3.2 EDS Analysis Reveal Significant Ca and P Content in Calcific Nodules

EDS spectra were collected from three regions on each nodule sample: cell, nodule body, and calcification. Regions were identified via backscattered electron SEM images and EDS mapping of the nodules (data not shown). Furthermore, distinct differences in surface topography were confirmed by secondary electron imaging between the nodule types with dystrophic nodules exhibiting rounded cellular structures across the surface of the nodule and osteogenic nodules having smooth regions in addition to spherical materials on the surface (Fig. 5.2A,D).

Spectra from dystrophic nodules reveal average percent weight concentrations of 0.52 ± 0.076 and 0.26 ± 0.10, 0.623 ± 0.034 and 0.53 ± 0.044, and 2.88 ± 0.34 and 1.48 ± 0.12 for Ca and P from cell, nodule body, and calcification regions respectively (Fig. 5.2B,C). Ca and P concentration in calcification regions were significantly higher than those in the nodule body and the cell. Although the percent weight concentration was higher, calcification areas in the dystrophic nodule were scarce and often found in regions that were deeper within the nodule and not at the surface. Spectra from osteogenic nodules show average percent weight concentrations of 0.51 ± 0.091 and 0.16 ± 0.099, 1.78 ± 0.214 and 1.33 ± 0.101, and 10.09 ± 0.903 and 5.31 ± 0.488 for Ca and P from cell, nodule body, and calcification regions respectively (Fig. 5.2E,F). Osteogenic nodule spectra show dramatically higher levels of Ca and P in spherical materials on the surface of the nodule compared to the nodule body and cells. Additionally, Ca and P concentrations from the osteogenic nodule body

were also higher than that of cells. Interestingly, osteogenic calcification possessed a higher concentration of Ca and P than dystrophic calcification.

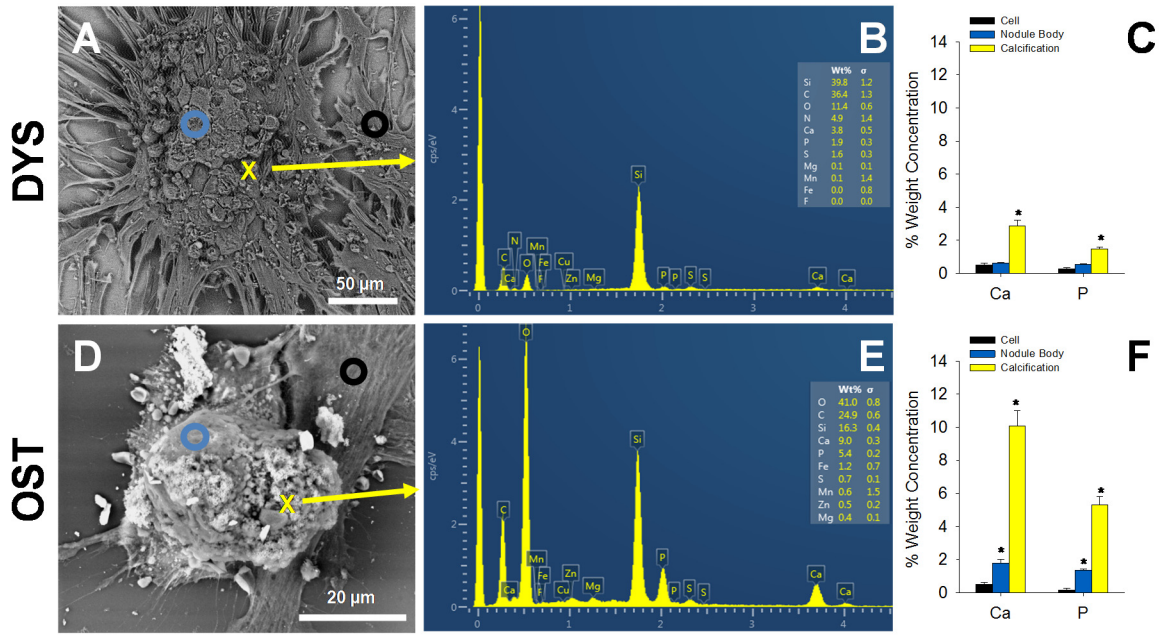

Fig. 5.2 – *EDS reveals significant Ca and P content in calcific nodules*. (A,D) Backscattered SEM image of calcific nodules with annotations showing regions of the nodules scanned with EDS. A black circle represents an EDS scan on cells; a blue circle represents an EDS scan on the nodule body; and a yellow X marks a point scanned to represent an area of calcification. (B) Representative EDS spectrum of a dystrophic nodule scanned at the yellow X in A. Ca and P scans show a weight percent of 2.8 and 1.5 respectively. (C) Relative percent weight concentration show significantly higher amounts of Ca and P in regions of calcification. (E) Representative EDS spectrum of an osteogenic nodule scanned at the yellow X in D shows a weight percent of 10.1 and 5.3 for Ca and P respectively. (F) Relative percent weight concentration show dramatically higher levels of Ca and P in calcification regions. * indicates $p \leq 0.05$

5.3.3 Biomechanical Analysis Reveals Nodule Heterogeneity

AFM scans of live cells, dystrophic nodules, and osteogenic nodules provide a wide distribution of modulus values that we represent by taking the averaged median value for each cell or CN after multiple successful scans. Averaged modulus median values of 214.712 kPa, 387.94 kPa, and 204.04 kPa were noted for cells, dystrophic nodules, and osteogenic nodules, respectively (Fig. 5.3A). No significant differences in modulus were found between the cell and CN groups suggesting that the nodule surfaces are comprised mostly of cellular material. Live AVICs scans revealed largely homogenous modulus properties, while certain regions of the osteogenic nodule body were similarly homogenous (Fig. 5.3C,D,I,J). However, osteogenic CN heterogeneity was noted as areas of the osteogenic nodule surface also contained significantly stiffer calcified spheres that were discernable via AFM (Fig. 5.3K,L). Dystrophic calcification scans indicated a more variable modulus map corresponding to changes in topography, but the modulus values were not significantly different than that of AVICs and osteogenic nodules (Fig. 5.3F,G).

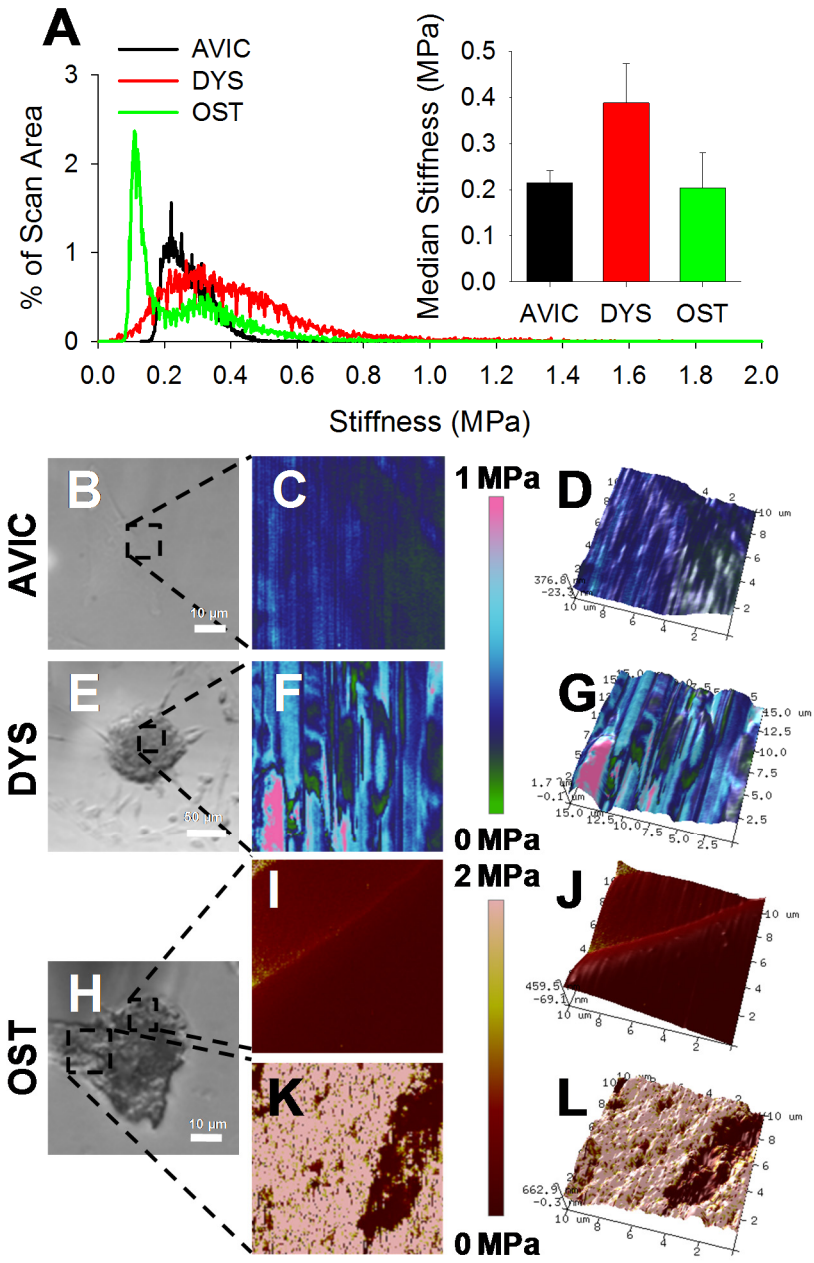

Fig. 5.3 – *Biomechanical analysis reveals nodule heterogeneity.* (A) Representative modulus scan distributions for cells and nodules. Inset graph shows average median modulus and reveals no significant difference between sample groups; however, osteogenic nodules had bimodal distribution, which likely skews downward their overall stiffness. (B,E,H) Regions scanned on AVIC, dystrophic, and osteogenic nodules via AFM are represented by the black dotted box. AVIC and osteogenic nodule body scans display consistent homogenous modulus scans (C,I) while dystrophic nodules exhibit heterogeneous modulus scans (F). Osteogenic nodules contain dramatically stiffer regions resembling spherical calcifications on the surface of the nodule body revealing the heterogeneous make up of osteogenic nodules. (D,G,J,L) 3-D topographical maps for AVIC, dystrophic, and osteogenic nodules were overlaid with the modulus map.

5.4 – Discussion

Since the seminal study describing CNs, much research has been conducted to evaluate the molecular processes that mediate the formation and evolution of these nodules [19]. However, there has been a lack of clarity regarding the intrinsic physiochemical and biophysical properties of the CNs formed *in vitro*. Characterization of these properties is necessary to provide the link between *in vitro* CN formation and *in vivo* valvular calcification and strengthen the impact of the findings from these *in vitro* systems. Additionally, the perception of CN formation has changed drastically in recent years from an understanding of one nodule expressing both dystrophic and osteogenic properties to distinct dystrophic and osteogenic nodules with specific properties [17, 19, 20, 22, 23]. Defining dystrophic and osteogenic nodule properties will help delineate characteristics unique to each nodule type and may provide important correlations between mechanistic information and biophysical properties. In this study, we sought to define the physiochemical and biophysical properties of dystrophic and osteogenic CNs formed via published *in vitro* systems.

Dystrophic and osteogenic CNs generated in this study were assessed to ensure that they generated distinct nodules that corresponded with previous findings [17, 148]. Dystrophic nodules were formed via TGF-β1 activation of AVICs under a 15% mechanical strain environment for 24 h. These nodules contained a necrotic core with a ring of apoptotic cells surrounding the nodule periphery as revealed by Annexin V/PI stain. Osteogenic nodules formed after six

days in calcifying media on compliant PA gels of 24 kPa. The whole nodule body stained positively for Calcein AM with no uptake of PI stain indicating viable cells. Both nodules also stained positively for Alizarin red, a calcium stain. These results confirm that two unique nodule types consistent with dystrophic and osteogenic calcification were formed.

Backscattered electron SEM images revealed dramatic differences in nodule chemical composition. Dystrophic nodules were comprised of round structures that covered the nodule body and were presumably dead cell bodies due to their uptake of PI. In addition, the backscattered images were fairly similar in brightness indicating similar physiochemical properties throughout the surface of the dystrophic nodule. Conversely, osteogenic nodules exhibited smooth regions in the nodule body with small spherical materials covering regions of the nodule body. These spherical objects appear much brighter in the backscattered image suggesting material that is higher in atomic number such as Ca and P.

EDS analysis of both nodule types show significantly higher Ca and P content than that of cells. For dystrophic nodules, however, the majority of the scans on the nodule revealed very low Ca and P values similar to those from cells. Regions that exhibited high Ca and P content seemed to be embedded between the rounded surface structures and were giving information about the material deeper within the nodule. Chen et al. revealed through TEM imaging of a dystrophic nodule that the bulk calcification was found beneath a layer of cells covering the surface [12]. Because the interaction volume for both backscattered electrons and X-ray generation is limited to a few microns in depth and varies

with atomic number, regions beneath the surface of an unpolished sample cannot be effectively characterized [159]. Taken together, our EDS data suggest that the dystrophic nodule surface is comprised mostly of cellular material, but there is evidence of Ca and P deeper within the nodule. Conversely, osteogenic nodules had abundant surface calcification. EDS confirmed that the spherical objects on the surface of osteogenic nodules were high in Ca and P concentration. These novel findings are consistent with a recent EDS analysis of *in vivo* valve calcification that described the presence of spherical calcifications on the surface of valve tissue [73]. Additionally, the nodule body of osteogenic CNs contained higher levels of Ca and P than cells indicating the presence of embedded bone matrix characteristic of osteogenesis. Both nodule types exhibited Ca and P ratios consistent with hydroxyapatite with dystrophic nodules having a Ca and P ratio of 2.0 and osteogenic nodules having a Ca and P ratio of 1.67 [160]. Further, osteogenic calcifications had significantly higher amounts of Ca and P when compared to dystrophic calcification. These physiochemical similarities and differences could prove to be important hallmarks distinguishing between calcification types [161].

AFM data for dystrophic and osteogenic nodules complemented the SEM-EDS data. For dystrophic nodules, the scans showed a high level of topographical heterogeneity as evidenced by the change in height throughout scans. This is consistent with the bumpy morphology of the dystrophic nodule surface. The modulus data shows approximately cellular stiffness throughout the majority of the scans supporting the notion that the dystrophic nodule surface is

mostly cellular. For osteogenic nodules, height and modulus scans along the nodule body were mostly homogenous with modulus readings in the range of cellular modulus. This suggests that although the osteogenic nodule body is high in Ca and P, it is mostly comprised of cells. This is consistent with the bone formation process which has been described to contain osteogenic cells embedded in the bone matrix that they are secreting [162]. Further, regions containing spherical objects were also identified via AFM. These regions were dramatically stiffer than the nodule body and the cells, suggesting they are non-cellular material. The increased stiffness of these spheres support the EDS spectrum and backscattered SEM images of osteogenic nodules further suggesting that these spherical objects are calcified. The presence of regions exhibiting distinct properties in the osteogenic nodule highlights the heterogeneous make up of osteogenic CNs, which distinguishes it from dystrophic CNs.

This physiochemical and biophysical analysis of CNs provides new insight into dystrophic and osteogenic calcification. Our data demonstrate that dystrophic and osteogenic nodules exhibit different properties. Dystrophic nodules were found to exhibit a bumpy topography with a modulus similar to cells. Ca and P were found in regions that appeared to be deeper within the nodule suggesting that dystrophic CNs have mineralized content beneath the surface. Osteogenic nodules displayed nodule heterogeneity with regions rich in stiff calcified spheres and smooth regions comprised mostly of cells. Levels of Ca and P were elevated in both the nodule body and the calcified spheres. These

findings demonstrate for the first time the unique physiochemical and biophysical characteristics of dystrophic and osteogenic CNs.

Future work includes the characterization of these systems over multiple time points. In this work, the time points for analysis were chosen based upon the literature; however, one major limitation in the CN assays is ambiguity regarding nodule endpoints. A thorough characterization of CN formation over time could generate further insight into how dystrophic and osteogenic nodules mature. Additionally, other techniques may be implemented in the analysis of CNs. This study utilized primarily surface/sub-surface techniques to analyze CNs. Although these techniques can comprehensively describe surface properties, they are limited in their ability to characterize the material properties beneath the surface. Tools such as TEM can be used to generate more information regarding the characteristics of CNs beneath the surface.

Chapter VI

Notch1 Mutation Leads to CAVD through Enhanced Myofibroblast Mechanotransduction

Text for Chapter VI taken from:

> **Chen, J., Ryzhova, L.M., Sewell-Loftin, M.K., Brown, C.B., Baldwin, H.S., Merryman, W.D., "Notch1 Mutation Leads to Valvular Calcification through Enhanced Cadherin-11 Mechanotransduction",** ***Arteriosclerosis, Thrombosis, and Vascular Biology,*** **(In Revision).**

6.1 – Introduction

CAVD is thought to occur in two forms, dystrophic and osteogenic, and is believed to be mediated by AVICs [17, 19, 22, 23, 148, 149]. Dystrophic calcification is more prevalent, found in 83% of valve explants and involves cell-death-mediated calcification through the nucleation of Ca and P [15, 19, 148, 149]. Dystrophic calcification proceeds as quiescent AVICs differentiate into activated myofibroblasts, which is a complex process regulated by a host of signaling pathways including TGF-β1, mitogen-activated protein kinase (MAPK), and phosphoinositide 3-kinase/protein kinase B (PI3K/Akt) signaling [16, 123, 146, 163, 164]. Hallmarks for myofibroblast-like AVICs include enhanced αSMA and cadherin-11 expression that confer increased contractility and strong

intercellular connections, respectively [21, 149]. The combinatorial effect of these proteins leads to increased intercellular tension and eventual cell-death-mediated calcification [148]. Alternatively, osteogenic calcification is found in 13% of calcified valves and is generated through the active secretion of osteoid matrix via osteoblast-like AVICs [15, 17]. The differentiation to osteoblast-like AVICs is induced by the treatment of potent osteogenic media and is thought to be mediated by BMP signaling, which leads to the expression of the transcriptional activator Runx2 [17, 165]. However, the role of dystrophic and osteogenic processes in the progression of CAVD *in vivo* is poorly understood. Genetic factors that promote CAVD has provided new physiologically relevant areas of investigation that may further the understanding of CAVD etiology [26, 27]. Specifically, the Notch1 mutation affects the intrinsic signaling of the cells, predisposing them for CAVD and creating a clinically relevant system to study CAVD.

Notch is a highly conserved cell-cell signaling pathway that plays a crucial role in proper cardiac development and remodeling [93, 166, 167]. Upon ligand binding, Notch receptors undergo proteolytic cleavage via γ-secretase and release of the Notch intracellular domain (NICD), which translocates to the nucleus to affect cell maintenance, proliferation, and apoptosis [96, 168]. Mutations in Notch can lead to a spectrum of congenital heart defects such as cardiomyopathy, tetralogy of Fallot, and valvular malformations [93, 169]. In addition to developmental abnormalities, dysregulated Notch function plays a major role in cardiac disease initiation and progression [170]. Specifically in the

aortic valve, mutations in Notch1 lead to CAVD with 100% penetrance in humans [27]. Furthermore, valvular calcification observed in Notch1 haploinsufficient patients is more severe, suggesting a direct role of Notch1 signaling in the calcification process.

Recent investigations of the role of Notch1 deficiency in CAVD have been variable. Acharya et al. demonstrated through chemical inhibition that Notch1 has an inhibitory role on the development of CAVD [99]. Further, Nigam et al. showed that Notch1 signaling specifically affects osteogenic pathways in AVICs, preventing the progression of osteogenic calcification [94]. Conversely, Zeng et al. recently indicated that Notch1 in fact promotes osteogenic calcification in human AVICs [171]. These disparate findings highlight the need for further studies in order to elucidate the pathological alterations due to Notch1 mutation. One major limitation of studies evaluating the effect of the Notch1 mutation is lack of a consistent method to recapitulate the effects of the mutation *in vitro*. Many studies utilize N-[N-(3,5-difluorophenacetyl-L-alanyl]-S-phenylglycine t-butyl ester (DAPT), a chemical inhibitor of γ-secretase, to mimic Notch1 haploinsufficiency; however, DAPT has potential off target effects [94, 99, 171]. Therefore, isolation and study of AVICs from Notch1$^{+/-}$ mice represents a more accurate approach to evaluate the Notch1 mutation *in vitro*.

In this study, we isolated Notch1 mutant AVICs from Notch1$^{+/-}$ Immortomice for the first time. Using these cells, we found that Notch1$^{+/-}$ AVICs display reduced αSMA and Runx2, but notably increased cadherin-11 expression. We determined that upregulated cadherin-11 expression is mediated

by enhanced protein kinase B (Akt) phosphorylation and activity in the mutant cells. Further, the inhibition of Akt phosphorylation led to a dramatic decrease in cadherin-11. The involvement of Notch signaling in cadherin-11 expression is a novel finding directly linking Notch1 heterozygosity with a hallmark of CAVD. Lastly, Notch1$^{+/-}$ AVICs were shown to be hypersensitive to mechanical strain resulting in significant increases in αSMA expression and formation of CNs. These findings reveal that CAVD arising from the Notch1$^{+/-}$ mutation proceed through increased cell-cell mechanotransduction via cadherin-11, which in a dynamic environment leads to differentiation of AVICs into myofibroblasts that then undergo dystrophic calcification.

6.2 – Methods

6.2.1 Overview

WT and Notch1$^{+/-}$ murine AVICs were isolated from WT and Notch1$^{+/-}$ Immortomice and expanded in culture. WT and mutant cells were assessed for calcification potential, protein expression alterations, cell signaling dysfunction, and response to mechanical strain. All experiments were conducted on BioFlex Pronectin plates unless otherwise indicated.

6.2.2 Notch1$^{+/-}$ Mice and Genotyping

On a CD1 background, mice carrying the Notch1^{tm1Con} allele were crossed to “immortomouse”(Charles River, 237 HO, 238 HE) to obtain the Notch1$^{+/-}$ Immorto genotype [172, 173]. Mouse lines were outcrossed onto CD1 and maintained as sibling matings. Genotyping was performed by polymerase chain reaction analysis using the primer pairs (f: GATATCGTGG TGCATACCCTCCTG; r: GTGGTC TAGGATGCTTGGGTCTAG) for the Notch1 WT allele, (f: GATATCGTGGTGCATACCCTCCTG; r: GTCAGTTTCATAGCC TGAAGAACG) for the Notch1 null allele, (f: CCTCTGAGCTATTC CAGAAGTAGTG; r: TTAGAGCTTTAAATCTCTGTAGGTAG) for the Immorto allele. All breeding and experimental procedures were done with prior approval by the Vanderbilt Institutional Animal Care and Use Committee.

6.2.3 Atomic Force Microscopy Analysis

Murine aortic valve leaflets from wild type and Notch1+/- mutants were processed as previously described for micromechanical measurement with AFM [158]. Briefly, 12 month old mice were sacrificed and whole hearts were excised into cold PBS. Samples were flash frozen without fixation in OCT and cryosectioned at 10 μm. Sections were prepared for AFM analysis by rinsing out the OCT in PBS, blocking with 10% FBS for 30 min. Slides were washed in PBS 3X, rinsed in ddH_2O, and immediately subjected to AFM analysis (Bruker, Santa Barbara, CA). Scanning was completed on multiple 30 μm X 30 μm areas using

borosilicate glass particle tips with a nominal diameter of 3 μm and spring constant of 0.03 N/m. The tip was calibrated to a 2.5 MPa poly(dimethysiloxane) standard prior to sample analysis. For each animal, a minimum of two scans on each of three sections were analyzed and a median modulus value was calculated for each scan. Median values were aggregated to create average modulus for the samples for statistical comparisons.

6.2.4 Von Kossa Staining

For calcification analysis, slides with sections adjacent to those analyzed via AFM were stained using the von Kossa protocol. Samples were fixed using 10% neutral buffered formalin prior to incubation with silver nitrate. After dehydration and mounting, samples were imaged using a Nikon Eclipse E800 microscope (Nikon Inc., Melville NY) with a Spot RT3 camera (Spot Imaging Solutions, Sterling Heights, MI).

6.2.5 Immunohistochemistry

Unfixed frozen 10 μm sections adjacent to those analyzed via AFM and von Kossa were stained for cadherin-11. Briefly, samples were fixed for 15 min in 4% paraformaldhyde, blocked for 1 h using 10% FBS, incubated with anti-cadherin-11 antibody at 1:100 (Cell Signaling, Boston, MA) in 1% FBS for 2 h at room temperature, washed with PBS + 0.01% Tween, incubated with 1:300 αSMA conjugated to Cy3 (Sigma, St. Louis, MO) and 1:300 Alexa-Flour 647 for 1

h at room temperature. Slides were mounted using ProLong Godl Anti-Fade reagent with DAPI (Invitrogen, Grand Island, NY) and imaged using Olympus BX53.

6.2.6 WT and Notch1$^{+/-}$ AVIC Isolation and Culture

WT and Notch1$^{+/-}$ AVICs were isolated and expanded *in vitro* for the first time. WT and Notch1$^{+/-}$ Immortomice (4-6 weeks) were euthanized, and aortic valve leaflets were excised. The tissue was digested in a 600 U/mL collagenase solution (Worthington Biochemical Corp, Lakewood, NJ) for 1 h at room temperature. Leaflets were carefully pipetted onto 0.1% gelatin coated TCPS and allowed to adhere for 2 days in immortalized media (10% FBS, 1% penicillin/streptomycin antibiotic, 10 U/mL INF-Y) at 33° C and 5% CO_2. Tissue cultures were monitored as AVICs migrated onto the tissue culture polystyrene. Each animal was able to generate one unique cell line, and cells were characterized via morphological assessment and confirmation of the presence of αSMA. Cells were expanded and cryopreserved for experimentation. Prior to experimentation, cells were transitioned at 37° C and 5% CO_2 overnight. Four independent cell lines for WT and Notch1$^{+/-}$ mice were used in this study. This murine AVIC system represents a strong *in* vitro model for studying Notch1 deficiency; however, cell signaling molecules could vary from human specimen.

6.2.7 AVIC Treatment and Analysis

All experiments were conducted on BioFlex Pronectin culture plates unless otherwise stated. These plates were chosen because the stiffness of the BioFlex substrate is approximately on the order of magnitude of the WT and Notch1$^{+/-}$ valve leaflets. In order to analyze signaling changes between WT and mutant AVICs, cells were serum starved for 3 h, treated with 1 ng/ml TGF-β1 (R&D Systems, Minneapolis, MN) and 100 ng/ml BMP2 (R&D Systems, Minneapolis, MN) for 30 minutes, and assessed via Western blotting. For inhibition of signaling pathways, cells were similarly serum starved for 3 h and treated with 10 μM U0126, a MEK1/2 inhibitor specific to Erk1/2 phosphorylation, and SB 203580 at 1 μM and 10 μM to inhibit p38 and Akt, respectively, for 30 minutes [174]. AVICs were lysed and analyzed via Western blotting. In order to assess the role of GSK-3β, GSK-3β activity was inhibited by the treatment of 20 μM LiCl (Sigma, St. Louis, MO) for 24 h in full media.

6.2.8 Immobilized Jagged1-Fc

The process of ligand immobilization was performed as previously described [175]. Briefly, tissue culture plates were incubated in a solution of goat anti-human IgG antibody (20 μg/ml) (Sigma, St. Louis, MO) in PBS for 30 minutes at 37°C and then blocked with growth media for 30 minutes. Plates were then incubated with either human IgG (10 μg/ml) (Sigma, St. Louis, MO) or Jag1-

Fc (10μg/ml) (R&D Systems, Minneapolis, MN) for 2 h at 37°C. After incubation, plates were washed two times in growth media and then seeded with cells.

6.2.9 Mechanical Strain Analysis and Calcific Nodule Assay

WT and Notch1$^{+/-}$ AVICs were plated on BioFlex Pronectin culture plates (Flexcell International Corporation, Hillsborough, NC) at 5x10^4 cells/cm^2 in normal growth media and were given a day to reach confluence. Growth media was replaced with fresh growth media and the cells were then subjected to equibiaxial strain via the Flexcell-4000 Tension System at a strain magnitude of 10% and a frequency of 1 Hz for designated times. For CN assays, WT and mutant cells were seeded on BioFlex plates at 7x10^4 cells/cm^2 in normal growth media. Normal growth media was then removed and replaced with growth media supplemented with 1 ng/ml TGF- β1 and then subjected to equibiaxial strain at a strain magnitude of 10% and a frequency of 1 Hz for 24 h. CNs were stained with Alizarin red and counted via standard light microscopy.

6.2.10 Assays for Cell Viability

AVICs were rinsed with PBS and stained with Annexin V conjugated with Alexa fluor 488 (5% solution in Annexin binding buffer; Invitrogen, Grand Island, NY) for 15 minutes to detect apoptotic cells. PI (0.4% solution in Annexin binding buffer; Invitrogen, Grand Island, NY) was used as a counter-stain for necrotic cells. Apoptosis and necrosis images were taken after 24 h of equibiaxial strain using a fluorescence microscope (Nikon TE300 Inverted Tissue Culture Microscope).

6.2.11 Immunofluorescence

AVICs were plated on fibronectin functionalized coverslips and treated with 1 ng/mL TGF-β1 for 24 h. The cells were then fixed in 3.7% formaldehyde, permeabilized with 0.1% Triton X-100, and blocked with 1% bovine serum albumin for 1 h at room temperature. A primary antibody to cadherin-11 (Cell Signaling, Boston, MA) was added to the coverslips for 3 h at room temperature. After thorough washing in PBS, a fluorescently labeled secondary antibody (Alexa Fluor 488, Invitrogen, Grand Island, NY) was added to the coverslip with a primary antibody to αSMA conjugated with Cy3 (Sigma, St. Louis, MO) for 1 h. The coverslips were then washed and sealed with ProLong Gold antifade reagent (Invitrogen, Grand Island, NY) overnight prior to imaging with a Nikon Eclipse E800 equipped with a Spot RT3 camera.

6.2.12 Western blotting

AVICs were washed twice in PBS and lysed with RIPA buffer supplemented with protease and phosphatase inhibitors (Roche, Basel, Switzerland) and centrifuged to remove membrane components. Protein quantification was conducted via BCA Protein Assay (Pierce, Rockford, IL), and samples were normalized. Proteins were separated via SDS-Page and transferred onto a nitrocellulose membrane (Li-Cor, Lincoln, NE). Membranes were blocked in milk for 1 h and incubated with primary antibody overnight at 4°C. Membranes were then washed 3X in PBS and incubated for 40 min with secondary antibody followed by 3 washes and imaged via Oddessy CLx (Li-Cor, Lincoln, NE).

6.2.13 Statistical Analysis

The data are reported as the mean of all replicates, and error is given as standard error of the mean. Statistical significance between treatments was determined by one-way ANOVA and Holm-Sidek tests.

6.3 – Results

6.3.1 Notch1 mutation is characterized by enhanced calcification, increased mechanical stiffness, and alterations to cadherin-11 and Runx2 expression

Tissue level characterization demonstrated that Notch1$^{+/-}$ valves have enhanced calcification, elevated cadherin-11, and increased mechanical stiffness. Von Kossa staining of the valve leaflets revealed higher uptake of stain in the Notch1$^{+/-}$ animals (Fig. 6.1A(a,b)). Accumulation of Von Kossa stain was evenly distributed throughout the tissue and no punctate stain was observed in the leaflets. Immunohistochemistry analysis of valve tissue revealed enhanced cadherin-11 staining in the Notch1$^{+/-}$ leaflets (Fig. 6.1A(c,d)). Further, biomechanical analysis of leaflet tissue via atomic force microscopy (AFM) indicated that Notch1$^{+/-}$ valve leaflets are significantly stiffer than WT leaflets (Fig. 6.1B). WT Immorto and Notch1$^{+/-}$ Immorto genotype was confirmed with PCR (Fig. 6.1C). Protein level analysis confirmed that Notch1$^{+/-}$ AVICs have reduced NICD cleavage (Fig. 6.1D). Notch1$^{+/-}$ AVICs also express less αSMA and Runx2 but significantly more cadherin-11 (Fig. 6.1E). Upon Jagged1 stimulation, αSMA

expression was unchanged (Fig. 6.1F), cadherin-11 expression was reduced (Fig. 6.1G), and Runx2 expression was increased (Fig. 6.1H).

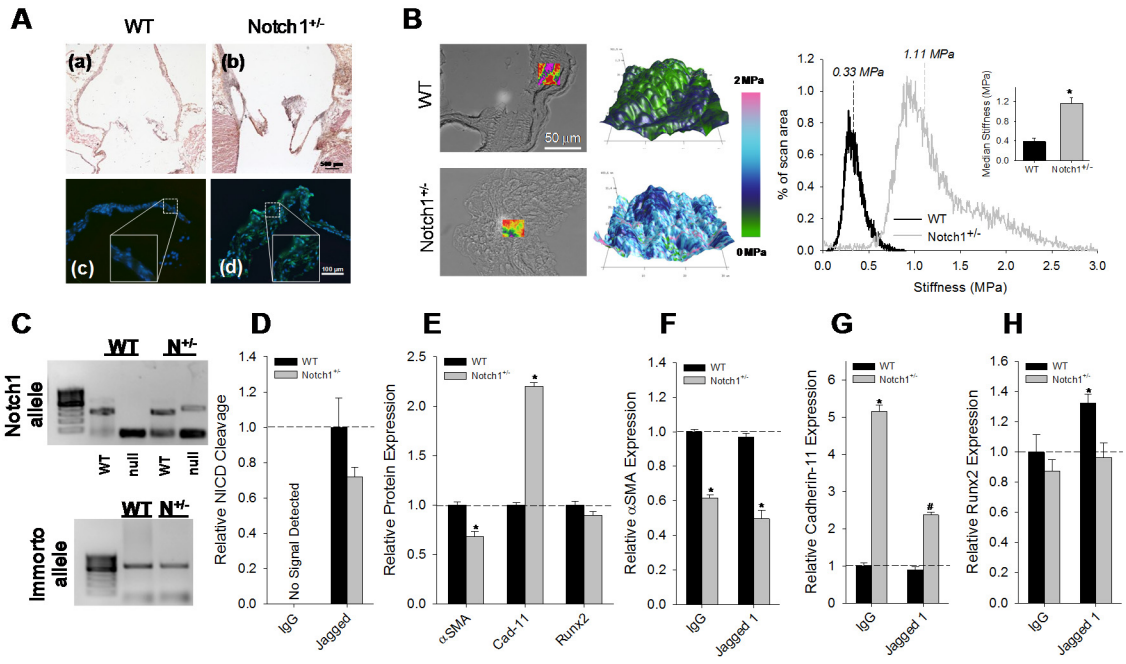

Fig. 6.1 – Notch1 mutation is characterized by enhanced calcification, increased mechanical stiffness, and alterations to cadherin-11 and Runx2 expression. Notch1$^{+/-}$ mice displayed increased calcification (brown) as evidenced by Von Kossa stain (A(a,b)) and cadherin-11 expression (green) by immunohistochemistry (A(c,d)). Aortic valve leaflets from Notch1$^{+/-}$ mice are significantly stiffer as revealed by AFM analysis. The drawn vertical lines represent median modulus values, which are aggregated and plotted in the bar graph (B). PCR confirms Notch1$^{+/-}$ heterozygosity and immortalization (C) and this results in decreased NICD cleavage (D). Notch1$^{+/-}$ AVICs display decreased αSMA and Runx2 expression but significantly increased cadherin-11 expression (E). Upon Notch1 activation via Jagged stimulation, αSMA is not significantly changed (F); however, cadherin-11 expression is decreased (G), whereas Runx2 expression is increased (H). * indicates significant difference ($P<0.05$) vs WT control and # indicates significant difference ($P<0.05$) vs Notch1$^{+/-}$ control.

6.3.2 Notch1$^{+/-}$ AVICs have dysregulated MAPK and PI3K/Akt Signaling

We evaluated the effect of TGF-β1 and BMP2 stimulation on important signaling pathways such as TGF-β/BMP, MAPK, and PI3K/Akt, which all have been shown to be involved in the calcification process [17, 19, 123, 149, 163]. Notch1$^{+/-}$ AVICs have higher basal levels of Smad3 and Smad1/5/8 phosphorylation, but TGF-β1 and BMP2 treatment led to insignificant phosphorylation differences between WT and mutant AVICs (Fig. 2A,B). Erk1/2 and p38, signaling molecules of the MAPK pathway, had significantly decreased levels of phosphorylation in the Notch1$^{+/-}$ AVICs (Fig. 2C,D). Conversely, Notch1$^{+/-}$ AVICs displayed significantly increased Akt phosphorylation at both Thr308 and Ser473 with minimal change with TGF-β1 and BMP2 stimulation (Fig. 2E,F).

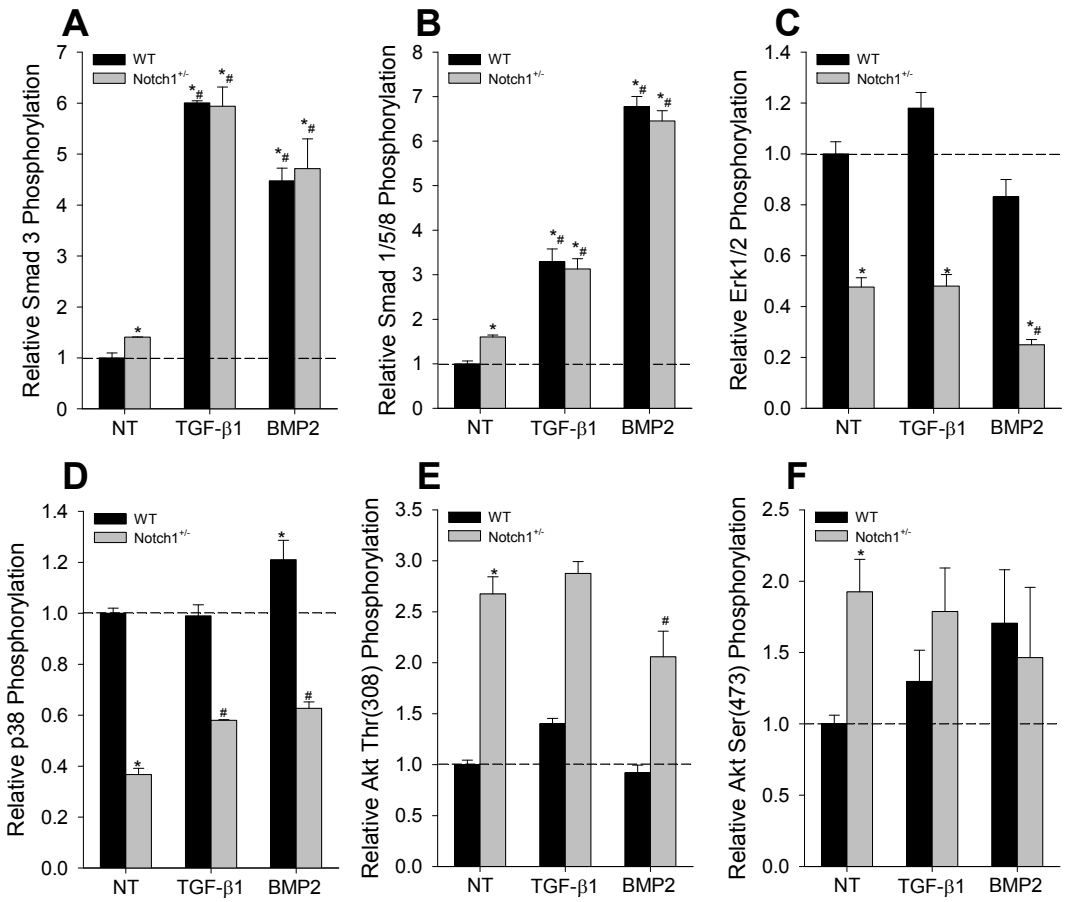

Fig 6.2 – Notch1$^{+/-}$ AVICs have dysregulated MAPK and PI3K/Akt Signaling. TGF-β1 and BMP2 stimulation leads to comparable increases in Smad3 and Smad1/5/8 phosphorylation in both WT and Notch1 deficient cells (A,B). MAPK signaling is dysregulated with significant decreases in Erk1/2 and p38 phosphorylation in the mutant cells (C,D). Additionally, PI3K/Akt signaling is enhanced in the mutant cells with increased Akt phosphorylation at both Thr308 and Ser473 (E,F). * indicates significant difference ($P<0.05$) vs WT control and # indicates significant difference ($P<0.05$) vs Notch1$^{+/-}$ control.

6.3.3 Upregulated cadherin-11 expression in Notch1$^{+/-}$ AVICs is enhanced Akt activity

Because Erk1/2, p38, and Akt signaling were abnormal in Notch1$^{+/-}$ cells, we sought to determine their role in cadherin-11 expression by inhibiting their activity. We treated WT and Notch1$^{+/-}$ AVICs with a MEK1/2 inhibitor (U0126), which prevents Erk1/2 phosphorylation, a p38 inhibitor, and an Akt inhibitor. U0126 and p38 inhibitor treatment did not significantly affect cadherin-11 expression in either cell type; however, Akt inhibition led to near complete abrogation of cadherin-11 expression (Fig. 6.3A). Because of the dramatic response due to Akt inhibition, we further evaluated the PI3K/Akt pathway. Akt phosphorylation was expectedly inhibited by the Akt inhibitor (Fig. 6.3B,C), and glycogen synthase kinase 3β (GSK-3β) phosphorylation increased with Akt inhibition (Fig. 6.3D). The role of GSK-3β activity in cadherin-11 expression was assessed with lithium chloride (LiCl) treatment, a GSK-3β inhibitor, which caused a significant reduction in GSK-3β activity and cadherin-11 (Fig. 6.3E,F).

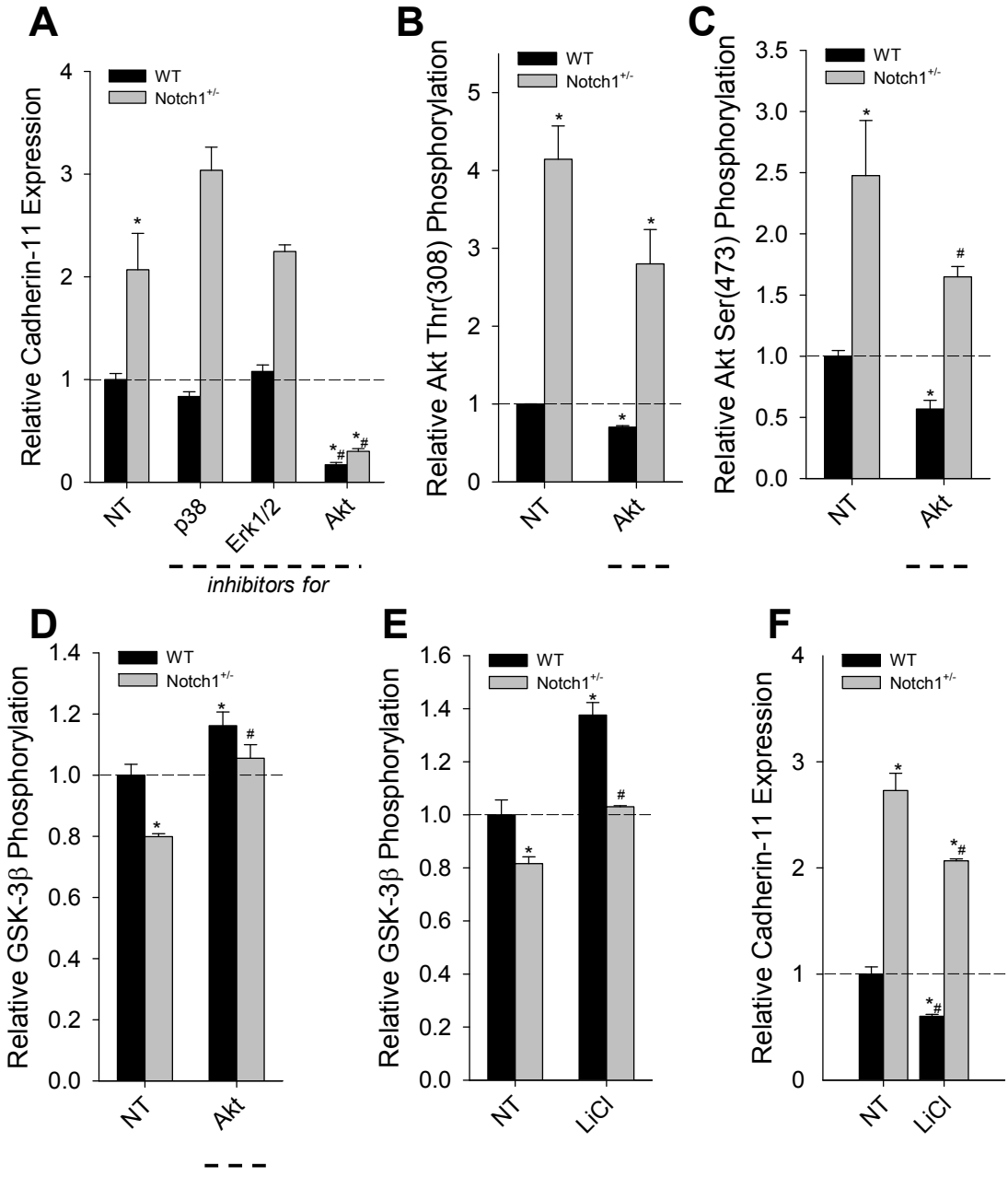

Fig 6.3 – *Upregulated cadherin-11 expression in Notch1$^{+/-}$ AVICs is mediated by enhanced Akt activity.* Cadherin-11 expression is significantly reduced by the Akt inhibitor in both WT and Notch1$^{+/-}$ AVICs (A). The inhibition of Akt leads to a significant decrease in Akt phosphorylation at Thr308 and Ser473 (B,C). Further, Akt inhibition leads to decreased GSK-3β activity as evidenced by an increase in GSK-3β phosphorylation (D). LiCl treatment reduces GSK-3β activity (E) and leads to a decrease in cadherin-11 expression (F). * indicates significant difference ($P<0.05$) vs WT control and # indicates significant difference ($P<0.05$) vs Notch1$^{+/-}$ control.

6.3.4 Deficient Notch1 signaling leads to hypersensitivity to mechanical strain and myofibroblast activation

Strain induced activation of Notch1 signaling is reduced in the Notch1$^{+/-}$ AVICs as evidenced by a decrease in NICD cleavage (Fig. 6.4A). With the application 10% cyclic mechanical strain, which approximates *in vivo* diastolic loading, αSMA expression is dramatically increased, cadherin-11 expression remains unchanged, and Runx2 expression is decreased (Fig. 6.4B-D). Notably, unstrained Notch1$^{+/-}$ AVICs have less αSMA than WT but exceed the WT cells when strained. WT and Notch1$^{+/-}$ AVICs both have increased phosphorylation of Erk1/2 and p38 under stretch (Fig. 6.4E,F). Similarly, Akt phosphorylation at Ser473 was increased with mechanical strain in both cell types. As with αSMA, phosphorylation of Akt Ser473 underwent larger increases due to strain in Notch1$^{+/-}$ AVICs (Fig. 6.4G). Akt phosphorylation at Thr308 (data not shown) and GSK-3β phosphorylation were not significantly affected due to mechanical strain (Fig. 6.4H).

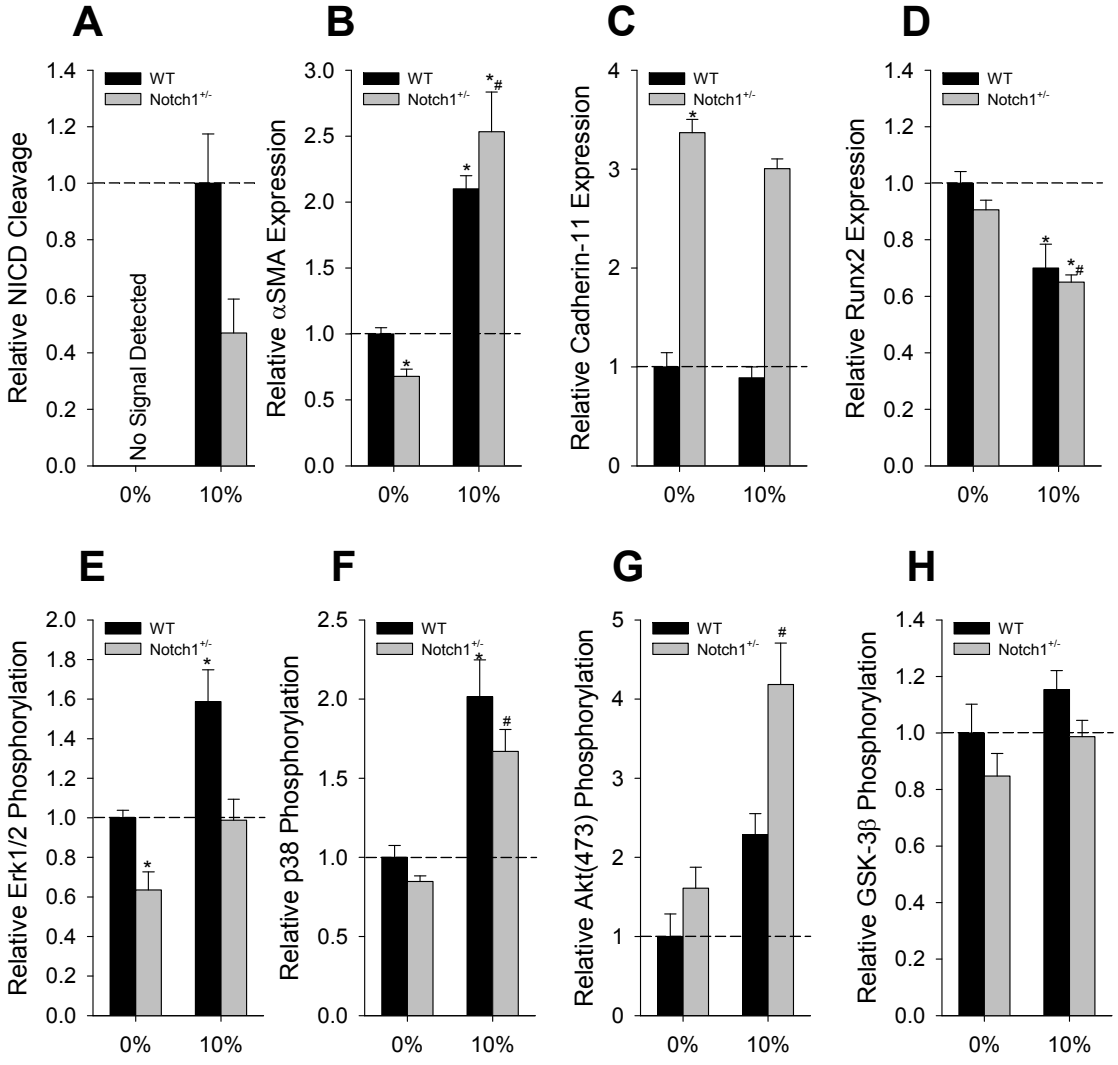

Fig. 6.4 – *Deficient Notch1 signaling leads to hypersensitivity to mechanical strain and myofibroblast activation.* Mechanical strain leads to increase release of NICD this activation is reduced in Notch1$^{+/-}$ cells (A). Mechanical strain leads to increased αSMA expression, no change in cadherin-11, and a significant reduction in Runx2 expression (B-D). MAPK signaling is enhanced with strain with similar relative increases between WT and Notch1$^{+/-}$ cells (E,F). However, Akt Ser473 display an exaggerated increase in mutant cells in the presence of strain (G). Furthermore, no significant changes were observed in GSK-3β phosphorylation (H). * indicates significant difference ($P<0.05$) vs WT control and # indicates significant difference ($P<0.05$) vs Notch1$^{+/-}$ control.

6.3.5 Notch1$^{+/-}$ AVICs have active cadherin-11 engagement and calcify through a dystrophic pathway

Immunostaining revealed that Notch1$^{+/-}$ AVICs have significantly more cadherin-11; however, WT cells have more αSMA than mutant cells (Fig. 6.5A,B). When treated with TGF-β1, however, both WT and Notch1$^{+/-}$ AVICs revealed increases in αSMA and cadherin-11 (Fig. 6.5C,D). CN formation was assessed in a physiologically relevant strain (10%) system as previously described [148]. Notch1$^{+/-}$ AVICs formed significantly more CNs than WT cells with and without TGF-β1; however, TGF-β1 treatment dramatically increased the number of nodules formed (Fig. 5E). Apoptosis and necrosis stains were conducted to describe nodule viability. Annexin V and PI stains revealed significant uptake of PI in the nodule center and faint Annexin V stain on the periphery of the nodule characteristic of dystrophic calcification (Fig. 6.5F,G,I,J). CNs from both genotypes were intensely stained via Alizarin red, a calcification stain (Fig. 6.5H,K).

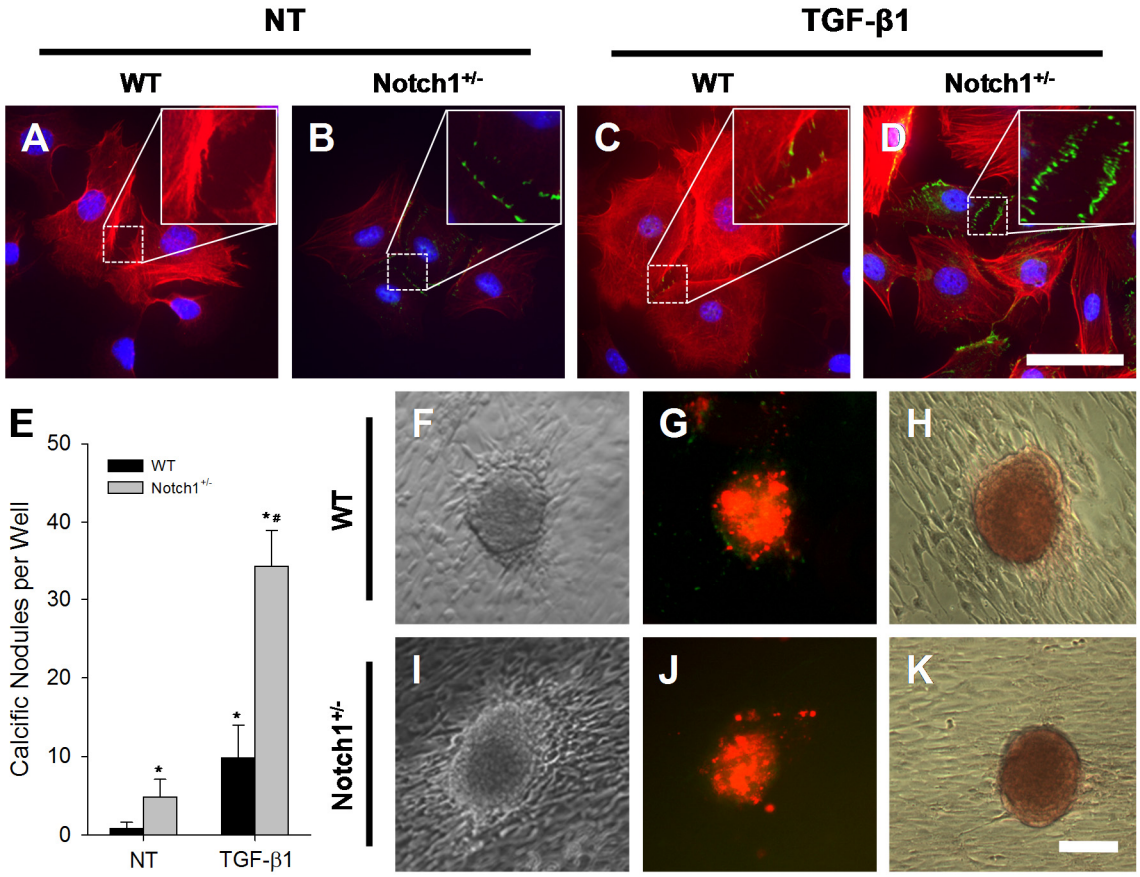

Fig. 6.5 – *Notch1+/- AVICs have active cadherin-11 engagement and calcify through a dystrophic pathway.* Notch1$^{+/-}$ AVICs show reduced αSMA expression (red) but enhanced cadherin-11 expression (green) (A,B). Upon TGF-β1 treatment, αSMA and cadherin-11 are both increased with Notch1$^{+/-}$ AVICs displaying comparable αSMA and more cadherin-11 stain than the WT cells (C,D). Dynamic nodule assay demonstrates more robust nodule formation in Notch1$^{+/-}$ cells in the presence and absence of TGF-β1 (E). Annexin/PI stain for apoptosis (green) and necrosis (red) reveals intense uptake of PI stain for both WT nodules (F,G) and Notch1$^{+/-}$ nodules (I,J). Additionally, WT and Notch1$^{+/-}$ nodules stained positively for Alizarin red, a calcium stain (red) (H,K). Scalebar = 100 μm. * indicates significant difference ($P<0.05$) vs WT control and # indicates significant difference ($P<0.05$) vs Notch1$^{+/-}$ control.

6.4 – Discussion

There are four notable findings in this study: (1) Notch1 mutation leads to AVICs with a myofibroblast-like phenotype as evidenced by increased cadherin-11 expression, (2) upregulated cadherin-11 expression is mediated by increased Akt activity, (3) Notch1$^{+/-}$ AVICs become fully activated myofibroblasts in the presence of mechanical strain, and (4) activated Notch1$^{+/-}$ AVICs lead to enhanced dystrophic calcification *in vitro*.

Previous studies evaluating the role of Notch1 mutation in CAVD have been variable and have primarily focused on Notch1 signaling in osteogenic calcification [27, 94, 95, 99, 176]. However, our data suggests that Notch1$^{+/-}$ AVICs suppress osteogenic differentiation and follow a myofibroblast-like phenotype. We found that Notch1$^{+/-}$ AVICs display decreased Runx2 expression (Fig. 6.1E), which is essential for osteogenic differentiation [177]. Moreover, the activation of Notch1 via Jagged1 ligand binding significantly increased the expression of Runx2 in WT cells (Fig. 6.1H), suggesting that the activation of Notch1 signaling could in fact induce osteogenic differentiation. This is consistent with a recent report highlighting the role of Notch1 in promoting osteogenic responses in human AVICs [171]. Conversely, several studies have indicated that canonical Notch1 signaling plays a protective role by preventing the transcription of Runx2 mRNA and subsequent osteogenic differentiation [27, 99]. However, in these systems, Notch1 deficiency was simulated through DAPT treatment which affects all Notch signaling and may have unknown off target effects that confound the data, and changes in mRNA level do not necessarily

translate to changes in protein expression, which we show here. Interestingly, Notch signaling has also been implicated in the regulation of myofibroblast differentiation. Sassoli et al. demonstrated that reduced Notch1 signaling lead to myofibroblast differentiation and αSMA expression in cardiac fibroblasts [178]. Further, Fan et al. showed that this phenotypic shift was associated with a reduction in Notch receptor and ligand expression [179]. Here, we show that Notch1 deficient AVICs exhibit myofibroblast-like properties that promote dystrophic CAVD.

The transition of fibroblasts to myofibroblasts is a complex process that often occurs after tissue injury [67, 77]. The myofibroblast is crucial to the tissue repair process but the persistence of this phenotype can lead to pathological remodeling of the ECM. Many factors influence this transition from fibroblasts to myofibroblasts including inflammatory signals and the mechanical environment [77]. Myofibroblast differentiation occurs through two stages, first to an intermediate cell phenotype, the protomyofibroblast, and then to the fully activated myofibroblast. Protomyofibroblasts possess myofibroblast-like properties with changes in focal adhesions proteins and stress fibers, but they do not express αSMA [67]. When in the presence of TGF-β1 and/or mechanical stretch, protomyofibroblasts become differentiated myofibroblasts characterized by αSMA and cadherin-11 [16]. In CAVD, myofibroblasts are thought to contribute directly to the thickening and stiffening of stenotic valves as well as the dystrophic calcification observed in diseased tissue explants [180]. We demonstrated in a previous study that the presence of cadherin-11 coupled with

increased contractility via αSMA leads to apoptosis and subsequent cell aggregation and calcification in AVICs [149]. Additionally, we found that human leaflets excised from patients with CAVD were highly enriched in cadherin-11 that was colocalized with αSMA in areas of significant calcification. In the present study, we found that reduced Notch1 signaling leads to significant alterations to myofibroblast markers. The expression of the myofibroblast marker cadherin-11 was dramatically increased in Notch1$^{+/-}$ AVICs (Fig. 1A,E). Activation of Notch1 signaling reduced cadherin-11 (Fig. 1G), suggesting that the increase in cadherin-11 expression was due to Notch1 deficient signaling. Surprisingly, the myofibroblast marker αSMA was reduced in the mutant cells and this reduction was not affected by Notch1 activation, suggesting that these changes are indirectly affected by dysregulated Notch1 signaling. Taken together, Notch1$^{+/-}$ AVICs represent a phenotype that resembles an intermediary myofibroblast expressing enhanced cadherin-11, reduced αSMA, and decreased osteogenic activity.

Cadherin-11 is a type II classical cadherin that plays significant roles in normal development and many diseases such as inflammatory disorders and cancer [70, 134, 181-184]. First observed in osteoblasts, cadherin-11 has now been associated with a variety of fibrotic diseases such as pulmonary fibrosis, dermal fibrosis, and CAVD [134, 149, 185]. Cadherin-11 is a unique intercellular junction from a biomechanical perspective because it resists two fold higher forces than typical cadherins such as N-cadherin, thus creating tighter, stronger junctions [120]. These unique characteristics are essential to the progression of

dystrophic calcification in CAVD, as we showed in a previous study that knockdown of cadherin-11 prevents calcification of porcine AVICs, even when exposed to TGF-β1 [149]. We identified a functional role of cadherin-11 in CAVD; however, the regulation of cadherin-11 expression is unknown in AVICs. In the present study, cadherin-11 expression is dramatically increased in Notch1 deficient AVICs; therefore, we examined downstream mediators from Notch1 that may alter cadherin-11 expression. MAPK and PI3K/Akt signaling were highly dysregulated in Notch1$^{+/-}$ AVICs with reduced p38 and Erk1/2 phosphorylation, but significantly increased Akt phosphorylation at both Ser473 and Thr308 (Fig. 2D-F). Using inhibitors for these pathways, we found that p38 and Erk1/2 inhibition did not significantly affect cadherin-11 levels, but the inhibition of Akt dramatically abrogated cadherin-11 expression (Fig. 3A). Akt is a central node in the PI3K/Akt pathway and is responsible for a plethora of cellular processes including cell survival, proliferation, metabolism, and migration [186]. When PI3K is activated, it converts phosphatidylinositol (3-5)-bisphosphate to phosphatidylinositol (3-5)-trisphosphate which recruits Akt to the plasma membrane leading to its phosphorylation via phosphoinositide-depedent kinase 1 (PDK1) and mammalian target of rapamycin complex 2 (mTORC2) at Thr308 and Ser473, respectively [187]. Activated Akt phosphorylates a wide variety of substrates mediating multiple cellular events. Interestingly, GSK-3β, a downstream substrate of Akt, has been implicated in cadherin-11 expression in prostate and breast cancer cells with the inactivation of GSK-3β leading to a reduction in cadherin-11 mRNA and protein levels [188]. We therefore assessed

the role of GSK-3β in our cells by inhibiting its activity via LiCl treatment. We found that LiCl led to a significant decrease in GSK-3β activity and a significant reduction in cadherin-11 expression; however, the decrease in cadherin-11 expression was modest when compared with the decrease observed with inhibition of Akt (Fig. 3F). This moderate decrease in cadherin-11 suggests that there are other downstream substrates of Akt that are involved in cadherin-11 expression but that GSK-3β plays a significant role. Future studies examining other Akt substrates would be beneficial in determining the signaling mechanisms involved in cadherin-11 expression. Here, we identify a novel mechanism by demonstrating that Notch1 deficient signaling leads to increased cadherin-11 expression through enhanced Akt signaling and, at least partially, through increased GSK-3β activity.

AVICs reside in a highly dynamic environment and undergo constant cyclic mechanical strain *in vivo*. Further, AVIC mechanobiology is directly influenced by mechanical strain, and we and others have previously shown that increased magnitude of strain plays a significant role in the initiation and progression of CAVD [35, 148, 189, 190]. We hypothesized that Notch1$^{+/-}$ AVICs may have alterations in their mechanotransductive response to strain that would lead to early disease and CAVD observed in Notch1 haploinsufficient patients. Our data show that Notch1 signaling is activated by mechanical strain, and this activation is decreased in Notch1$^{+/-}$ AVICs (Fig. 6.4A). We hypothesized that this decrease in mechanically induced NICD cleavage in the mutant cells may lead to deleterious changes that contribute to CAVD. Our data reveal that mechanical

strain led to increased αSMA expression with no change in cadherin-11 expression, and a drastic reduction in Runx2 expression (Fig. 6.4B-D). Notably, Notch1$^{+/-}$ AVICs had higher αSMA expression than WT cells under strain. Analysis of signaling proteins revealed an exaggerated Akt Ser473 phosphorylation response to mechanical strain in Notch1$^{+/-}$ AVICs (Fig. 6.4G). Interestingly, Wang et al. connected Akt Ser473 phosphorylation with αSMA expression by demonstrating that stiffer substrates activate Akt Ser473 and push the cell towards a myofibroblast phenotype [163]. Akt signaling has been shown to be regulated by Notch1; however, their relationship is not well understood [191-193]. In our system, Notch1$^{+/-}$ AVICs have increased Akt phosphorylation suggesting that Notch1 activation decreases Akt phosphorylation. It is possible that Notch1 plays a protective role in preventing myofibroblast differentiation by modulating Akt Ser473 activity. The loss of this regulatory mechanism in the Notch1$^{+/-}$ cells allows for an unfettered increase in phosphorylation of Akt Ser473 and subsequent αSMA upregulation.

In the presence of mechanical strain, Notch1$^{+/-}$ AVICs become fully activated myofibroblasts as evidenced by the presence of both αSMA and cadherin-11. Interestingly, the presence of mechanical strain also decreased Runx2 expression (Fig. 6.4D) further supporting the notion of Notch1$^{+/-}$ AVICs being pushed toward a myofibroblast phenotype. WT cells, however, did not exhibit significant changes to cadherin-11 expression due to mechanical strain and therefore do not represent a fully activated myofibroblast. We hypothesized that the presence of cadherin-11 in the Notch1$^{+/-}$ AVICs would lead to the

development of more severe calcification. We subjected WT and mutant cells to a dynamic CN assay as previously described and found significantly more CNs generated by the mutant cells with and without TGF-β1 stimulation (Fig. 6.5E) [148]. As expected, TGF-β1 treatment led to the development of significantly more CNs in both cell types. Immunostaining images revealed that TGF-β1 led to the full activation of WT cells and enhanced αSMA and cadherin-11 expression in the Notch1$^{+/-}$ AVICs (Fig. 6.5A-D). Furthermore, these nodules stained positively for cell death and resembled dystrophic CNs as previously described (Fig. 6.5G,J) [148]. These findings reveal a role of cadherin-11 for modulating calcification severity and provide evidence that enhanced cadherin-11 contributes to the development of CAVD in Notch1 haploinsufficient patients.

In this study, we demonstrate that Notch1$^{+/-}$ AVICs become fully activated myofibroblasts (increased αSMA and cadherin-11 expression), which leads to dystrophic calcification in a dynamic mechanical environment. The effect of Notch1 deficient signaling is manifest in enhanced Akt and GSK-3β activity as well as the loss of the regulation of strain induced Akt Ser 473 activation, resulting in enhanced cadherin-11 and αSMA, respectively (Fig 6.6). However, the loss of Notch1 signaling affects other relevant pathways that may contribute substantially to the regulation of AVIC phenotype. Here, we observed significant alterations to three pathways that have been implicated in myofibroblast differentiation and the development of valvular disease: TGF-β/BMP, MAPK, and PI3K/Akt. Significant cross-talk has been observed between these pathways; however, the interplay between these signaling components is not well

understood [194]. It is beyond the scope of this study to elucidate the intricate interactions and convergence between these pathways; however, our data does present novel information regarding myofibroblast differentiation and creates new directions for CAVD research.

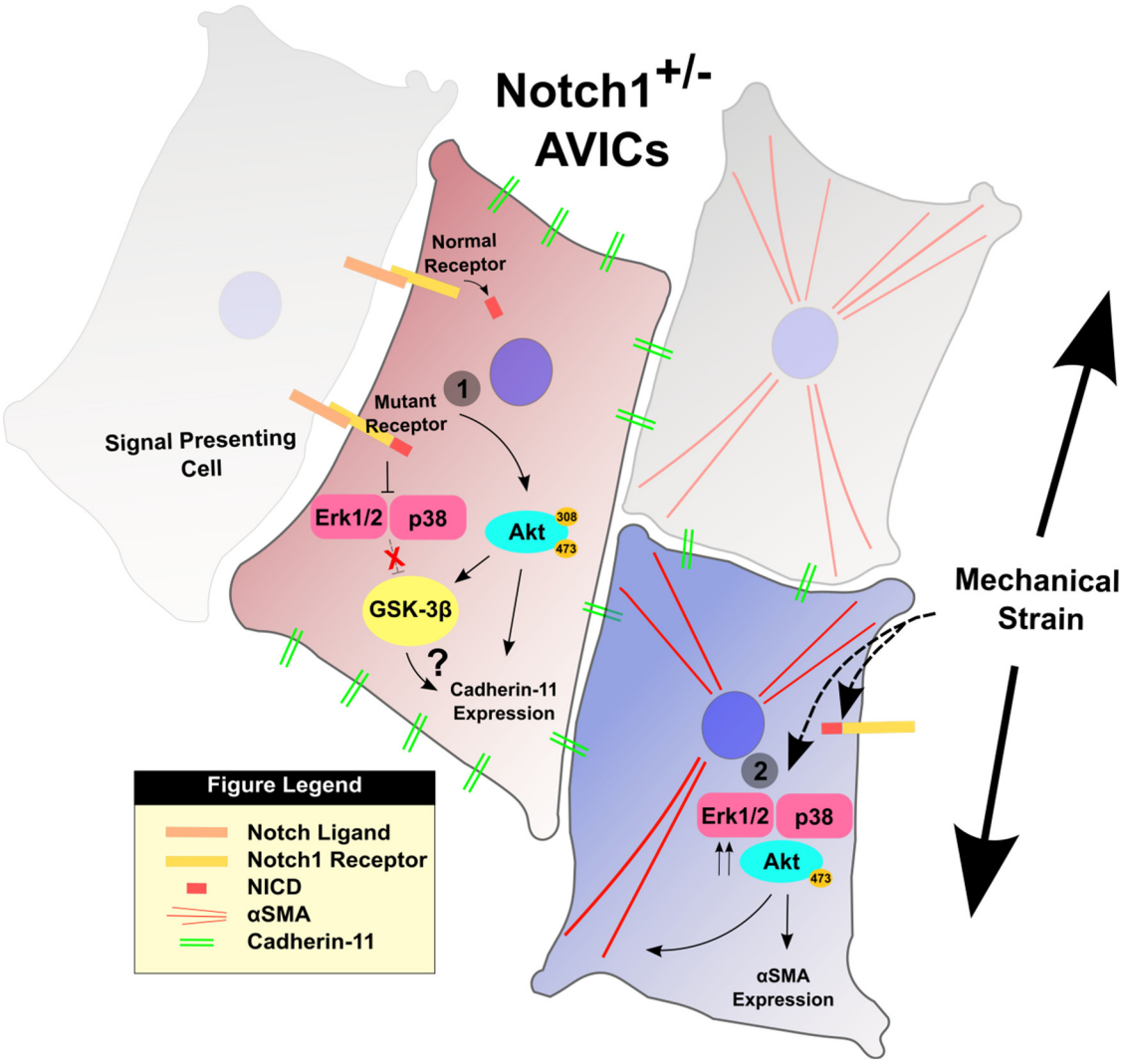

Fig. 6.6 *–Proposed mechanism for myofibroblast activation in Notch1$^{+/-}$ AVICs.* Notch1$^{+/-}$ AVICs have decreased NICD cleavage upon Notch1 activation leading to two significant alterations that lead to myofibroblast differentiation and valvular calcification. (1) First, deficient Notch1 signaling leads to an increase in Akt phosphorylation at both Thr308 and Ser473 and enhanced GSK-3β activity. Increased Akt signaling leads to increased cadherin-11 expression and is partially mediated by GSK-3β. (2) Notch1$^{+/-}$ cells exhibit reduced mechanically induced NICD cleavage leading to an exaggerated increase in Akt Ser473 phosphorylation which leads to increased αSMA expression.

The goal of elucidating CAVD mechanism is to identify significant contributors to disease that are targetable through pharmacological treatment [7]. The findings in this report are significant because they provide paradigm shifting evidence that Notch1 mutation leads to dystrophic, but not osteogenic, CAVD. Furthermore, the clear and distinct role of increased cadherin-11 in the Notch1$^{+/-}$ AVICs is significant because it has been demonstrated as a critical component of valvular calcification, and inhibition of cadherin-11 function may be a promising approach for treating CAVD. Additionally, the discovery of the role of PI3K/Akt signaling in αSMA and cadherin-11 expression presents many targetable proteins such as PDK1, mTORC2, and GSK-3β that should to be further explored.

Chapter VII

Societal Implications and Future Directions

7.1 – Summary and Impact of Results

The overall goal of this work was to investigate the role of mechanical strain and Notch1 haploinsufficiency in the initiation and evolution of CAVD. The motivation for this work was to examine factors that could generate insight towards valvular calcification *in vivo* and therefore allow for strategic approaches in the development of a pharmacological therapy for CAVD. We began addressing this goal in aim 1 by describing the role of mechanical strain in the formation of CNs. We found that mechanical strain plays an important role in the development of dystrophic CNs by disrupting the intercellular tension that is generated by activated AVICs. We found that increased strain corresponded to an increase in CN formation. Furthermore, we discovered that the nodules formed stained positively for Annexin V and PI, which indicated that this was a cell-death-mediated process. In addition to its role in disrupting the cell monolayer, we also noted that mechanical strain played a significant role in the maturation and growth of the CN. When mechanical strain was applied for 5 minutes, we observed a disruption and aggregation of cells but no CN formation;

however, with 24 hrs of continuous cyclic stretch, the aggregates formed CNs with a necrotic core. In order to describe this phenomenon, we employed a descriptive model using a modified Lamé solution, which demonstrated that continuous applied mechanical strain onto an aggregate result in the magnification of radial stretch at the aggregate periphery. These findings suggest that upon disruption of the cells and subsequent aggregation, mechanical strain is enhanced at the edge of the aggregate leading to more cell death and CN growth. The results of this study revealed that strain plays a two part role in the initiation and maturation of CNs by disrupting AVIC tension leading to aggregation, and magnifying strain around the aggregate causing CN growth. Also, this data indicates that mechanical strain promotes dystrophic calcification suggesting that *in vivo* AV calcification may have a preference for dystrophic processes.

In our investigation of mechanical strain, we became interested in how this tension based phenomenon was controlled by the AVICs. We determined that AVIC activation via TGF-β1 led to the increase of αSMA; however, increased contractility did not generate tension by itself, rather contractility must be couple with intercellular connections in order to produce tension. We tested this hypothesis by evaluating changes in AVIC cadherins upon AVIC activation and found that cadherin-11 was significantly upregulated due to TGF-β1 treatment. We found that cadherin-11 function was crucial in the build-up of tension needed for dystrophic calcification to proceed. Upon siRNA silencing of cadherin-11, CNs were unable to form even in the presence of TGF-β1 and strain. Here, we have

identified for the first time cadherin-11 as a critical regulator of dystrophic calcification. Furthermore, we found that cadherin-11 is highly enhanced in human diseased AV explants indicating its promise as a target for pharmacological intervention.

In aim 2, we delineated and defined the physiochemical and biophysical properties of *in vitro* valvular calcification. We confirmed that these assays generate structures that are similar to valvular calcification observed *in vivo*. Furthermore, we confirmed that dystrophic nodule formation was a cell-death-mediated process with the presence of a necrotic core, and osteogenic nodule formation was an active process containing living cells. Both nodule types were composed of hydroxyapatite as confirmed by EDS, yet they exhibited differences in morphology and calcification profile. Finally, AFM data revealed that CN surfaces were comprised mostly of cellular material with dystrophic nodules containing a layer of dead cells with calcification embedded within the nodule and osteogenic nodules containing osteogenic AVICs aggregated together laying down osteoid matrix on the nodule surface. These results demonstrate two independent processes resulting in two unique aggregate structures that ultimately represent the vast majority of valvular calcification. Further, these studies reveal that CNs resemble properties of calcification observed in diseased valve explants, which strengthens the impact of the *in vitro* assays.

In aim 3, we investigated the role of Notch1 signaling in the development of CAVD. We found that Notch1$^{+/-}$ valves contained more calcification and were significantly stiffer than WT age-matched littermates. Immunohistochemistry

revealed that Notch1$^{+/-}$ valves also had enhanced cadherin-11 expression. Interestingly, Notch1$^{+/-}$ AVICs exhibited significantly reduced Runx2 expression suggesting that these mutant cells were not undergoing osteogenic differentation. We identified the PI3K/Akt pathway as an important regulator of cadherin-11 expression and demonstrating important roles of Akt and its downstream substrates. Additionally, Notch1$^{+/-}$ AVICs responded to mechanical strain in a hypersensitive manner by drastically increasing Akt phosphorylation and subsequent αSMA expression. Furthermore, we observed dystrophic calcification when subjecting WT and Notch1$^{+/-}$ AVICs to a dynamic CN assay. These findings suggest that Notch1 deficiency leads to enhanced myofibroblast markers that promote dystrophic calcification. Notably, these findings also suggest that dystrophic calcification is promoted in this clinically relevant system.

7.2 Future Directions

We believe that the results presented in this dissertation provide novel insights into the mechanisms involved in valvular calcification *in vivo*. We have identified critical regulators of AVIC biology and have provided compelling evidence that CAVD progresses through primarily dystrophic processes *in vivo*. However, in order for this work to lead to the development of novel therapeutic strategies, much work remains. We have identified cadherin-11 as a crucial mediator of CN evolution *in vitro*, and we have observed its presence in regions of calcification from diseased explants; however, there is a need to demonstrate its role in the evolution of CAVD *in vivo*. Animal models of valvular calcification

such as the Notch1$^{+/-}$ mouse can be used to study the role of cadherin-11 *in vivo*. For example, crossing Notch1$^{+/-}$ mice with other transgenic animals that have cadherin-11 removed would be an exciting avenue to establish the role of cadherin-11 in CAVD. Furthermore, animal studies utilizing drugs that target cadherin-11 function would be necessary to demonstrate the efficacy of such an approach.

In addition, our understanding of cadherin-11 biology is very limited. Recent studies have demonstrated that cadherin-11 is a mechanotransduction protein and facilitates signaling through the cadherin-11 complex. It is unclear what cadherin-11 signaling modulates; however, investigating downstream targets of cadherin-11 could reveal new insights regarding the function of cadherin-11. Further mechanistic studies teasing out the signaling components involved in cadherin-11 expression are also needed in order to modulate cadherin-11 for therapeutic purposes. We have demonstrated that PI3K/Akt signaling and more specifically Akt is involved in the expression of cadherin-11; however, Akt activates a host of downstream substrates, and it is unclear which molecule is involved in cadherin-11 expression. The literature has identified several potential mediators such as β-catenin, which we have not yet explored. Furthermore, our data shows that PI3K/Akt signaling is involved in the expression of other hallmarks of CAVD, namely αSMA. The PI3K/Akt signaling pathways has only recently been shown to be involved in valvular disease and is largely unexplored in the context of CAVD, but we have demonstrated its role in the expression of the two major markers of myofibroblast activation and dystrophic

calcification. Future examination may lead to the discovery of other targets for valvular disease.

As the impact of CAVD grows in the coming years, the search for an effective pharmacological treatment becomes more pertinent. Research elucidating CAVD etiology is essential for the identification of targets that can halt or slow down the progression of CAVD. Efforts to generate insight regarding this disease process involve investigations into AVIC biology regulation and its development into valvular calcification. Further, efforts to establish and recognize the different stages of valvular calcification and the processes that are involved in each respective stage are necessary to avoid confusion in the interpretation of results. As we continue to identify the relevant cues involved in the modulation of CAVD and clarify the stages of CAVD, we will be able to advance our understanding of CAVD etiology and find other promising targets for CAVD treatment.

Appendix

Because AVICs aggregate as sheets, the cell-cell adhesion strength is greater than the cell-surface adhesion strength, and we treat this problem as a planar representation. Therefore, the underlying assumptions are the same as plane stress problems in linear elasticity that have been foundational in determining strength of materials and predicting mechanical failure. We think this description is relevant for several stages of nodule development.

The classical Lamé solution to the thick-walled cylinder (1833) can be used to describe how a calcified nodule alters the equibiaxial strain field felt by surrounding cells in our assay. This solution is more commonly used to assess how internal and external pressures of a thin slice of a long cylinder translate into radial and circumferential stresses and strains. By reversing the signs of the pressure terms in the Lamé equations, we have a mathematical solution for an outer disc responding to internal and external stresses around a central circular core. We simplify the geometry of our system to two concentric discs: an inner disc containing the cellular aggregate/nodule and an outer ring of surrounding monolayer/tissue (Fig. 3.7A). Assuming the circular core is small, these equations can be simplified. Given a range of inner stress values at the periphery of this core, we can calculate both the magnitudes and the gradient of stress and strain with radial position (Fig. 3.7B-D).

Besides greatly simplifying the complex three dimensional geometry of the heart valve, the key limitation of this model is the equations are for infinitesimal

strains, meaning they are directly proportional to length ratio. Real descriptions of strain are nonlinear functions of length ratio. Interestingly, the trends predicted by the Lamé theory for length ratio are consistent with both more advanced strain representations and experimental measurements [195-197] for the cases we have presented. While the magnitudes and decay lengths should be different in actual biological tissue due to both material properties and geometry, we expect these principles to hold true. For example, in the valve leaflet, pathological strain is mainly applied along the circumferential direction, but any rigid material (e.g. the nodule) should still enhance the strain profile while further emphasizing the critical role AVICs have in maintaining the integrity of the valve leaflet.

$a =$ radius of aggregate

$R =$ radius of the entire monolayer

$r =$ radial distance, a≤r≤R

$E_Y =$ Young's modulus of the monolayer

$\upsilon =$ Poisson's ratio of the monolayer

$\sigma_o =$ externally applied stress, due to pressure in the aorta during diastole

$\sigma_i =$ internally applied stress, due to contractility of cells in the nodule or rigidity of the nodule

$\sigma_r =$ radial stress

$\sigma_\theta =$ circumferential stress

$\varepsilon_r =$ radial strain

$\varepsilon_\theta =$ circumferential strain

ε_z = axial strain

u = displacement

The modified Lamé solution for external and internally applied tensile stresses:

$$\sigma_r(r) = [1/(R^2 - a^2)][(R^2\sigma_o - a^2\sigma_i) - (\sigma_o - \sigma_i)(aR/r)^2] \quad (1)$$

$$\sigma_\theta(r) = [1/(R^2 - a^2)][(R^2\sigma_o - a^2\sigma_i) + (\sigma_o - \sigma_i)(aR/r)^2] \quad (2)$$

$$\varepsilon_r(r) = (1/E_Y)[1/(R^2 - a^2)][(1 - v)(R^2\sigma_o - a^2\sigma_i) - (1 + v)(\sigma_o - \sigma_i)(aR/r)^2] \quad (3)$$

$$\varepsilon_\theta(r) = (1/E_Y)[1/(R^2 - a^2)][(1 - v)(R^2\sigma_o - a^2\sigma_i) - (1 + v)(\sigma_o - \sigma_i)(aR/r)^2] \quad (4)$$

$$\varepsilon_z = (-2v/E_Y)\,(R^2\sigma_o - a^2\sigma_i)/(R^2 - a^2) \quad (5)$$

$$u(r) = (1/E_Y)[r/(R^2 - a^2)][(1 - v)(R^2\sigma_o - a^2\sigma_i) + (1 + v)(\sigma_o - \sigma_i)(aR/r)^2] \quad (6)$$

For $(R \gg a)$:

$$\sigma_r(r) = \sigma_o - (\sigma_o - \sigma_i)(a/r)^2 \quad (7)$$

$$\sigma_\theta(r) = \sigma_o + (\sigma_o - \sigma_i)(a/r)^2 \quad (8)$$

$$\varepsilon_r(r) = (1/E_Y)[(1 - v)\sigma_o - (1 + v)(\sigma_o - \sigma_i)(a/r)^2] \quad (9)$$

$$\varepsilon_\theta(r) = (1/E_Y)[(1 - v)\sigma_o + (1 + v)(\sigma_o - \sigma_i)(a/r)^2] \quad (10)$$

$$\varepsilon_z = -2v\sigma_o/E_Y \quad (11)$$

$$u(r) = (r/E_Y)[(1 - v)\sigma_o + (1 + v)(\sigma_o - \sigma_i)(a/r)^2] \quad (12)$$

Equibiaxial case $(\sigma_o = \sigma_i\,,\ R \gg a)$:

$$\sigma_{eqb} = \sigma_o \tag{13}$$

$$\varepsilon_{eqb} = (1 - \upsilon)\sigma_o / E_Y \tag{14}$$

Evaluating magnitudes normalized with the equibiaxial case at the periphery of the nodule for $(R \gg a)$:

$$\sigma_r(a)/\sigma_{eqb} = \sigma_i/\sigma_o \tag{15}$$

$$\sigma_\theta(a)/\sigma_{eqb} = 2 - (\sigma_i/\sigma_o) \tag{16}$$

$$\varepsilon_r(a)/\varepsilon_{eqb} = [(1 + \upsilon)(\sigma_i/\sigma_o) - 2\upsilon]/(1 - \upsilon) \tag{17}$$

$$\varepsilon_\theta(a)/\varepsilon_{eqb} = [2 - (1 + \upsilon)(\sigma_i/\sigma_o)]/(1 - \upsilon) \tag{18}$$

REFERENCES

1. Goldbarg, S.H., et al., *Insights into degenerative aortic valve disease.* J Am Coll Cardiol, 2007. **50**(13): p. 1205-13.
2. Mozaffarian, D., et al., *Heart disease and stroke statistics-2015 update: a report from the american heart association.* Circulation, 2015. **131**(4): p. e29-e322.
3. Carabello, B.A. and W.J. Paulus, *Aortic stenosis.* Lancet, 2009. **373**(9667): p. 956-66.
4. Nkomo, V.T., et al., *Burden of valvular heart diseases: a population-based study.* Lancet, 2006. **368**(9540): p. 1005-11.
5. Soler-Soler, J. and E. Galve, *Worldwide perspective of valve disease.* Heart, 2000. **83**(6): p. 721-5.
6. Chrysohoou, C., D. Tsiachris, and C. Stefanadis, *Aortic stenosis in the elderly: challenges in diagnosis and therapy.* Maturitas, 2011. **70**(4): p. 349-53.
7. Hutcheson, J.D., E. Aikawa, and W.D. Merryman, *Potential drug targets for calcific aortic valve disease.* Nat Rev Cardiol, 2014. **11**(4): p. 218-31.
8. Stewart, R.A., *Clinical trials in heart valve disease.* Curr Opin Cardiol, 2009. **24**(4): p. 279-87.
9. Freeman, R.V. and C.M. Otto, *Spectrum of calcific aortic valve disease: pathogenesis, disease progression, and treatment strategies.* Circulation, 2005. **111**(24): p. 3316-26.

10. Merryman, W.D., *Insights into (the interstitium of) degenerative aortic valve disease.* J Am Coll Cardiol, 2008. **51**(14): p. 1415; author reply 1416.

11. Chalajour, F., et al., *Identification and characterization of cells with high angiogenic potential and transitional phenotype in calcific aortic valve.* Exp Cell Res, 2007. **313**(11): p. 2326-35.

12. Chen, J.H., et al., *Identification and characterization of aortic valve mesenchymal progenitor cells with robust osteogenic calcification potential.* Am J Pathol, 2009. **174**(3): p. 1109-19.

13. Taylor, P.M., et al., *The cardiac valve interstitial cell.* Int J Biochem Cell Biol, 2003. **35**(2): p. 113-8.

14. Liu, A.C., V.R. Joag, and A.I. Gotlieb, *The emerging role of valve interstitial cell phenotypes in regulating heart valve pathobiology.* Am J Pathol, 2007. **171**(5): p. 1407-18.

15. Mohler, E.R., 3rd, et al., *Bone formation and inflammation in cardiac valves.* Circulation, 2001. **103**(11): p. 1522-8.

16. Hinz, B., et al., *Myofibroblast development is characterized by specific cell-cell adherens junctions.* Mol Biol Cell, 2004. **15**(9): p. 4310-20.

17. Yip, C.Y., et al., *Calcification by valve interstitial cells is regulated by the stiffness of the extracellular matrix.* Arterioscler Thromb Vasc Biol, 2009. **29**(6): p. 936-42.

18. Rodriguez, K.J. and K.S. Masters, *Regulation of valvular interstitial cell calcification by components of the extracellular matrix.* J Biomed Mater Res A, 2009. **90**(4): p. 1043-53.

19. Mohler, E.R., 3rd, et al., *Identification and characterization of calcifying valve cells from human and canine aortic valves.* J Heart Valve Dis, 1999. **8**(3): p. 254-60.

20. Jian, B., et al., *Progression of aortic valve stenosis: TGF-beta1 is present in calcified aortic valve cusps and promotes aortic valve interstitial cell calcification via apoptosis.* Ann Thorac Surg, 2003. **75**(2): p. 457-65; discussion 465-6.

21. Walker, G.A., et al., *Valvular myofibroblast activation by transforming growth factor-beta: implications for pathological extracellular matrix remodeling in heart valve disease.* Circ Res, 2004. **95**(3): p. 253-60.

22. Benton, J.A., et al., *Statins block calcific nodule formation of valvular interstitial cells by inhibiting alpha-smooth muscle actin expression.* Arterioscler Thromb Vasc Biol, 2009. **29**(11): p. 1950-7.

23. Chen, J.H. and C.A. Simmons, *Cell-matrix interactions in the pathobiology of calcific aortic valve disease: critical roles for matricellular, matricrine, and matrix mechanics cues.* Circ Res, 2011. **108**(12): p. 1510-24.

24. Rajamannan, N.M., et al., *Calcific aortic valve disease: not simply a degenerative process: A review and agenda for research from the National Heart and Lung and Blood Institute Aortic Stenosis Working*

Group. Executive summary: Calcific aortic valve disease-2011 update. Circulation, 2011. **124**(16): p. 1783-91.

25. Leopold, J.A., *Cellular mechanisms of aortic valve calcification.* Circ Cardiovasc Interv, 2012. **5**(4): p. 605-14.
26. Garg, V., *Molecular genetics of aortic valve disease.* Curr Opin Cardiol, 2006. **21**(3): p. 180-4.
27. Garg, V., et al., *Mutations in NOTCH1 cause aortic valve disease.* Nature, 2005. **437**(7056): p. 270-4.
28. Balachandran, K., P. Sucosky, and A.P. Yoganathan, *Hemodynamics and mechanobiology of aortic valve inflammation and calcification.* Int J Inflam, 2011. **2011**: p. 263870.
29. David Merryman, W., *Mechano-potential etiologies of aortic valve disease.* J Biomech, 2010. **43**(1): p. 87-92.
30. Butcher, J.T., C.A. Simmons, and J.N. Warnock, *Mechanobiology of the aortic heart valve.* J Heart Valve Dis, 2008. **17**(1): p. 62-73.
31. Sacks, M.S., W. David Merryman, and D.E. Schmidt, *On the biomechanics of heart valve function.* J Biomech, 2009. **42**(12): p. 1804-24.
32. Grashow, J.S., A.P. Yoganathan, and M.S. Sacks, *Biaixal stress-stretch behavior of the mitral valve anterior leaflet at physiologic strain rates.* Ann Biomed Eng, 2006. **34**(2): p. 315-25.

33. Butcher, J.T. and R.M. Nerem, *Valvular endothelial cells and the mechanoregulation of valvular pathology.* Philos Trans R Soc Lond B Biol Sci, 2007. **362**(1484): p. 1445-57.

34. Balachandran, K., et al., *Elevated cyclic stretch alters matrix remodeling in aortic valve cusps: implications for degenerative aortic valve disease.* Am J Physiol Heart Circ Physiol, 2009. **296**(3): p. H756-64.

35. Balachandran, K., et al., *Elevated cyclic stretch induces aortic valve calcification in a bone morphogenic protein-dependent manner.* Am J Pathol, 2010. **177**(1): p. 49-57.

36. Yacoub, M.H. and J.J. Takkenberg, *Will heart valve tissue engineering change the world?* Nat Clin Pract Cardiovasc Med, 2005. **2**(2): p. 60-1.

37. Lindroos, M., et al., *Prevalence of aortic valve abnormalities in the elderly: an echocardiographic study of a random population sample.* J Am Coll Cardiol, 1993. **21**(5): p. 1220-5.

38. Iung, B. and A. Vahanian, *Valvular heart diseases in elderly people.* Lancet, 2006. **368**(9540): p. 969-71.

39. Schoen, F.J. and R.J. Levy, *Calcification of tissue heart valve substitutes: progress toward understanding and prevention.* Ann Thorac Surg, 2005. **79**(3): p. 1072-80.

40. Sacks, M.S. and A.P. Yoganathan, *Heart valve function: a biomechanical perspective.* Philos Trans R Soc Lond B Biol Sci, 2007. **362**(1484): p. 1369-91.

41. Schoen, F.J., *Evolving concepts of cardiac valve dynamics: the continuum of development, functional structure, pathobiology, and tissue engineering.* Circulation, 2008. **118**(18): p. 1864-80.

42. Merryman, W.D., et al., *Synergistic effects of cyclic tension and transforming growth factor-beta1 on the aortic valve myofibroblast.* Cardiovasc Pathol, 2007. **16**(5): p. 268-76.

43. Vesely, I. and R. Noseworthy, *Micromechanics of the fibrosa and the ventricularis in aortic valve leaflets.* J Biomech, 1992. **25**(1): p. 101-13.

44. Vesely, I. and D. Boughner, *Analysis of the bending behaviour of porcine xenograft leaflets and of natural aortic valve material: bending stiffness, neutral axis and shear measurements.* J Biomech, 1989. **22**(6-7): p. 655-71.

45. Frater, R.W., et al., *Endothelial covering of biological artificial heart valves.* Ann Thorac Surg, 1992. **53**(3): p. 371-2.

46. Leask, R.L., N. Jain, and J. Butany, *Endothelium and valvular diseases of the heart.* Microsc Res Tech, 2003. **60**(2): p. 129-37.

47. Lester, W.M., et al., *Interstitial cells from the atrial and ventricular sides of the bovine mitral valve respond differently to denuding endocardial injury.* In Vitro Cell Dev Biol, 1993. **29A**(1): p. 41-50.

48. Siney, L. and M.J. Lewis, *Nitric oxide release from porcine mitral valves.* Cardiovasc Res, 1993. **27**(9): p. 1657-61.

49. Butcher, J.T. and R.M. Nerem, *Valvular endothelial cells regulate the phenotype of interstitial cells in co-culture: effects of steady shear stress.* Tissue Eng, 2006. **12**(4): p. 905-15.

50. Deck, J.D., *Endothelial cell orientation on aortic valve leaflets.* Cardiovasc Res, 1986. **20**(10): p. 760-7.

51. Filip, D.A., A. Radu, and M. Simionescu, *Interstitial cells of the heart valves possess characteristics similar to smooth muscle cells.* Circ Res, 1986. **59**(3): p. 310-20.

52. Messier, R.H., Jr., et al., *Dual structural and functional phenotypes of the porcine aortic valve interstitial population: characteristics of the leaflet myofibroblast.* J Surg Res, 1994. **57**(1): p. 1-21.

53. Simionescu, D.T., J.J. Lovekamp, and N.R. Vyavahare, *Degeneration of bioprosthetic heart valve cusp and wall tissues is initiated during tissue preparation: an ultrastructural study.* J Heart Valve Dis, 2003. **12**(2): p. 226-34.

54. Simionescu, D.T., J.J. Lovekamp, and N.R. Vyavahare, *Glycosaminoglycan-degrading enzymes in porcine aortic heart valves: implications for bioprosthetic heart valve degeneration.* J Heart Valve Dis, 2003. **12**(2): p. 217-25.

55. Simionescu, D.T., J.J. Lovekamp, and N.R. Vyavahare, *Extracellular matrix degrading enzymes are active in porcine stentless aortic bioprosthetic heart valves.* J Biomed Mater Res, 2003. **66A**(4): p. 755-63.

56. Mendelson, K. and F.J. Schoen, *Heart valve tissue engineering: concepts, approaches, progress, and challenges.* Ann Biomed Eng, 2006. **34**(12): p. 1799-819.

57. Latif, N., et al., *Characterization of structural and signaling molecules by human valve interstitial cells and comparison to human mesenchymal stem cells.* J Heart Valve Dis, 2007. **16**(1): p. 56-66.

58. Ku, C.H., et al., *Collagen synthesis by mesenchymal stem cells and aortic valve interstitial cells in response to mechanical stretch.* Cardiovasc Res, 2006. **71**(3): p. 548-56.

59. Schneider, P.J. and J.D. Deck, *Tissue and cell renewal in the natural aortic valve of rats: an autoradiographic study.* Cardiovasc Res, 1981. **15**(4): p. 181-9.

60. Rajamannan, N.M., et al., *Human aortic valve calcification is associated with an osteoblast phenotype.* Circulation, 2003. **107**(17): p. 2181-4.

61. Jaiswal, N., et al., *Osteogenic differentiation of purified, culture-expanded human mesenchymal stem cells in vitro.* J Cell Biochem, 1997. **64**(2): p. 295-312.

62. Gaur, T., et al., *Canonical WNT signaling promotes osteogenesis by directly stimulating Runx2 gene expression.* J Biol Chem, 2005. **280**(39): p. 33132-40.

63. Lian, J.B. and C.M. Gundberg, *Osteocalcin. Biochemical considerations and clinical applications.* Clin Orthop Relat Res, 1988(226): p. 267-91.

64. Monzack, E.L. and K.S. Masters, *Can valvular interstitial cells become true osteoblasts? A side-by-side comparison.* J Heart Valve Dis, 2011. **20**(4): p. 449-63.

65. Gabbiani, G., G.B. Ryan, and G. Majne, *Presence of modified fibroblasts in granulation tissue and their possible role in wound contraction.* Experientia, 1971. **27**(5): p. 549-50.

66. Hinz, B., et al., *Mechanical tension controls granulation tissue contractile activity and myofibroblast differentiation.* Am J Pathol, 2001. **159**(3): p. 1009-20.

67. Tomasek, J.J., et al., *Myofibroblasts and mechano-regulation of connective tissue remodelling.* Nat Rev Mol Cell Biol, 2002. **3**(5): p. 349-63.

68. Hinz, B., *The myofibroblast: paradigm for a mechanically active cell.* J Biomech, 2010. **43**(1): p. 146-55.

69. Skalli, O., et al., *Alpha-smooth muscle actin, a differentiation marker of smooth muscle cells, is present in microfilamentous bundles of pericytes.* J Histochem Cytochem, 1989. **37**(3): p. 315-21.

70. Chang, S.K., et al., *Cadherin-11 regulates fibroblast inflammation.* Proc Natl Acad Sci U S A, 2011. **108**(20): p. 8402-7.

71. Chen, J.H., et al., *beta-catenin mediates mechanically regulated, transforming growth factor-beta1-induced myofibroblast differentiation of aortic valve interstitial cells.* Arterioscler Thromb Vasc Biol, 2011. **31**(3): p. 590-7.

72. Vaslef, S.N. and W.C. Roberts, *Early descriptions of aortic valve stenosis.* Am Heart J, 1993. **125**(5 Pt 1): p. 1465-74.

73. Bertazzo, S., et al., *Nano-analytical electron microscopy reveals fundamental insights into human cardiovascular tissue calcification.* Nat Mater, 2013. **12**(6): p. 576-83.

74. Mohler, E.R., 3rd, *Mechanisms of aortic valve calcification.* Am J Cardiol, 2004. **94**(11): p. 1396-402, A6.

75. Rajamannan, N.M., *Calcific aortic stenosis: lessons learned from experimental and clinical studies.* Arterioscler Thromb Vasc Biol, 2009. **29**(2): p. 162-8.

76. Gu, X. and K.S. Masters, *Role of the Rho pathway in regulating valvular interstitial cell phenotype and nodule formation.* Am J Physiol Heart Circ Physiol.

77. Hinz, B., *Formation and function of the myofibroblast during tissue repair.* J Invest Dermatol, 2007. **127**(3): p. 526-37.

78. Kim, K.M., *Apoptosis and calcification.* Scanning Microsc, 1995. **9**(4): p. 1137-75; discussion 1175-8.

79. Butcher, J.T., et al., *Transcriptional profiles of valvular and vascular endothelial cells reveal phenotypic differences: influence of shear stress.* Arterioscler Thromb Vasc Biol, 2006. **26**(1): p. 69-77.

80. Sucosky, P., et al., *Altered shear stress stimulates upregulation of endothelial VCAM-1 and ICAM-1 in a BMP-4- and TGF-beta1-dependent pathway.* Arterioscler Thromb Vasc Biol, 2009. **29**(2): p. 254-60.

81. Owens, G.K., *Role of mechanical strain in regulation of differentiation of vascular smooth muscle cells.* Circ Res, 1996. **79**(5): p. 1054-5.

82. Williams, B., *Mechanical influences on vascular smooth muscle cell function.* J Hypertens, 1998. **16**(12 Pt 2): p. 1921-9.

83. Wang, J.H. and B.P. Thampatty, *An introductory review of cell mechanobiology.* Biomech Model Mechanobiol, 2006. **5**(1): p. 1-16.

84. Ross, R., *The pathogenesis of atherosclerosis--an update.* N Engl J Med, 1986. **314**(8): p. 488-500.

85. Chicurel, M.E., C.S. Chen, and D.E. Ingber, *Cellular control lies in the balance of forces.* Curr Opin Cell Biol, 1998. **10**(2): p. 232-9.

86. Grodzinsky, A.J., et al., *Cartilage tissue remodeling in response to mechanical forces.* Annu Rev Biomed Eng, 2000. **2**: p. 691-713.

87. Ingber, D.E., *Mechanobiology and diseases of mechanotransduction.* Ann Med, 2003. **35**(8): p. 564-77.

88. Riley, G.P., et al., *Matrix metalloproteinase activities and their relationship with collagen remodelling in tendon pathology.* Matrix Biol, 2002. **21**(2): p. 185-95.

89. Robicsek, F., M.J. Thubrikar, and A.A. Fokin, *Cause of degenerative disease of the trileaflet aortic valve: review of subject and presentation of a new theory.* Ann Thorac Surg, 2002. **73**(4): p. 1346-54.

90. Goffin, J.M., et al., *Focal adhesion size controls tension-dependent recruitment of alpha-smooth muscle actin to stress fibers.* J Cell Biol, 2006. **172**(2): p. 259-68.

91. Wipff, P.J., et al., *Myofibroblast contraction activates latent TGF-beta1 from the extracellular matrix.* J Cell Biol, 2007. **179**(6): p. 1311-23.

92. Balachandran, K., et al., *Elevated cyclic stretch induces aortic valve calcification in a bone morphogenic protein-dependent manner.* Am J Pathol. **177**(1): p. 49-57.

93. High, F.A. and J.A. Epstein, *The multifaceted role of Notch in cardiac development and disease.* Nat Rev Genet, 2008. **9**(1): p. 49-61.

94. Nigam, V. and D. Srivastava, *Notch1 represses osteogenic pathways in aortic valve cells.* J Mol Cell Cardiol, 2009. **47**(6): p. 828-34.

95. Nus, M., et al., *Diet-induced aortic valve disease in mice haploinsufficient for the Notch pathway effector RBPJK/CSL.* Arterioscler Thromb Vasc Biol, 2011. **31**(7): p. 1580-8.

96. Bray, S.J., *Notch signalling: a simple pathway becomes complex.* Nat Rev Mol Cell Biol, 2006. **7**(9): p. 678-89.

97. Kopan, R. and M.X. Ilagan, *The canonical Notch signaling pathway: unfolding the activation mechanism.* Cell, 2009. **137**(2): p. 216-33.

98. Artavanis-Tsakonas, S., K. Matsuno, and M.E. Fortini, *Notch signaling.* Science, 1995. **268**(5208): p. 225-32.

99. Acharya, A., et al., *Inhibitory role of Notch1 in calcific aortic valve disease.* PLoS One, 2011. **6**(11): p. e27743.

100. Tang, Y., S. Urs, and L. Liaw, *Hairy-related transcription factors inhibit Notch-induced smooth muscle alpha-actin expression by interfering with*

Notch intracellular domain/CBF-1 complex interaction with the CBF-1-binding site. Circ Res, 2008. **102**(6): p. 661-8.

101. Roger, V.L., et al., *Heart disease and stroke statistics--2011 update: a report from the American Heart Association.* Circulation, 2011. **123**(4): p. e18-e209.
102. Merryman, W.D., *Mechano-potential etiologies of aortic valve disease.* J Biomech, 2009. **43**(1): p. 87-92.
103. Helske, S., et al., *Aortic valve stenosis: an active atheroinflammatory process.* Curr Opin Lipidol, 2007. **18**(5): p. 483-91.
104. Rajamannan, N.M., *Mechanisms of aortic valve calcification: the LDL-density-radius theory: a translation from cell signaling to physiology.* Am J Physiol Heart Circ Physiol, 2010. **298**(1): p. H5-15.
105. Merryman, W.D., *What modulates the aortic valve interstitial cell phenotype?* Future Cardiol, 2008. **4**(3): p. 247-52.
106. Kennedy, J.A., et al., *Inhibition of calcifying nodule formation in cultured porcine aortic valve cells by nitric oxide donors.* Eur J Pharmacol, 2009. **602**(1): p. 28-35.
107. Chen, J.H., et al., *beta-catenin mediates mechanically regulated, transforming growth factor-beta1-induced myofibroblast differentiation of aortic valve interstitial cells.* Arterioscler Thromb Vasc Biol. **31**(3): p. 590-7.

108. Gu, X. and K.S. Masters, *Regulation of valvular interstitial cell calcification by adhesive peptide sequences.* J Biomed Mater Res A, 2010. **93**(4): p. 1620-30.

109. Benton, J.A., H.B. Kern, and K.S. Anseth, *Substrate properties influence calcification in valvular interstitial cell culture.* J Heart Valve Dis, 2008. **17**(6): p. 689-99.

110. Cushing, M.C., J.T. Liao, and K.S. Anseth, *Activation of valvular interstitial cells is mediated by transforming growth factor-beta1 interactions with matrix molecules.* Matrix Biol, 2005. **24**(6): p. 428-37.

111. Robicsek, F. and M.J. Thubrikar, *Mechanical stress as cause of aortic valve disease. Presentation of a new aortic root prosthesis.* Acta Chir Belg, 2002. **102**(1): p. 1-6.

112. Haskett, D., et al., *Microstructural and biomechanical alterations of the human aorta as a function of age and location.* Biomech Model Mechanobiol, 2010. **9**(6): p. 725-36.

113. Balachandran, K., et al., *An ex vivo study of the biological properties of porcine aortic valves in response to circumferential cyclic stretch.* Ann Biomed Eng, 2006. **34**(11): p. 1655-65.

114. Simmons, C.A., et al., *Mechanical stimulation and mitogen-activated protein kinase signaling independently regulate osteogenic differentiation and mineralization by calcifying vascular cells.* J Biomech, 2004. **37**(10): p. 1531-41.

115. Merryman, W.D., et al., *Differences in tissue-remodeling potential of aortic and pulmonary heart valve interstitial cells.* Tissue Eng, 2007. **13**(9): p. 2281-9.

116. Merryman, W.D., et al., *Correlation between heart valve interstitial cell stiffness and transvalvular pressure: implications for collagen biosynthesis.* Am J Physiol Heart Circ Physiol, 2006. **290**(1): p. H224-31.

117. Wipff, P.J., et al., *Myofibroblast contraction activates latent TGF-β1 from the extracellular matrix.* J Cell Biol, 2007. **179**(6): p. 1311-23.

118. Gu, X. and K.S. Masters, *Role of the Rho pathway in regulating valvular interstitial cell phenotype and nodule formation.* Am J Physiol Heart Circ Physiol, 2011. **300**(2): p. H448-58.

119. Follonier, L., et al., *Myofibroblast communication is controlled by intercellular mechanical coupling.* J Cell Sci, 2008. **121**(Pt 20): p. 3305-16.

120. Pittet, P., et al., *Fibrogenic fibroblasts increase intercellular adhesion strength by reinforcing individual OB-cadherin bonds.* J Cell Sci, 2008. **121**(Pt 6): p. 877-86.

121. Merryman, W.D., et al., *The effects of cellular contraction on aortic valve leaflet flexural stiffness.* J Biomech, 2006. **39**(1): p. 88-96.

122. Yip, C.Y. and C.A. Simmons, *The aortic valve microenvironment and its role in calcific aortic valve disease.* Cardiovasc Pathol, 2011. **20**(3): p. 177-82.

123. Gu, X. and K.S. Masters, *Role of the MAPK/ERK pathway in valvular interstitial cell calcification.* Am J Physiol Heart Circ Physiol, 2009. **296**(6): p. H1748-57.

124. Hutcheson, J.D., Venkataraman, R., Baudenbacher, F. J., Merryman, W. D., *Intracellular Ca2+ accumlation is starin-dependent and correlates with apoptosis in aortic valve fibroblasts.* Journal of Biomechanics, (in press).

125. Piper, C., et al., *Can progression of valvar aortic stenosis be predicted accurately?* Ann Thorac Surg, 2003. **76**(3): p. 676-80; discussion 680.

126. Weinberg, E.J., F.J. Schoen, and M.R. Mofrad, *A computational model of aging and calcification in the aortic heart valve.* PLoS One, 2009. **4**(6): p. e5960.

127. Weinberg, E.J., et al., *Hemodynamic environments from opposing sides of human aortic valve leaflets evoke distinct endothelial phenotypes in vitro.* Cardiovasc Eng, 2010. **10**(1): p. 5-11.

128. Weinberg, E.J. and M.R. Kaazempur Mofrad, *Transient, three-dimensional, multiscale simulations of the human aortic valve.* Cardiovasc Eng, 2007. **7**(4): p. 140-55.

129. Serini, G. and G. Gabbiani, *Mechanisms of myofibroblast activity and phenotypic modulation.* Exp Cell Res, 1999. **250**(2): p. 273-83.

130. Rajamannan, N.M., *Calcific aortic valve disease: cellular origins of valve calcification.* Arterioscler Thromb Vasc Biol, 2011. **31**(12): p. 2777-8.

131. Fisher, C.I., J. Chen, and W.D. Merryman, *Calcific nodule morphogenesis by heart valve interstitial cells is strain dependent.* Biomech Model Mechanobiol, 2012.

132. Cushing, M.C., et al., *Fibroblast growth factor represses Smad-mediated myofibroblast activation in aortic valvular interstitial cells.* FASEB J, 2008. **22**(6): p. 1769-77.

133. Lee, D.M., et al., *Cadherin-11 in synovial lining formation and pathology in arthritis.* Science, 2007. **315**(5814): p. 1006-10.

134. Schneider, D.J., et al., *Cadherin-11 contributes to pulmonary fibrosis: potential role in TGF-beta production and epithelial to mesenchymal transition.* FASEB J, 2012. **26**(2): p. 503-12.

135. Heupel, W.M., et al., *Different Ca2+ affinities and functional implications of the two synaptic adhesion molecules cadherin-11 and N-cadherin.* Mol Cell Neurosci, 2008. **37**(3): p. 548-58.

136. Hutcheson, J.D., et al., *5-HT2B antagonism arrests non-canonical TGF-β1-induced valvular myofibroblast differentiation.* J Mol Cell Cardiol, 2012. **In press**.

137. Samarakoon, R. and P.J. Higgins, *Integration of non-SMAD and SMAD signaling in TGF-beta1-induced plasminogen activator inhibitor type-1 gene expression in vascular smooth muscle cells.* Thromb Haemost, 2008. **100**(6): p. 976-83.

138. Li, J., et al., *MEK/ERK and p38 MAPK regulate chondrogenesis of rat bone marrow mesenchymal stem cells through delicate interaction with TGF-beta1/Smads pathway.* Cell Prolif, 2010. **43**(4): p. 333-43.

139. Jiang, W., et al., *Role of cross-talk between the Smad2 and MAPK pathways in TGF-beta1-induced collagen IV expression in mesangial cells.* Int J Mol Med, 2010. **26**(4): p. 571-6.

140. Greenberg, R.S., et al., *FAK-dependent regulation of myofibroblast differentiation.* FASEB J, 2006. **20**(7): p. 1006-8.

141. Otto, C.M., et al., *Characterization of the early lesion of 'degenerative' valvular aortic stenosis. Histological and immunohistochemical studies.* Circulation, 1994. **90**(2): p. 844-53.

142. Iung, B. and A. Vahanian, *Epidemiology of valvular heart disease in the adult.* Nat Rev Cardiol, 2011. **8**(3): p. 162-72.

143. Dweck, M.R., N.A. Boon, and D.E. Newby, *Calcific aortic stenosis: a disease of the valve and the myocardium.* J Am Coll Cardiol, 2012. **60**(19): p. 1854-63.

144. Langanay, T., et al., *Aortic valve replacement in the elderly: the real life.* Ann Thorac Surg, 2012. **93**(1): p. 70-7; discussion 77-8.

145. Thomas, M., et al., *Thirty-day results of the SAPIEN aortic Bioprosthesis European Outcome (SOURCE) Registry: A European registry of transcatheter aortic valve implantation using the Edwards SAPIEN valve.* Circulation, 2010. **122**(1): p. 62-9.

146. Hutcheson, J.D., et al., *5-HT(2B) antagonism arrests non-canonical TGF-beta1-induced valvular myofibroblast differentiation.* J Mol Cell Cardiol, 2012. **53**(5): p. 707-14.

147. Yip, C.Y., et al., *Inhibition of pathological differentiation of valvular interstitial cells by C-type natriuretic peptide.* Arterioscler Thromb Vasc Biol, 2011. **31**(8): p. 1881-9.

148. Fisher, C.I., J. Chen, and W.D. Merryman, *Calcific nodule morphogenesis by heart valve interstitial cells is strain dependent.* Biomech Model Mechanobiol, 2013. **12**(1): p. 5-17.

149. Hutcheson, J.D., et al., *Cadherin-11 regulates cell-cell tension necessary for calcific nodule formation by valvular myofibroblasts.* Arterioscler Thromb Vasc Biol, 2013. **33**(1): p. 114-20.

150. Bowler, M.A., Merryman, W.D., *In vitro Models of Aortic Valve Calcification: Solidifying a System* Cardiovascular Pathology, 2014.

151. Valente, M., U. Bortolotti, and G. Thiene, *Ultrastructural substrates of dystrophic calcification in porcine bioprosthetic valve failure.* Am J Pathol, 1985. **119**(1): p. 12-21.

152. Zhao, Y., et al., *Characterization of dystrophic calcification induced in mice by cardiotoxin.* Calcif Tissue Int, 2009. **85**(3): p. 267-75.

153. Cloyd, K.L., et al., *Characterization of porcine aortic valvular interstitial cell 'calcified' nodules.* PLoS One, 2012. **7**(10): p. e48154.

154. Wang, H., et al., *Redirecting valvular myofibroblasts into dormant fibroblasts through light-mediated reduction in substrate modulus.* PLoS One, 2012. **7**(7): p. e39969.

155. Engler, A.J., et al., *Matrix elasticity directs stem cell lineage specification.* Cell, 2006. **126**(4): p. 677-89.

156. Tse, J.R. and A.J. Engler, *Preparation of hydrogel substrates with tunable mechanical properties.* Curr Protoc Cell Biol, 2010. **Chapter 10**: p. Unit 10 16.

157. Gregory, C.A., et al., *An Alizarin red-based assay of mineralization by adherent cells in culture: comparison with cetylpyridinium chloride extraction.* Anal Biochem, 2004. **329**(1): p. 77-84.

158. Sewell-Loftin, M.K., et al., *A novel technique for quantifying mouse heart valve leaflet stiffness with atomic force microscopy.* J Heart Valve Dis, 2012. **21**(4): p. 513-20.

159. Goldstein, J., *Scanning electron microscopy and x-ray microanalysis*. 3rd ed. 2003, New York: Kluwer Academic/Plenum Publishers. xix, 689 p.

160. Bonucci, E., *Biological calcification : normal and pathological processes in the early stages*. 2007, Berlin New York: Springer. xxi, 592 p.

161. Benjamin Kramer, M.J.S., *Composition of Bone: IV. Primary Calcification.* The Journal of Biological Chemistry, 1928. **79**: p. 147-160.

162. Gilbert, S.F., *Developmental biology*. 6th ed. 2000, Sunderland, Mass.: Sinauer Associates. xviii, 749 p.

163. Wang, H., et al., *Hydrogels preserve native phenotypes of valvular fibroblasts through an elasticity-regulated PI3K/AKT pathway.* Proc Natl Acad Sci U S A, 2013. **110**(48): p. 19336-41.

164. Hinz, B., et al., *The myofibroblast: one function, multiple origins.* Am J Pathol, 2007. **170**(6): p. 1807-16.

165. Ducy, P., et al., *A Cbfa1-dependent genetic pathway controls bone formation beyond embryonic development.* Genes Dev, 1999. **13**(8): p. 1025-36.

166. MacGrogan, D., L. Luna-Zurita, and J.L. de la Pompa, *Notch Signaling in Cardiac Valve Development and Disease.* Birth Defects Research Part a-Clinical and Molecular Teratology, 2011. **91**(6): p. 449-459.

167. MacGrogan, D., M. Nus, and J.L. de la Pompa, *Notch Signaling in Cardiac Development and Disease.* Notch Signaling, 2010. **92**: p. 333-365.

168. Gude, N. and M. Sussman, *Notch signaling and cardiac repair.* J Mol Cell Cardiol, 2012. **52**(6): p. 1226-32.

169. Niessen, K. and A. Karsan, *Notch signaling in cardiac development.* Circulation Research, 2008. **102**(10): p. 1169-81.

170. Rusanescu, G., R. Weissleder, and E. Aikawa, *Notch signaling in cardiovascular disease and calcification.* Curr Cardiol Rev, 2008. **4**(3): p. 148-56.

171. Zeng, Q., et al., *Notch1 promotes the pro-osteogenic response of human aortic valve interstitial cells via modulation of ERK1/2 and nuclear factor-kappaB activation.* Arterioscler Thromb Vasc Biol, 2013. **33**(7): p. 1580-90.

172. Conlon, R.A., A.G. Reaume, and J. Rossant, *Notch1 is required for the coordinate segmentation of somites.* Development, 1995. **121**(5): p. 1533-45.

173. Jat, P.S., et al., *Direct derivation of conditionally immortal cell lines from an H-2Kb-tsA58 transgenic mouse.* Proc Natl Acad Sci U S A, 1991. **88**(12): p. 5096-100.

174. Lali, F.V., et al., *The pyridinyl imidazole inhibitor SB203580 blocks phosphoinositide-dependent protein kinase activity, protein kinase B phosphorylation, and retinoblastoma hyperphosphorylation in interleukin-2-stimulated T cells independently of p38 mitogen-activated protein kinase.* J Biol Chem, 2000. **275**(10): p. 7395-402.

175. Varnum-Finney, B., et al., *Immobilization of Notch ligand, Delta-1, is required for induction of notch signaling.* J Cell Sci, 2000. **113 Pt 23**: p. 4313-8.

176. Bosse, K., et al., *Endothelial nitric oxide signaling regulates Notch1 in aortic valve disease.* J Mol Cell Cardiol, 2013. **60**: p. 27-35.

177. Komori, T., *Regulation of skeletal development by the Runx family of transcription factors.* J Cell Biochem, 2005. **95**(3): p. 445-53.

178. Sassoli, C., et al., *Relaxin prevents cardiac fibroblast-myofibroblast transition via notch-1-mediated inhibition of TGF-beta/Smad3 signaling.* PLoS One, 2013. **8**(5): p. e63896.

179. Fan, Y.H., et al., *Notch signaling may negatively regulate neonatal rat cardiac fibroblast-myofibroblast transformation.* Physiol Res, 2011. **60**(5): p. 739-48.

180. Li, C., S. Xu, and A.I. Gotlieb, *The progression of calcific aortic valve disease through injury, cell dysfunction, and disruptive biologic and physical force feedback loops.* Cardiovasc Pathol, 2013. **22**(1): p. 1-8.

181. Simonneau, L., et al., *Cadherin 11 expression marks the mesenchymal phenotype: towards new functions for cadherins?* Cell Adhes Commun, 1995. **3**(2): p. 115-30.

182. Chu, K., et al., *Cadherin-11 promotes the metastasis of prostate cancer cells to bone.* Mol Cancer Res, 2008. **6**(8): p. 1259-67.

183. Kiener, H.P., et al., *Cadherin-11 induces rheumatoid arthritis fibroblast-like synoviocytes to form lining layers in vitro.* Am J Pathol, 2006. **168**(5): p. 1486-99.

184. Zhou, J., et al., *Cadherin-11 expression patterns in heart valves associate with key functions during embryonic cushion formation, valve maturation and calcification.* Cells Tissues Organs, 2013. **198**(4): p. 300-10.

185. Wu, M., et al., *Identification of cadherin 11 as a mediator of dermal fibrosis and possible role in systemic sclerosis.* Arthritis Rheumatol, 2014. **66**(4): p. 1010-21.

186. Manning, B.D. and L.C. Cantley, *AKT/PKB signaling: navigating downstream.* Cell, 2007. **129**(7): p. 1261-74.

187. Xu, N., et al., *Akt: a double-edged sword in cell proliferation and genome stability.* J Oncol, 2012. **2012**: p. 951724.

188. Farina, A.K., et al., *Post-transcriptional regulation of cadherin-11 expression by GSK-3 and beta-catenin in prostate and breast cancer cells.* PLoS One, 2009. **4**(3): p. e4797.

189. Wang, J., et al., *Mechanical force regulation of myofibroblast differentiation in cardiac fibroblasts.* Am J Physiol Heart Circ Physiol, 2003. **285**(5): p. H1871-81.

190. Tock, J., et al., *Induction of SM-alpha-actin expression by mechanical strain in adult vascular smooth muscle cells is mediated through activation of JNK and p38 MAP kinase.* Biochem Biophys Res Commun, 2003. **301**(4): p. 1116-21.

191. Meurette, O., et al., *Notch activation induces Akt signaling via an autocrine loop to prevent apoptosis in breast epithelial cells.* Cancer Res, 2009. **69**(12): p. 5015-22.

192. Gutierrez, A. and A.T. Look, *NOTCH and PI3K-AKT pathways intertwined.* Cancer Cell, 2007. **12**(5): p. 411-3.

193. Hales, E.C., et al., *Notch1 receptor regulates AKT protein activation loop (Thr308) dephosphorylation through modulation of the PP2A phosphatase in phosphatase and tensin homolog (PTEN)-null T-cell acute lymphoblastic leukemia cells.* J Biol Chem, 2013. **288**(31): p. 22836-48.

194. Guo, X. and X.F. Wang, *Signaling cross-talk between TGF-beta/BMP and other pathways.* Cell Res, 2009. **19**(1): p. 71-88.

195. Balestrini, J.L., et al., *Applying controlled non-uniform deformation for in vitro studies of cell mechanobiology.* Biomech Model Mechanobiol, 2010. **9**(3): p. 329-44.

196. David, G. and J.D. Humphrey, *Redistribution of stress due to a circular hole in a nonlinear anisotropic membrane.* J Biomech, 2004. **37**(8): p. 1197-203.

197. Mori, D., et al., *Stress distribution in a circular membrane with a central fixation.* J Biomech Eng, 2005. **127**(3): p. 549-53.